

*NASA Conference Publication 3069*

# **Eighteenth NASTRAN<sup>®</sup> Users' Colloquium**

*Computer Software Management and Information Center  
University of Georgia  
Athens, Georgia*

Proceedings of a colloquium held in  
Portland, Oregon  
April 23-27, 1990

**NASA**

National Aeronautics and  
Space Administration

Office of Management

Scientific and Technical  
Information Division

**1990**



## FOREWORD

NASTRAN® (NASA STRUCTURAL ANALYSIS) is a large, comprehensive, nonproprietary, general purpose finite element computer code for structural analysis which was developed under NASA sponsorship and became available to the public in late 1970. It can be obtained through COSMIC® (Computer Software Management and Information Center), Athens, Georgia, and is widely used by NASA, other government agencies, and industry.

NASA currently provides continuing maintenance of NASTRAN through COSMIC. Because of the widespread interest in NASTRAN, and finite element methods in general, the Eighteenth NASTRAN Users' Colloquium was organized and held at The Red Lion Portland Center, Portland, Oregon on April 23-27, 1990. (Papers from previous colloquia held in 1971, 1972, 1973, 1975, 1976, 1977, 1978, 1979, 1980, 1982, 1983, 1984, 1985, 1986, 1987, 1988 and 1989 are published in NASA Technical Memorandums X-2378, X-2637, X-2893, X-3278, X-3428, and NASA Conference Publications 2018, 2062, 2131, 2151, 2249, 2284, 2328, 2373, 2419, 2481, 2505 and 3029.) The Eighteenth Colloquium provides some comprehensive general papers on the application of finite element methods in engineering, comparisons with other approaches, unique applications, pre- and post-processing or auxiliary programs, and new methods of analysis with NASTRAN.

Individuals actively engaged in the use of finite elements or NASTRAN were invited to prepare papers for presentation at the Colloquium. These papers are included in this volume. No editorial review was provided by NASA or COSMIC; however, detailed instructions were provided each author to achieve reasonably consistent paper format and content. The opinions and data presented are the sole responsibility of the authors and their respective organizations.

NASTRAN® and COSMIC® are registered trademarks of the National Aeronautics and Space Administration.



CONTENTS

	Page
FOREWORD . . . . .	iii
1. A NASTRAN TRAINER FOR DYNAMICS . . . . . by H. R. Grooms, P.J. Hinz and G. L. Commerford (Rockwell International)	1 <sub>7</sub>
2. PCI - A PATRAN-NASTRAN MODEL TRANSLATOR . . . . . by T. J. Sheerer (Chrysler Technologies Airborne Systems, Inc.)	14 <sub>2</sub>
3. A GENERIC INTERFACE BETWEEN COSMIC/NASTRAN AND PATRAN . . . . . by Paul N. Roschke, Prakrit Premthamkorn, and James C. Maxwell (Texas A&M University)	20 <sub>3</sub>
4. ACCURACY OF THE QUAD4 THICK SHELL ELEMENT . . . . . by William R. Case, Tiffany D. Bowles, Alicia K. Croft and Mark A. McGinnis (NASA/Goddard Space Flight Center)	30 <sub>2</sub>
5. EIGENVALUE COMPUTATIONS WITH THE QUAD4 CONSISTENT-MASS MATRIX . . . . . By Thomas A. Butler (Los Alamos National Laboratory)	61 <sub>3</sub>
6. NASTRAN MIGRATION TO UNIX . . . . . by Gordon C. Chan and Horace Q. Turner (UNISYS Corporation)	73 <sub>2</sub>
7. OBTAINING EIGENSOLUTIONS FOR MULTIPLE FREQUENCY RANGES IN A SINGLE NASTRAN EXECUTION . . . . . by P. R. Pamidi and W. K. Brown (RPK Corporation)	77 <sub>1</sub>
8. RANDOM VIBRATION ANALYSIS OF SPACE FLIGHT HARDWARE USING NASTRAN by S. K. Thampi and S. N. Vidyasagar (GE Government Services)	90 <sub>3</sub>
9. OBTAINING AN EQUIVALENT BEAM . . . . . by Thomas G. Butler (Butler Analyses)	107 <sub>2</sub>
10. LOW VELOCITY IMPACT ANALYSIS WITH NASTRAN . . . . . by Daniel A. Trowbridge (Analex Corporation) and Joseph E. Grady and Robert A. Aiello (NASA Lewis Research Center)	115 <sub>10</sub>

CONTENTS  
(Continued)

	Page
11. TRANSITIONING OF POWER FLOW IN BEAM MODELS WITH BENDS . . . . .	135
by Stephen A. Hambric	
(David Taylor Research Center)	111
12. COUPLED BE/FE/BE APPROACH FOR SCATTERING FROM FLUID-FILLED STRUCTURES . . . . .	150
by Gordon C. Everstine and Raymond S. Cheng	
(David Taylor Research Center)	112
13. MONITORING OF RITZ MODAL GENERATION . . . . .	165
by Mladen Chargin	
(NASA Ames Research Center)	
and Thomas G. Butler	
(Butler Analyses)	

H.R. Grooms, P.J. Hinz, and G.L. Commerford  
Rockwell International

### OVERVIEW

As the use of the finite element method proliferates, the need for training becomes more and more pronounced. An automated tool to familiarize engineers with static solutions has been developed and used. This tool (Figure 1) is part of an overall structural analysis/expert training system (ref. 1). Experiences with this tool and comments from users (ref. 2) have underlined the need for a dynamic version of the trainer.

This paper presents an automated training tool that engineers can use to master the application of NASTRAN to dynamic problems. The paper consists of the following sections:

- Overview
- Background
- Existing Programs
- Scope, Purpose, and System Organization
- Example Problems
- Conclusions
- References

Example problems have been selected to make classical solutions available for comparison. These comparisons can be used to evaluate the solution.

### BACKGROUND

The solution of dynamic problems involves some complications that do not exist with static problems:

- How many degrees of freedom should be retained for the eigenvalue solution?
- Which discrete mass items are so large or important that they should be retained for eigenvalue solution?
- How many frequencies and mode shapes are needed and to what accuracy?

An engineer may think that most of the mass associated with a structure can be traced to the structural members themselves; this is not necessarily true. With many aircraft and spacecraft, the nonstructural masses (e.g., hydraulic lines, fuel tanks,

environmental control equipment, etc.) have a pronounced influence on the overall mass distribution and may have the greatest dynamic effect.

The example problems have distributed masses and lumped masses that the user must consider in the solution approach. These examples help the user develop judgment when deciding on the number and the particular degrees of freedom to be retained, and on how to discretize the distributed mass.

#### EXISTING PROGRAMS

Various researchers have developed computer programs for structural analysis and design applications. Ginsburg (ref. 3) addressed computer literacy, while Woodward and Morris discussed improved productivity through interactive processing (ref. 4). Wilson and Holt (ref. 5) developed a system for computer-assisted learning in structural engineering. Sadd and Rolph (ref. 6) described the various ways in which design engineers could be trained to use the finite element method. Self-adapting menus for CAD software are covered by Ginsburg (ref. 7).

Bykat (ref. 8) is developing a system that will have features for training, analysis control, and interrogation.

#### SCOPE, PURPOSE, AND SYSTEM ORGANIZATION

The NASTRAN trainer was designed to be a stand-alone tool. The trainer is user friendly--a knowledge of job control language or the operating system is not required. A user can sit down at a terminal and, in very little time, start solving an example problem. The trainer is organized so that a user must complete the static problems (ref. 2) before the dynamics problems can be accessed. This organization prevents a user who has no familiarity with the finite element method from starting with the dynamics section.

The trainer is organized into three main modules: (1) overview, (2) user's guide, and (3) problem set. Figure 2 shows some details of each module. The user accesses these modules by using the primary menu. More details of the NASTRAN environment sections are given in Figure 3.

#### EXAMPLE PROBLEMS

The example problems, shown in Figures 4 through 11 and summarized in Table 1, become progressively more difficult to solve. The first problem is a simply supported beam with a single lumped mass at the center.

There are various courses and classes to instruct engineers in solving dynamics problems. These courses usually emphasize the theory. A vital part of solving any large dynamics problems is deciding how many and which degrees of freedom should be retained for the eigenvalue solution. This is usually a matter of judgment, and it takes solving many problems to develop this judgment.

Example 2 was solved using three different approaches. The user was trying to answer some fundamental questions that must be addressed every time a dynamics problem is solved using the finite element method:

- Is the model fine enough?
- Have the distributed masses been lumped into enough locations?
- Have enough degrees of freedom been retained in the eigensolution?

Figure 12 summarizes the different approaches. Table 2 compares the computed three lowest natural frequencies with the exact results.

### CONCLUSIONS

An automated training tool that helps engineers become familiar with using NASTRAN to solve dynamic problems has been presented. The tool allows the user to proceed at his own pace by using a set of eight example problems. The examples were selected so that classical solutions are available and displayed, enabling the user to make comparisons.

### REFERENCES

1. Grooms, H.R., W.J. Merriman, and P.J. Hinz: An Expert/Training System for Structural Analysis. ASME Conference on Pressure Vessels and Piping, New Orleans, Louisiana, June 1985.
2. Grooms, H.R., P.J. Hinz, and K. Cox: Experiences With a NASTRAN Trainer. 16th NASTRAN Users' Colloquium, Arlington, Virginia, April 1988.
3. Ginsburg, S: Computer Literacy: Mainframe Monsters and Pacman. Symposium on Advances and Trends in Structures and Dynamics, Washington, D.C., October 1984.
4. Woodward, W.S., and J.W. Morris: Improving Productivity in Finite Element Analysis Through Interactive Processing. Finite Elements in Analysis and Design, Vol. 1, No. 1, 1985.
5. Wilson, E.L., and M. Holt: CAL-80-Computer Assisted Learning of Structural Engineering. Symposium on Advances and Trends in Structures and Dynamics, Washington, D.C., October 1984.
6. Sadd, M.H., and W.D. Rolph III: On Training Programs for Design Engineers in the Use of Finite Element Analysis. Computers and Structures, Vol. 26, No. 12, 1987.
7. Ginsburg, S: Self-Adapting Menus for CAD Software. Computers and Structures, Vol. 23, No. 4, 1986.
8. Bykat, A: Design of FEATS, a Finite Element Applications Training System. 16th NASTRAN Users' Colloquium, Arlington, Virginia, April 1988.

**Table 1. Example Problems**

<b>Example</b>	<b>Description</b>	<b>Significant Features</b>
1	Beam simply supported on both ends with lumped mass in middle	Motion in one plane only, lumped mass only
2	Beam simply supported on both ends with uniformly distributed mass	Motion in one plane only, distributed mass
3	Beam fixed on one end with a lumped mass at the free end	Motion in any direction, lumped mass only
4	Beam fixed on one end with a uniformly distributed mass	Motion in any direction with uniformly distributed mass
5	Rectangular plate clamped on one edge, all other edges free with a uniformly distributed mass	Plate bending with distributed mass
6	Rectangular plate, free-free with uniformly distributed mass	Free-free (implies six modes with zero frequency)
7	Two beams connected by springs, each with distributed and lumped mass	Multibody problem, free-free
8	Problem 7 with a forcing function added	Forcing function

**Table 2. Comparison of Natural Frequencies for Example 2**

<b>Mode \ Approach</b>	<b>Exact Solution</b>	<b>First Approach</b>	<b>Second</b>	<b>Third</b>
1	9.870	9.867	9.869	9.872
2	39.48	39.19	39.47	39.74
3	88.83	83.21	88.66	93.62

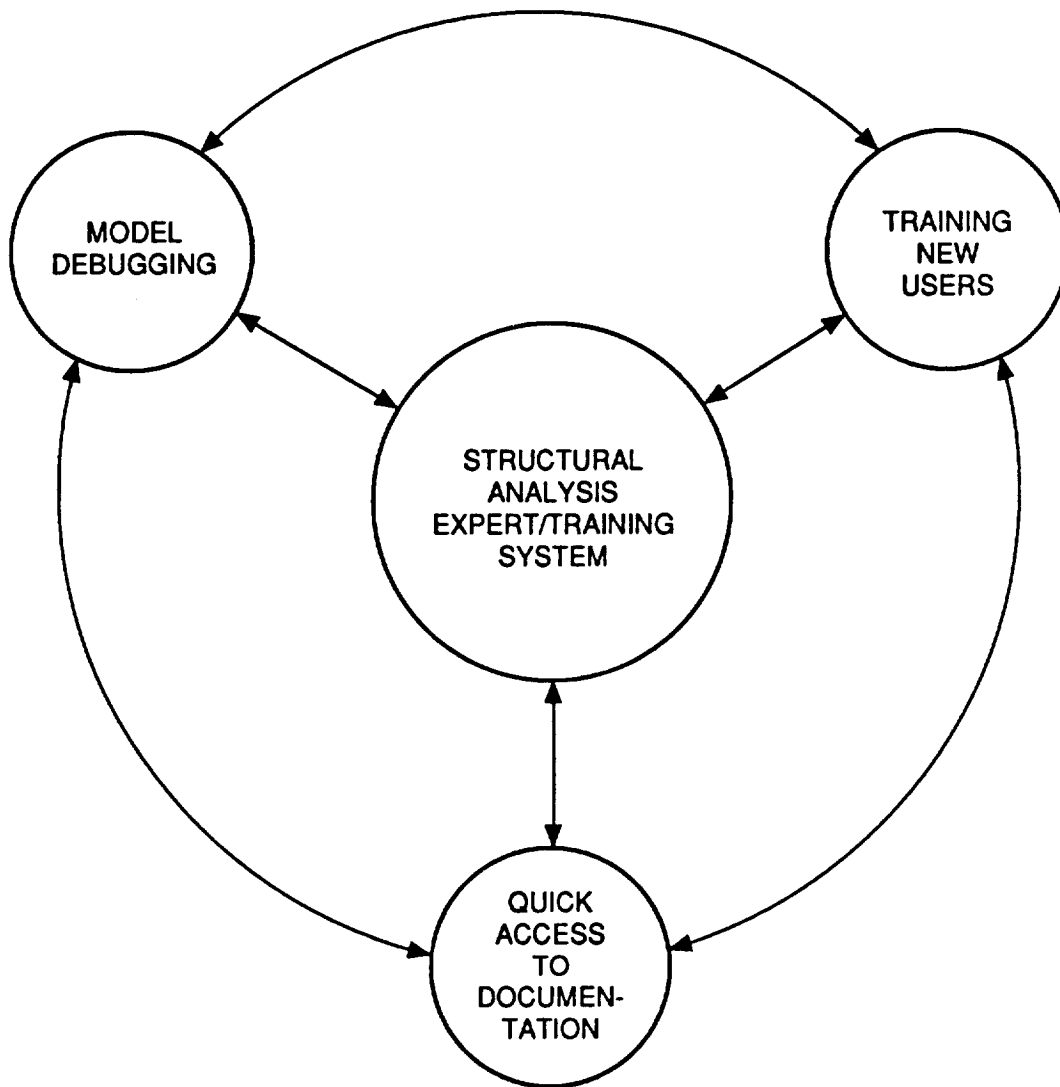


*Figure 1. Functional Expert Training System*

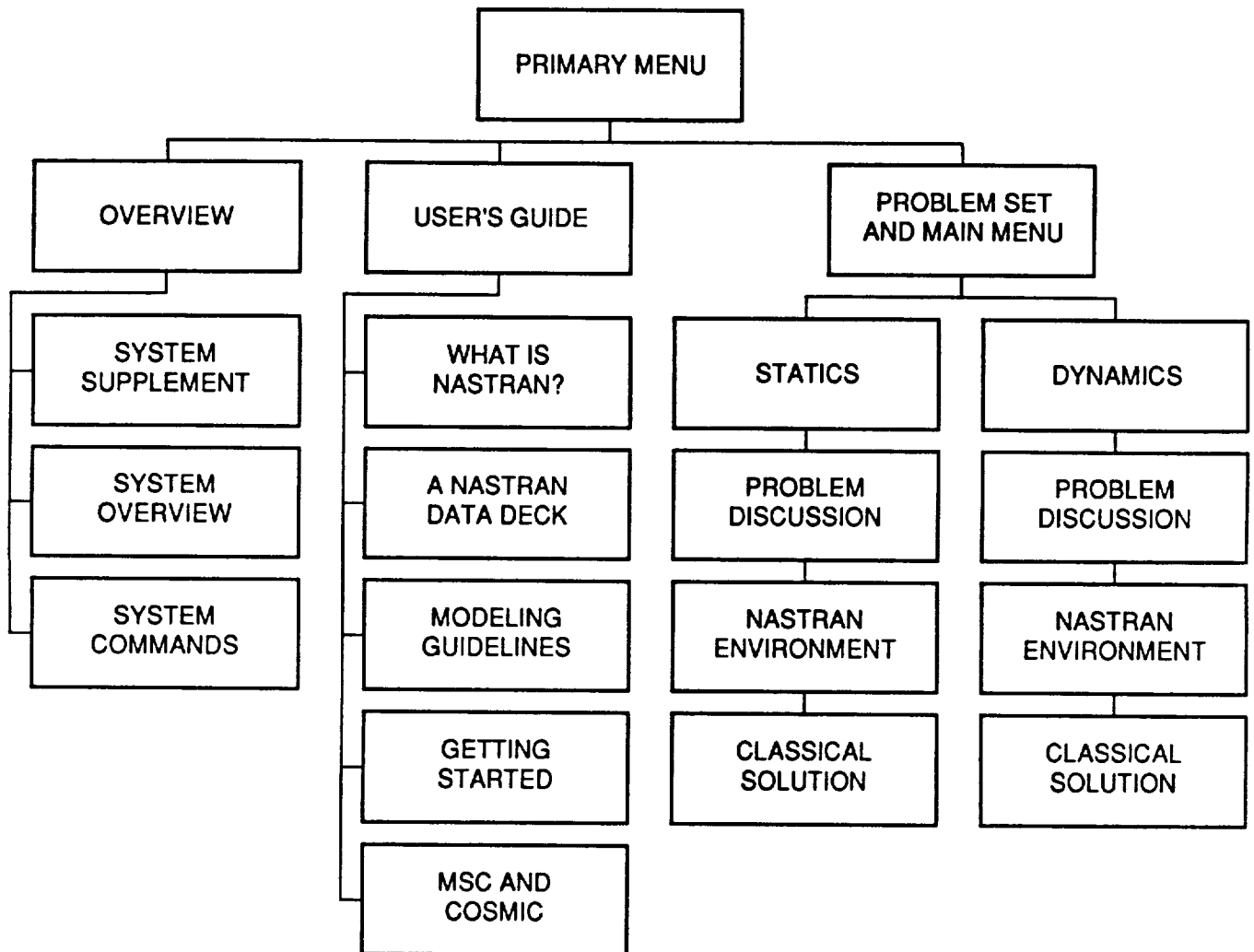


Figure 2. Organization of NASTRAN Trainer

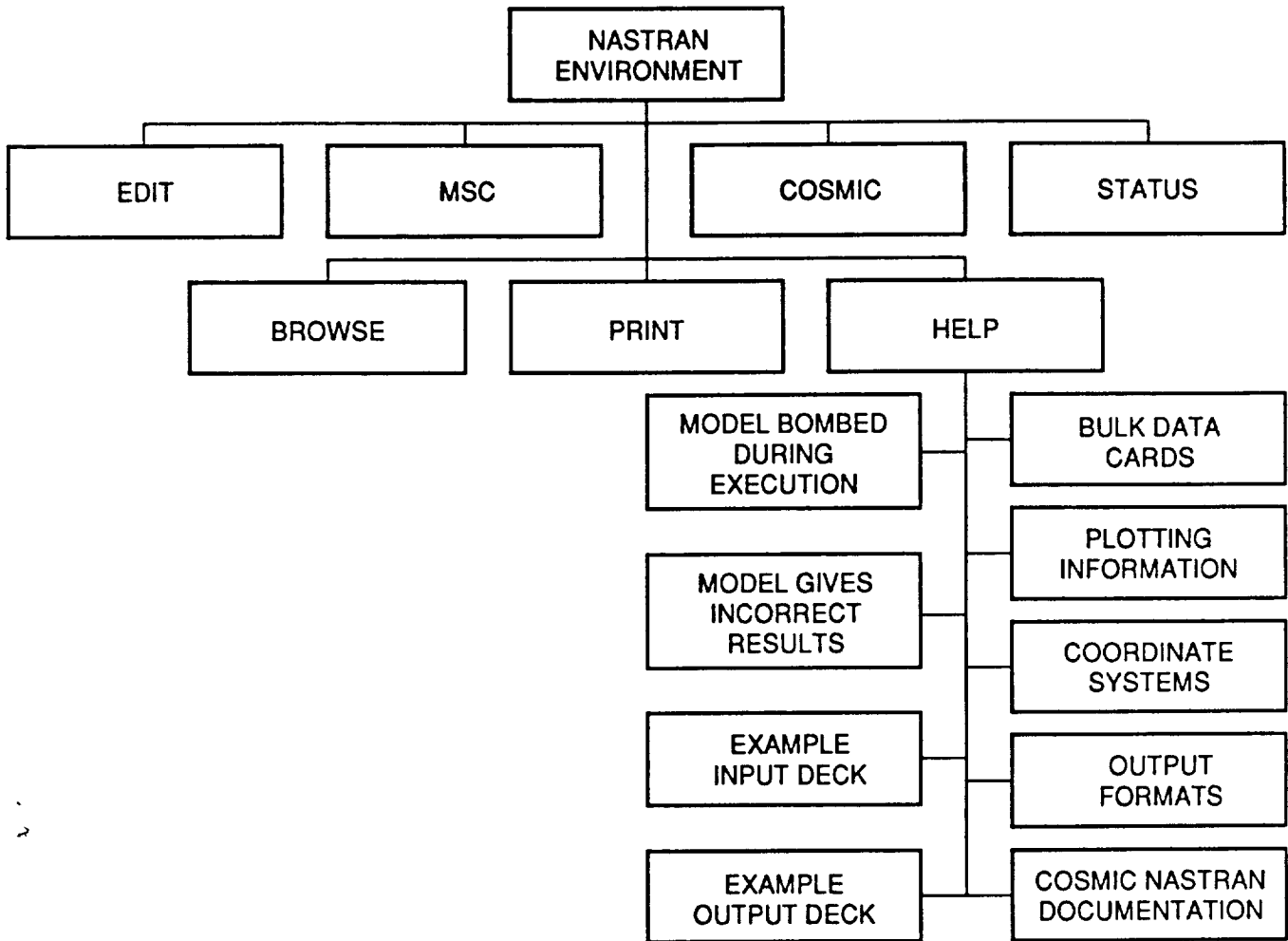


Figure 3. Organization of Program

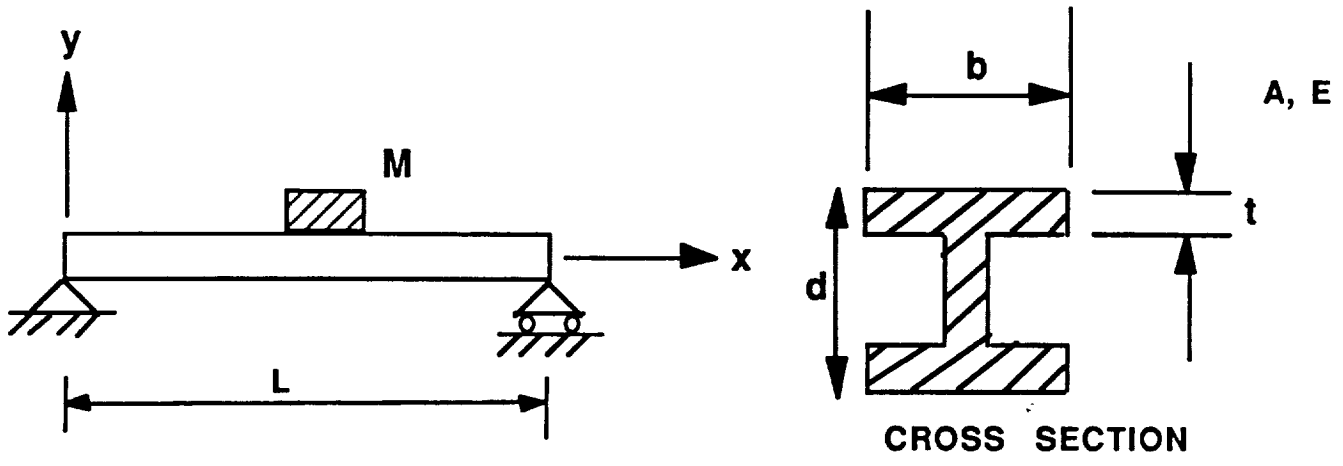


Figure 4. Simply Supported Beam with Concentrated Mass (Example 1)

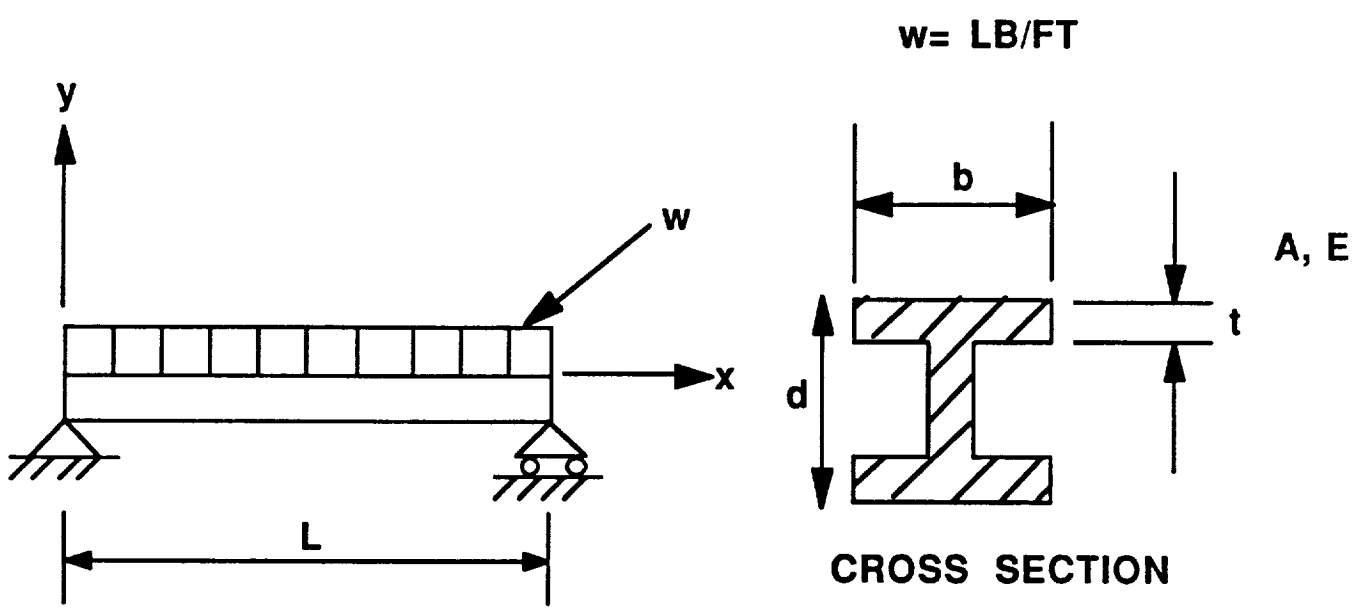


Figure 5. Simply Supported Beam with Uniformly Distributed Mass (Example 2)

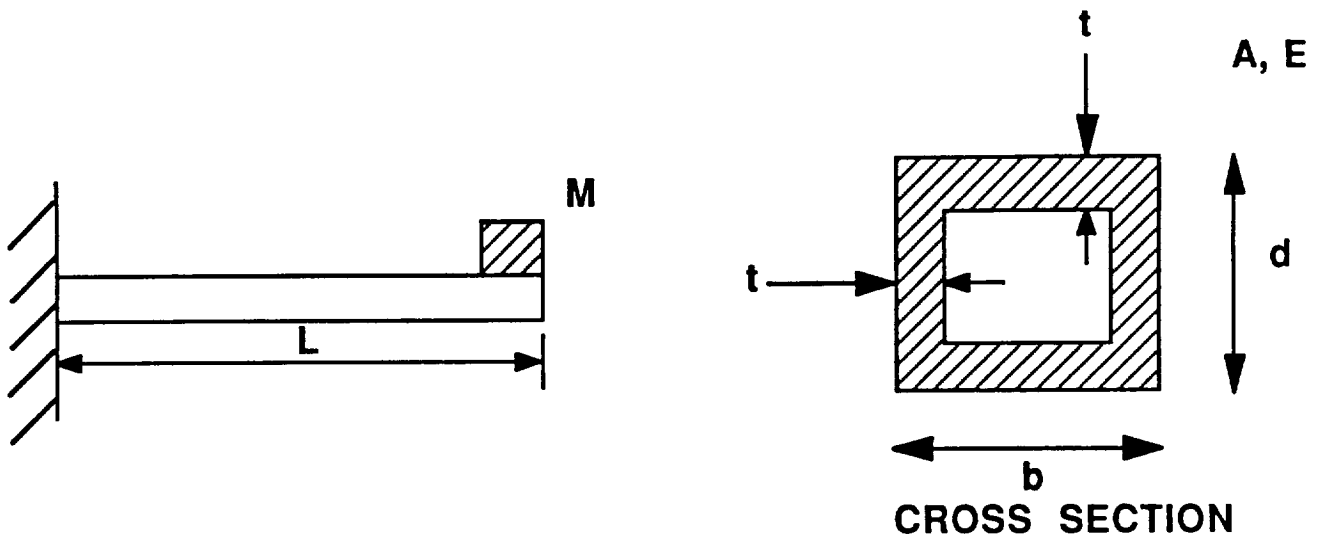


Figure 6. Cantilever Beam with Concentrated Mass (Example 3)

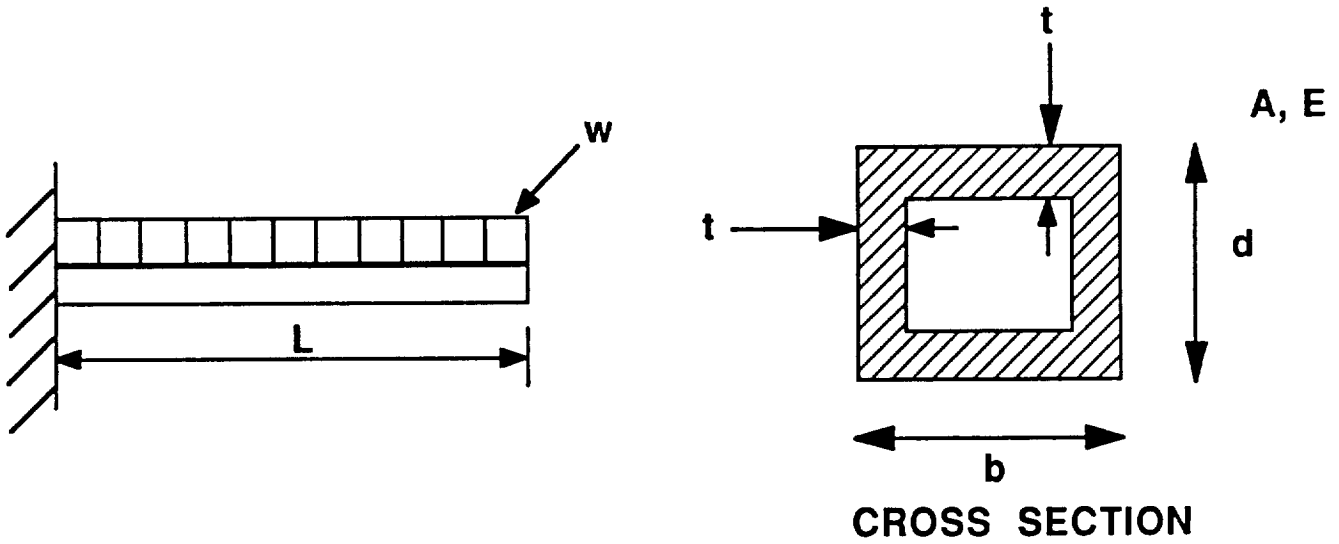


Figure 7. Cantilever Beam with Uniformly Distributed Mass (Example 4)

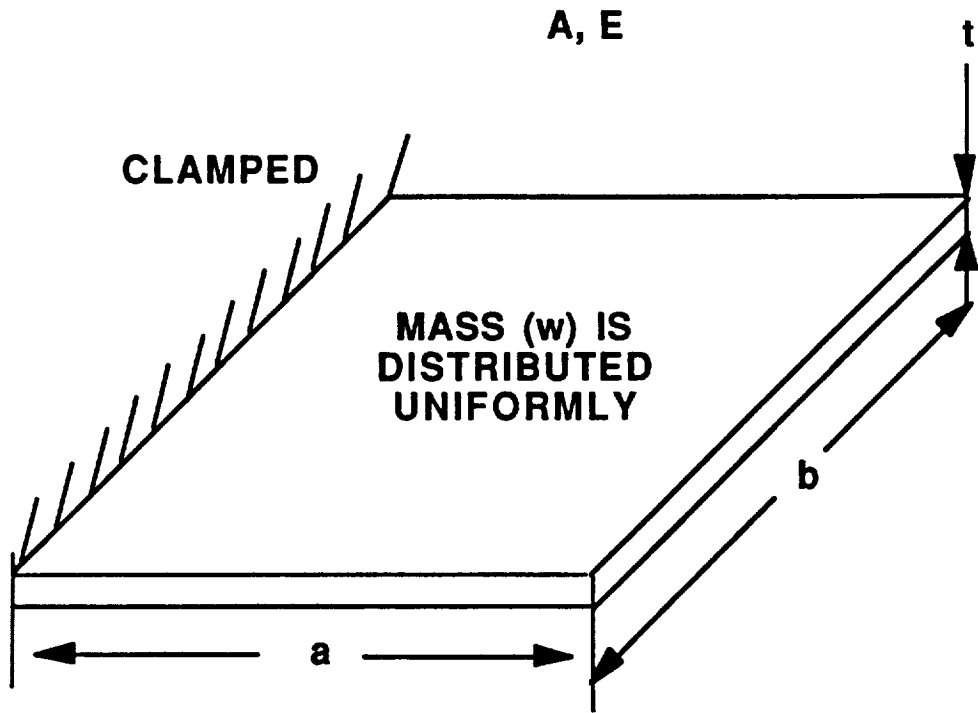


Figure 8. Rectangular Plated Clamped at One Edge (Example 5)

A, E

t = THICKNESS

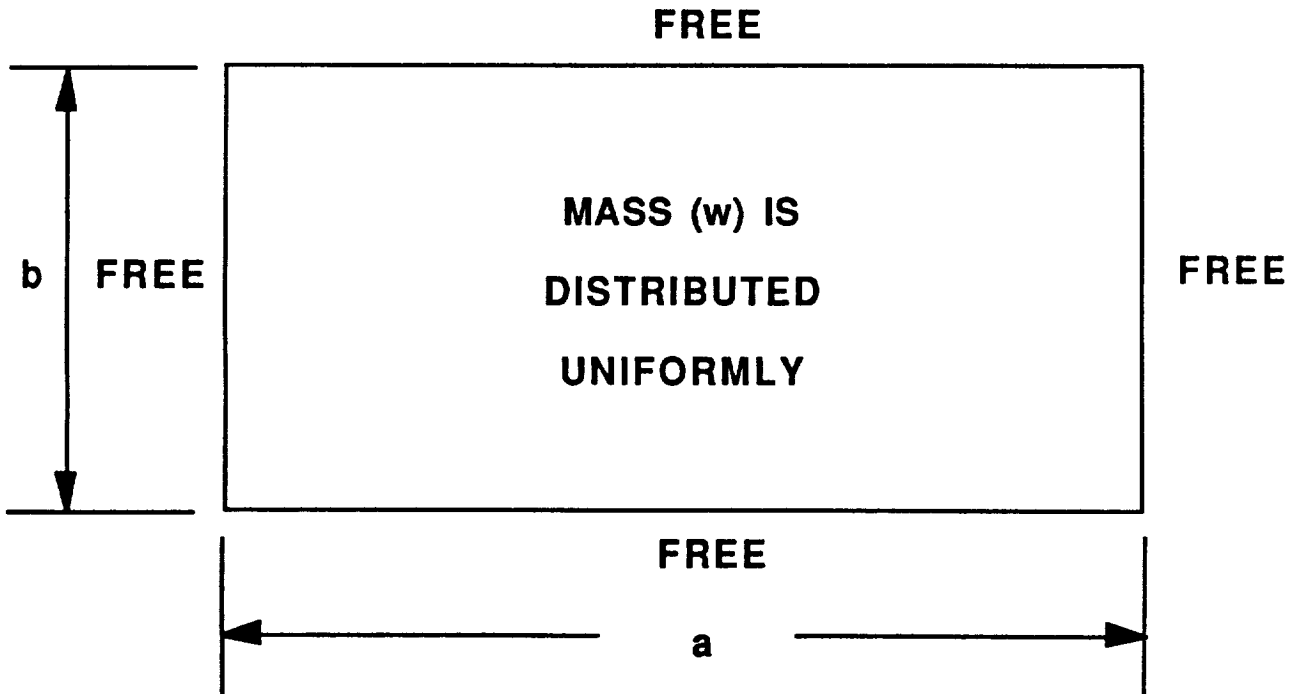


Figure 9. Rectangular Plate Free on All Sides (Example 6)

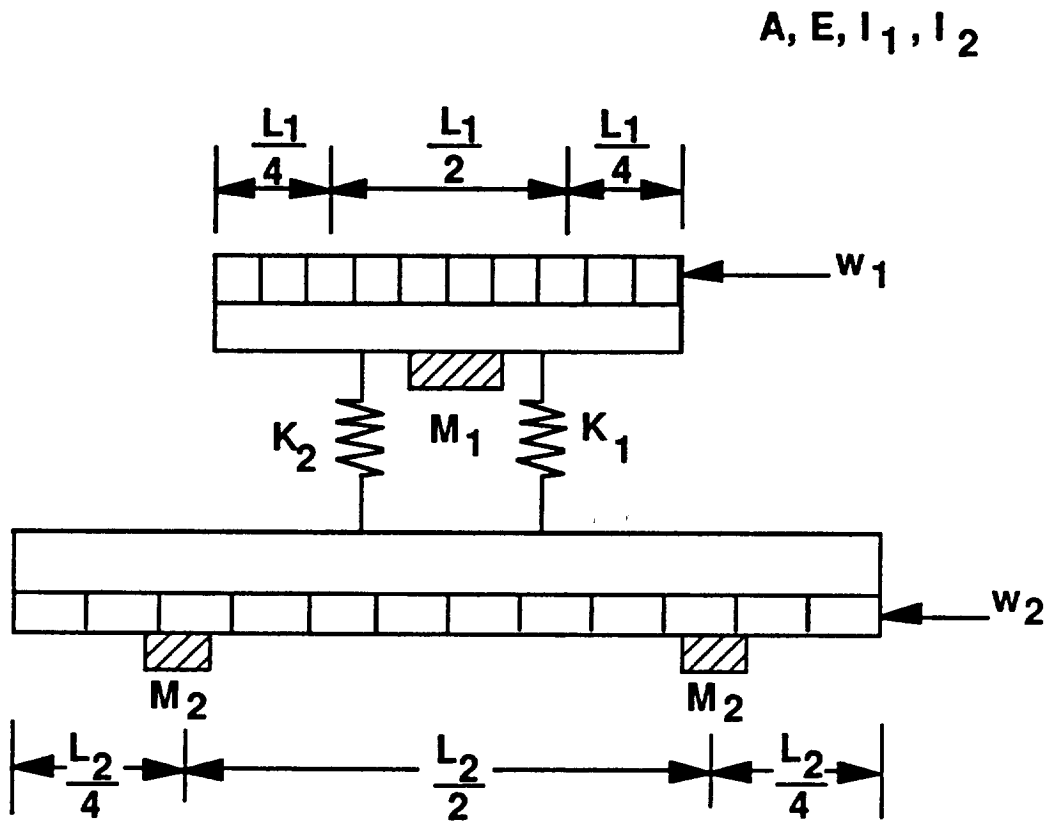


Figure 10. Two Beams Connected by Two Springs (Example 7)

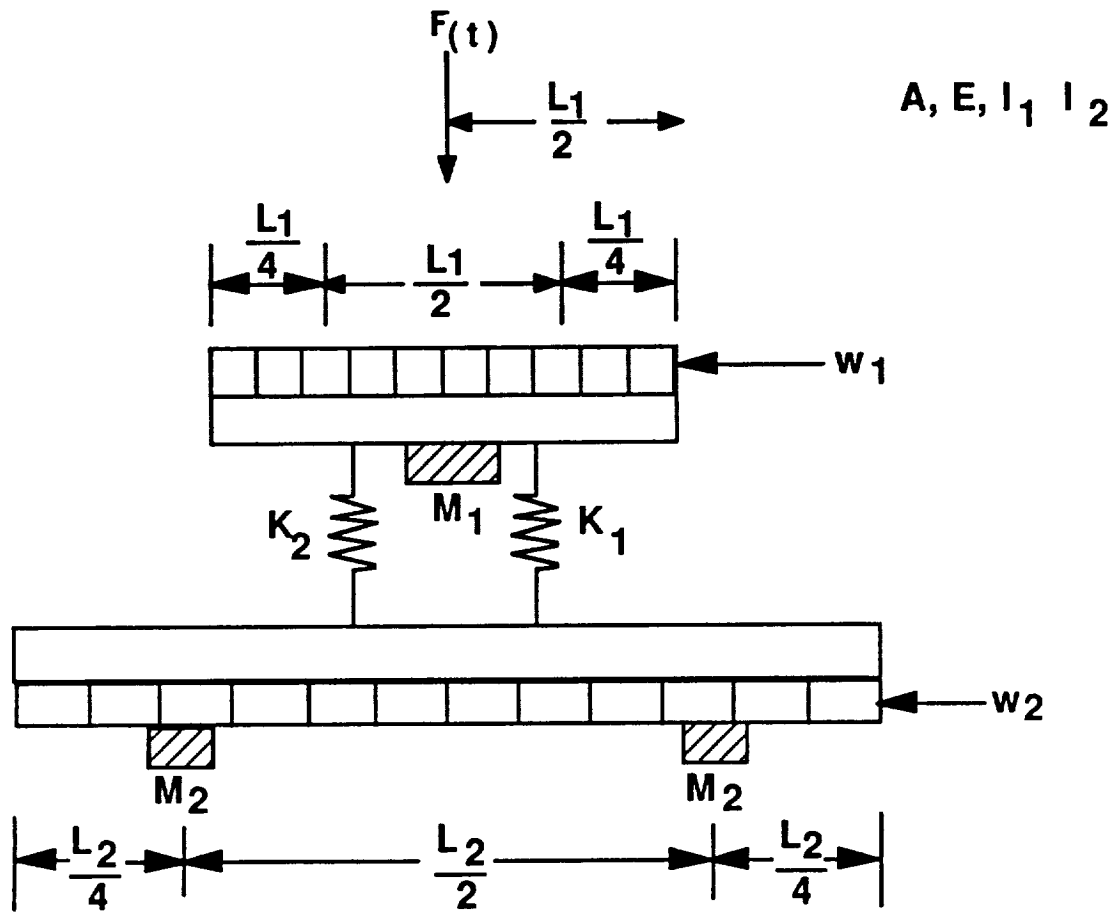


Figure 11. Two Beams Connected by Two Springs Driven by a Forcing Function (Example 8)

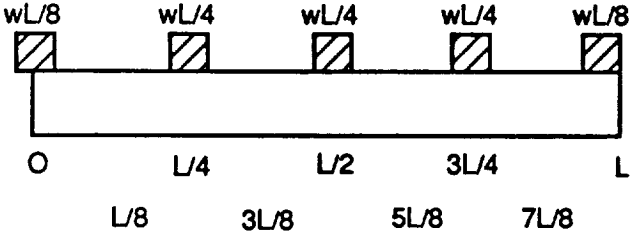
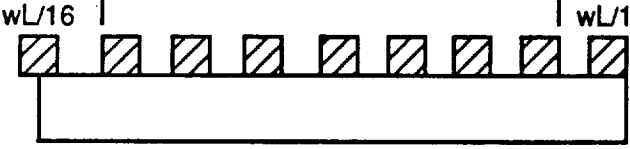
APPROACH		NO. OF ELEMENTS	NO. OF MASSES	DOFs IN EIGEN-SOLUTION
1	 <p>Diagram for Approach 1: A beam of length <math>L</math> is divided into four equal segments of length <math>L/4</math>. Five masses are placed at the ends and midpoints: <math>wL/8</math> at <math>0</math> and <math>L</math>, <math>wL/4</math> at <math>L/4</math> and <math>3L/4</math>, and <math>wL/4</math> at <math>L/2</math> and <math>5L/8</math>. The beam is divided into four elements of length <math>L/4</math> each.</p>	4	5	3
2	 <p>Diagram for Approach 2: A beam of length <math>L</math> is divided into eight equal segments of length <math>L/8</math> each. Nine masses are placed at the ends and midpoints: <math>wL/16</math> at <math>0</math> and <math>L</math>, and <math>wL/8</math> at <math>L/8</math>, <math>3L/8</math>, <math>5L/8</math>, and <math>7L/8</math>. The beam is divided into eight elements of length <math>L/8</math> each.</p>	8	9	7
3	<p>SAME AS APPROACH 2, EXCEPT SAME DOFs SAVED FOR EIGENSOLUTION AS APPROACH 1</p>	8	9	3

Figure 12. Three Approaches to Example 2

PCI - A PATRAN-NASTRAN MODEL TRANSLATOR

T.J. SHEERER

CP275167  
CHRYSLER TECHNOLOGIES AIRBORNE SYSTEMS, INC.

WACO, TX

INTRODUCTION

The existence of several derivative versions of NASTRAN, which differ significantly in element definitions and result formulation, has caused some difficulties in the interface between NASTRAN and pre- and post- processors such as PATRAN or SUPERTAB. In particular, the PATRAN-COSMIC/NASTRAN interface provided by PDA Engineering has not been updated at the same rate as the equivalent interface with MSC/NASTRAN, and has significantly less capabilities. Many model entities supported by both PATRAN and COSMIC/NASTRAN are not supported by the translator. The well-documented PATRAN neutral file, which is now supported by several other vendors, has provided a means for the user to create his own interface program for model translation, while it has also been possible to pass results from NASTRAN to PATRAN with a user-written program using OUTPUT2 statements and format information from the Patran Users' Manual. In recent years PDA engineering has provided as part of PATRAN a library of subroutines known as gateway utilities, which extract data directly from the PATRAN database file and which can be called from a FORTRAN program. As this eliminates the task of reading the neutral file the work of creating a translator can be produced by the user with little effort. This has been done with the object of producing a PATRAN-COSMIC NASTRAN model translator comparable in scope to the PATRAN-MSC/NASTRAN translator, but also allowing a greater degree of user control than is found therein. The different parts of the program were developed in several locations, as the counterpart to a results translator developed for Texas Instruments by Texas A and M University, which also emphasizes flexibility. Both these programs are public domain programs under the terms of the development agreement between Texas Instruments and Texas A.M.U., and enhancements developed at Chrysler have also been passed to T.A.M.U.

## PROGRAM STRUCTURE

PCI supports a range of elements comparable with PATNAS and significantly greater than PATCOS. The structure of the program is such that, in effect, it supports elements not currently extant. In the PATCOS program element types are hard-wired, and if a different NASTRAN card is required a text editor must be used to change the bulk data file. If, for example, the QUAD4 element is required in a model, all elements of this type must be edited from type QUAD2 to QUAD4, since PATCOS does not currently support the QUAD4. Similar difficulties arise with other elements. The PATNAS translator does support a wide range of elements identified by configuration codes, but the equivalence between elements and configuration code is controlled from within PATRAN, and the user can not translate to an element developed in-house, or a newly introduced element, or simply an element not supported by the translator. PCI uses a different approach by having a user text file of twenty NASTRAN element names for each element configuration. This file may be edited by the user to assign whatever correspondence he desires between configuration code and NASTRAN element type. Since most element cards in NASTRAN follow the same pattern of (NAME,PID/MID,NODES) it is not generally necessary to write a new subroutine when adding an element. Frequently the only parameter changed is field one of the NASTRAN data card, and this is controlled from a text file. Because NASTRAN and PATRAN use a different numbering sequence for higher elements it is convenient to use several subroutines to write NASTRAN elements, but frequently only one routine is required for each shape/node combination. All 3-node shells, for example, are written by the same routine. The PATRAN configuration field is used to select an element name from a range of twenty for each configuration of shape/nodes. The user-generated text file ETYPES.DAT contains these names for configurations 1 through 20. Any elements having the default configuration of zero in the PATRAN database are assigned the value 1 in the translator.

Table (1) shows the basic PATRAN element types supported by PCI and the NASTRAN elements obtainable from them. For comparison the elements supported by PATCOS and PATNAS are also shown. Note that, in general, failure by PCI to support elements listed for PATNAS is because they are not supported in COSMIC/NASTRAN. In practice, alteration of the text file of element configurations will allow support of these elements if and when they become available

TABLE 1: GEOMETRIC ELEMENT TRANSLATION  
CAPABILITIES OF PATCOS, PATNAS AND PCI

SHAPE/NODES	PATCOS	PATNAS	PCI
BAR/2	CBAR	CBAR CBEAM CROD	CBAR  CROD
TRIA/3	CTRIA2	CTRIA1 CTRIA2 CTRIA3  CTRIARG	CTRIA1 CTRIA2  CTRBSC CTRIARG CTRMEM CTRPLT
QUAD/4	CQUAD2	CQUAD1 CQUAD2 CQUAD4 CQDMEM1 CQDMEM2 CSHEAR  CTRAPARG	CQUAD1 CQUAD2 CQUAD4 CQDMEM1 CQDMEM2 CSHEAR CTWIST CQDPLT CQDMEM  CTRAPAX
TRIA/6	CTRIM6	CTRIA6 CTRIAX6	CTRIM6 CTRSHL CTRPLT1
QUAD/8	CIS2D8	CQUAD8	CIS2D8
HEX/8	CIHEX1	CHEXA CHEX8	CIHEX1 CHEXA1 CHEXA2
QUAD/20	CIHEX2	CHEXA CHEX8	CIHEX1 CHEXA1 CHEXA2
QUAD/32			CIHEX3

PCI also supports the SCALAR and damping elements CELAS2 and CDAMP2 by generating a scalar element for each degree of freedom specified in a PATRAN SPRING element. The concentrated mass element CONM2 is obtainable from the PATRAN MASS directive. MPCs and rigid elements are supported. Table (2) summarizes the support for these elements. Node translation with embedded SPCs is fully supported.

---

TABLE 2: SCALAR, DAMPER AND MASS ELEMENT SUPPORT

---

PATRAN DIRECTIVE	NATRAN CARD WRITTEN BY PCI
MPC	MPC
MPC,RRD	CRIGIDR
MPC,RBAR	CRIGD1
MPC,RBE1	CRBE1
MPC,RBE2	CRBE2
MPC,RBE3	CRBE3
BAR/2/n OR SPRING	CELAS2
BAR/2/n OR MASS	CONM2
BAR/2/n	CDAMP2

---

LOAD AND CONSTRAINT TRANSLATION:

PCI supports constraint (SPC), nodal force and pressure translation. FORCE and SPC cards are translated in an element-dependent manner as shown in Table (3). Only normal element pressures are supported. PCI will select the appropriate PLOAD card for the element type. In many circumstances involving higher order elements several PLOAD cards must be generated for a single PATRAN pressure load.

---

TABLE 3: PCI SUPPORT OF LOADS AND SPCS

---

NASTRAN CARD	USED IN ELEMENTS	SUPPORT
PLOAD4	CQUAD4	YES
PLOAD2	OTHER 1ST ORDER SHELL	YES
PLOAD3	ISOPARAMETRIC SOLID	NOT YET
PLOAD	2ND ORDER SHELL	YES

---

COORDINATE SYSTEMS:

The various PATRAN coordinate systems are translated to CORD2 cards in NASTRAN, as in the PATNAS translator. Additionally, PATRAN nodes, which are stored in the database in the basic coordinate system, have their locations output to NASTRAN in the local system associated with the nodes. This is of great importance if, for example, constraints are to be applied in a local system.

The PATRAN database includes, associated with each coordinate system, a 3x3 matrix T such that

$$[T] \begin{Bmatrix} x_1 \\ y_1 \\ z_1 \end{Bmatrix} = \begin{Bmatrix} x_b \\ y_b \\ z_b \end{Bmatrix}$$

where the suffixes l, b, denote local and basic coordinate systems respectively. The translator inverts the matrix to produce the matrix  $T^{-1}$  where

$$[T]^{-1} \begin{Bmatrix} x_b \\ y_b \\ z_b \end{Bmatrix} = \begin{Bmatrix} x_1 \\ y_1 \\ z_1 \end{Bmatrix}$$

and prints the local values to the NASTRAN data deck.

PROPERTY GENERATION:

It is generally no more difficult to enter property and material cards in NASTRAN than in PATRAN. For this reason property generation has not been implemented in PCI.

## CONCLUSIONS:

The amount of programming required to develop a PATRAN-NASTRAN translator was surprisingly small. The approach taken produced a highly flexible translator comparable with the PATNAS translator and superior to the PATCOS translator. The coding required varied from around ten lines for a shell element to around thirty for a bar element, and the time required to add a feature to the program is typically less than an hour. The use of a lookup table for element names makes the translator also applicable to other versions of NASTRAN. The saving in time as a result of using PDA's Gateway utilities was considerable.

During the writing of the program it became apparent that, with a somewhat more complex structure, it would be possible to extend the element data file to contain all data required to define the translation from PATRAN to NASTRAN by mapping of data between formats. Similar data files on property, material and grid formats would produce a completely universal translator from PATRAN to any FEA program, or indeed any CAE system.

32 21  
108

## A GENERIC INTERFACE BETWEEN COSMIC/NASTRAN AND PATRAN

Paul N. Roschke, Prakit Premthamkorn, and James C. Maxwell  
Texas A&M University

### SUMMARY

Despite its powerful analytical capabilities, COSMIC/NASTRAN lacks adequate post-processing adroitness. PATRAN<sup>1</sup>, on the other hand is widely accepted for its graphical capabilities. A nonproprietary, public domain code mnemonically titled CPI (for COSMIC/NASTRAN-PATRAN Interface) is designed to manipulate a large number of files rapidly and efficiently between the two parent codes. In addition to PATRAN's results file preparation, CPI also prepares PATRAN's P/PLOT data files for xy plotting. The user is prompted for necessary information during an interactive session. Current implementation supports NASTRAN's displacement approach including the following rigid formats: (1) static analysis, (2) normal modal analysis, (3) direct transient response, and (4) modal transient response. A wide variety of data blocks are also supported. Error trapping is given special consideration. A sample session with CPI illustrates its simplicity and ease of use.

### INTRODUCTION

#### Overview

The standard gateway that interfaces COSMIC/NASTRAN's analysis results to PATRAN's post-processing makes use of NASTRAN's FORTRAN-written results files. These files can be requested via DMAP ALTER's OUTPUT2 statement in NASTRAN's executive data deck. They contain data in mixed ASCII and binary code format. However, they can not be used as direct input to PATRAN. Similarly, PATRAN also supports communications with external codes via specially formatted results files. Format of these files is predetermined according to PATRAN and differs for each data type. Generally, they can be categorized into three groups according to their formats: (1) nodal results files, (2) element results files, and (3) beam results files. The number of results files can be as many as required. Therefore, in order to interface COSMIC/NASTRAN to PATRAN for post-processing purposes, an interface that is capable of translating from NASTRAN's analysis results to PATRAN-recognizable files is required.

Fig. 1 shows code and file relationships among the analysis and post-processing modules. The flow begins with the input of NASTRAN's analysis data deck. DMAP ALTER statements must be included in the executive control deck in order to obtain a FORTRAN-written results file. Generally, this file is assigned an extension of .PAT. This NASTRAN results file is then translated by the COSMIC/NASTRAN-PATRAN Interface (CPI). Output from CPI is a group of PATRAN-compatible results files and/or a P/PLOT-compatible data file. These files are ready for PATRAN post-processing.

---

<sup>1</sup> PATRAN is a trademark of PDA Engineering

PATRAN also requires access to a neutral file containing geometrical properties of the model. This file can be obtained via the COSPAT<sup>2</sup> translator, but not by means of CPI.

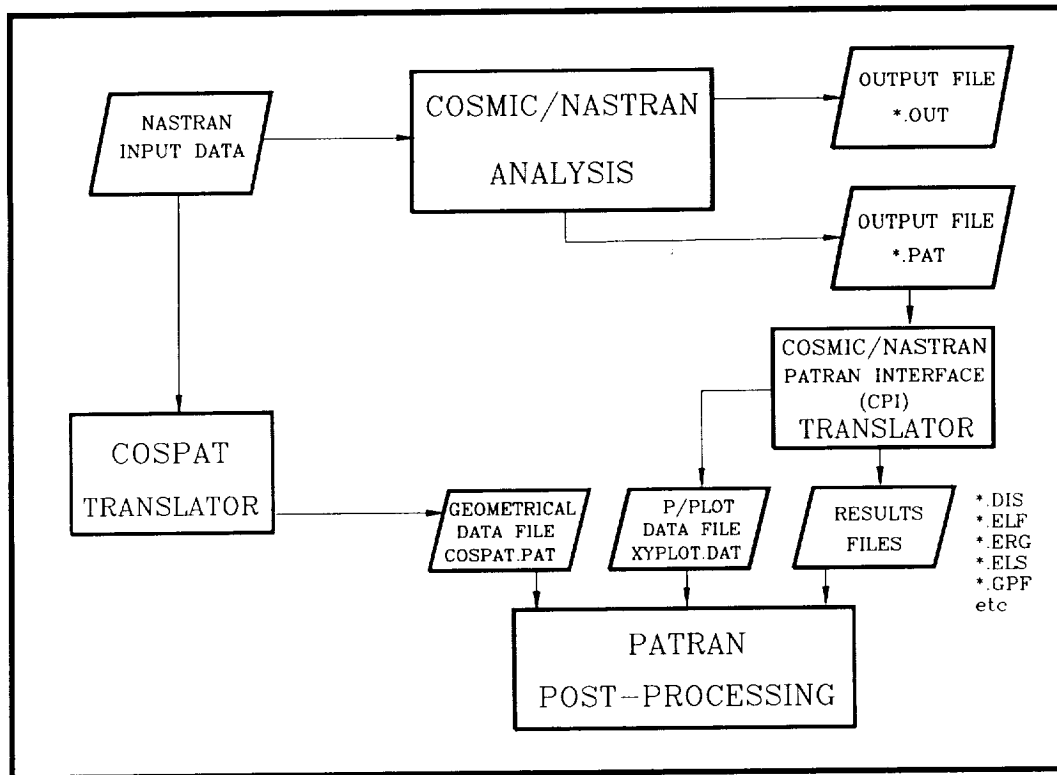


Fig. 1 Code and File Relationships

### Program Description

COSMIC/NASTRAN-PATRAN Interface (CPI) translates COSMIC/NASTRAN's FORTRAN-written results files to PATRAN compatible results files. These results files can be requested via the OUTPUT2 instruction in the executive control deck. CPI provides the operation in two modes:

**Mode 1 - Whole Model Translation:** CPI translates all data blocks contained in the NASTRAN results file (\*.PAT) and creates PATRAN compatible results files corresponding to data blocks found in the input data file. The user is prompted for the prefix name of an output file. Different prefixes allow the user to distinguish between groups of output files when many results files are translated in a single execution. Up to 6 characters per prefix is acceptable. Created output files and translated data blocks are summarized on the screen during CPI's execution.

**Mode 2 - XY-Plot Data Preparation:** CPI creates data for the specified node or element from a set of data blocks. CPI prompts the user for necessary information, i.e. node number and component number for nodal data, and searches the input file for any data on

<sup>2</sup> COSPAT is a COSMIC/NASTRAN to PATRAN interface, developed by COSMIC, University of Georgia, Athens, Georgia.

this node. Each data set is written to PATRAN's P/PLOT compatible data file. CPI names this file XYPLOT.DAT. When this command is selected, CPI automatically reviews the data blocks available in the current input file. The user is then prompted to enter the number corresponding to the data block name shown above this prompt.

Currently, CPI supports NASTRAN's displacement approach including, but not limited to, the following rigid formats:

- (1) Static Analysis (Rigid Format 1)
- (2) Normal Modal Analysis (Rigid Format 3)
- (3) Direct Transient Response (Rigid Format 9)
- (4) Modal Transient Response (Rigid Format 12)

Table 1 shows data blocks supported by CPI. It should be noted that CPI supports any rigid format as long as the data blocks listed are encountered. Rigid formats named above are only a guide to the rigid formats most frequently giving rise to these data blocks. CPI recognizes data blocks, not rigid formats. Table 2 shows elements currently supported by CPI.

**Table 1. Data Blocks Supported by CPI**

Data Block	Content
OUGV1	Nodal Displacements
HOUGV1	Nodal Temperature
OQG1	Single Point Constraint
OPG1	Load Vectors
OPHIG	Eigenvectors
OUPV1	Displacement Vectors
ONRGY1	Strain Energy
OES1(X)	Element Stress
OEF1	Element Forces
OGPFB1	Grid Point Balance Forces

**Table 2. Elements Supported by CPI**

Element Name	ID Number	Element Name	ID Number
CROD	1	CQDPLT	15
CQDMEM2	63	CBEAM	2
CTRIA2	17	CTUBE	3
CQUAD2	18	CTRIA1	6
CQUAD1	19	CTRBSC	7
CBAR	34	CTRPLT	8
CTRIARG	36	CTRMEM	9
CTRAPRG	37	CONROD	10
CQDMEM1	62	CTETRA	39
CWEDGE	40	CHEXA1	41
CHEXA2	42	CIHEX1	65
CIHEX2	66	CIHEX3	67

## PROGRAM USAGE AND SAMPLE SESSION

COSMIC/NASTRAN-PATRAN INTERFACE (CPI) is an interactive program. A user can manipulate the program by selecting from menu commands and answering questions. No special commands are needed. CPI also provides extensive error trapping to ensure appropriate input and output.

The following sample session (adapted from Ref. 5) illustrates execution of CPI for transient dynamic analysis results in which a series of time steps is involved. A simple three node model which is 350 cm. high, and has a cross sectional area of  $6.45 \text{ cm}^2$  (see Fig. 2), is used to model a rocket trajectory. Time versus loading of the rocket is shown in Fig. 3.

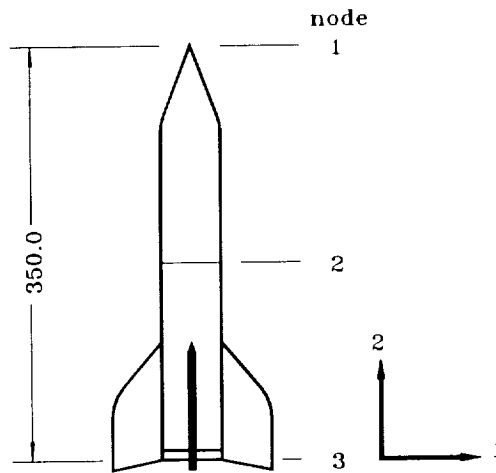


**Fig. 2 Sample 2 - Geometric Properties**

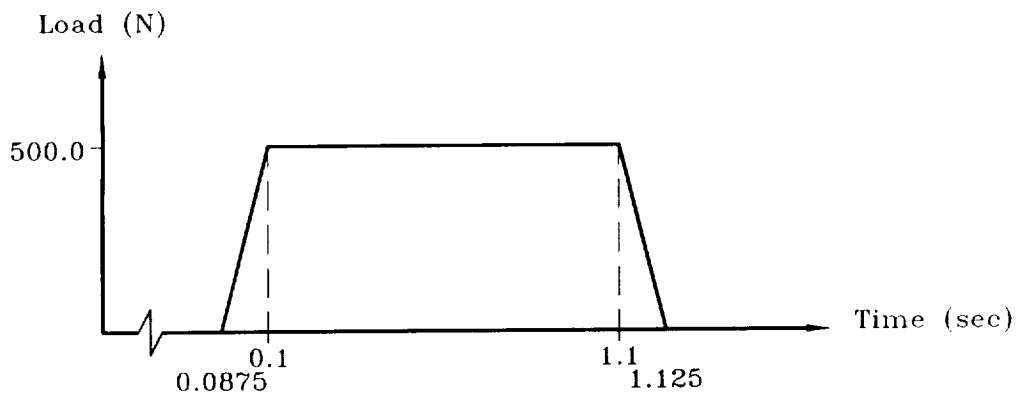


**Fig. 3 Sample 2 - Load vs. Time**

After invocation, CPI's opening header appears on the screen and CPI prompts the user for the name of the NASTRAN results file to be translated. The user then enters the NASTRAN results file name with its extension. Alternatively, the user can leave the translator and return to the operating system by entering "EXIT" (or "exit" or "E" or simply "e"). Here, the NASTRAN results file name is assigned the name "ROCKET.PAT."

```

*****
**
**          COSMIC/NASTRAN - PATRAN INTERFACE          **
**
**                ** C P I **                **
**
**          TEXAS A&M UNIVERSITY          **
**                &                **
**          TEXAS INSTRUMENTS          **
**
**                (JUNE 1989)                **
**
*****

```

```

ENTER NASTRAN RESULTS FILE NAME OR "EXIT"
>ROCKET.PAT

```

Once the results file has been named, CPI reads the results file header and echoes it to the screen for verification. Next a menu and a prompt for selection appear on the screen. The response to CPI should be one of the following:

- > 1 Select 1 to translate the entire file and create appropriate PATRAN-compatible results files.
- > 2 Select 2 to translate the data and create PATRAN's P/PLOT-compatible data files which contain requested nodal or element data.
- > 3 Select 3 to specify a new NASTRAN results file.
- > 4 Select 4 to exit CPI and return to the operating system.

If the first option is chosen, translation proceeds as follows:

```

DATE : 7/27/89
HEADER: NASTRAN FORT TAPE ID CODE -
LABEL : XXXXXXXX

```

```

-----
>>>>> ENTER YOUR SELECTION <<<<<<
-----

```

- 1) WHOLE MODEL TRANSLATOR
- 2) XY-PLOT DATA
- 3) ENTER NEW RESULTS FILE
- 4) EXIT

```

> 1
ENTER FILENAME PREFIX (UP TO 6 CHARACTERS) OR [RETURN]
(EXAMPLE DEFAULT FORMAT: S_I_.DIS)
> ROCKET
IS "ROCKET" THE CORRECT PREFIX? [Y]
><RETURN>

```

----- FILE CREATED -----	----- FROM DATA BLOCK -----
ROCKETS01I1.DIS	OUPV1
ROCKETS01I2.DIS	OUPV1
ROCKETS01I3.DIS	OUPV1
"	"
"	"
"	"
ROCKETS01I50.DIS	OUPV1
ROCKETS01I51.DIS	OUPV1
-----	-----

-----  
>>>>>> ENTER YOUR SELECTION <<<<<<<<  
-----

- 1) WHOLE MODEL TRANSLATOR
- 2) XY-PLOT DATA
- 3) ENTER NEW RESULTS FILE
- 4) EXIT

>

At this point the entire model is translated with the creation of the 51 files shown on the screen during execution. Each file corresponds to a new time step and a new geometric location of the rocket. It is apparent that running each file with PATRAN to obtain specific data for a given node and component can become tedious. Therefore, a routine has been incorporated into CPI to allow the user to create a file that contains only user-specified data available for plotting with P/PLOT.

When the second option is chosen, CPI reviews data block names existing in the current results file. The user is asked to select a data block name. CPI classifies data blocks into two groups: (1) nodal data, and (2) element data. If the selected data block contains nodal data, CPI prompts for a node number and a component number (1-6). In general, the six components of nodal data are:

- Component 1: X-direction translation vector
- Component 2: Y-direction translation vector
- Component 3: Z-direction translation vector
- Component 4: X-direction rotational vector
- Component 5: Y-direction rotational vector
- Component 6: Z-direction rotational vector

If the selected data block is an element data block, the user is prompted for an element number and a column number.

Next, CPI searches for the requested data and, upon completion of gathering the data, requests a data header extension of the current XY-plot data. Up to 38 characters is acceptable. Execution proceeds as follows:

```

-----
>>>>>> ENTER YOUR SELECTION <<<<<<<
-----

      1) WHOLE MODEL TRANSLATOR
      2) XY-PLOT DATA
      3) ENTER NEW RESULTS FILE
      4) EXIT
> 2
-----
                DATA BLOCK REVIEW
-----

                        1) OUPV1
-----

ENTER DESIRED BLOCKNAME NUMBER
(OR "0" TO EXIT)
> 1
ENTER NODE NUMBER
> 2
WHICH COMPONENT (1-6)?
> 2
ENTER PLOT TITLE EXTENSION FOR DATA SET: 1
DEFAULT TITLE: YDATA, DATA SET: 1; NODE: 2; COMPONENT:
2-
> Y-TRAJECTORY OF ROCKET
    %%% NUMBER OF DATA WRITTEN = 51 %%%
-----
                DATA BLOCK REVIEW
-----

                        1) OUPV1
-----

ENTER DESIRED BLOCKNAME NUMBER
(OR "0" TO EXIT)
> 0
-----
>>>>>> ENTER YOUR SELECTION <<<<<<<
-----

      1) WHOLE MODEL TRANSLATOR
      2) XY-PLOT DATA
      3) ENTER NEW RESULTS FILE
      4) EXIT
> 4
CPI Execution Completed

```

At this point a file called XYPLOT.DAT exists and upon input of this file into P/PLOT, data is readily graphed for the Y coordinates (component 2) of node 2 of the rocket for each of the 51 time steps (Fig. 4).

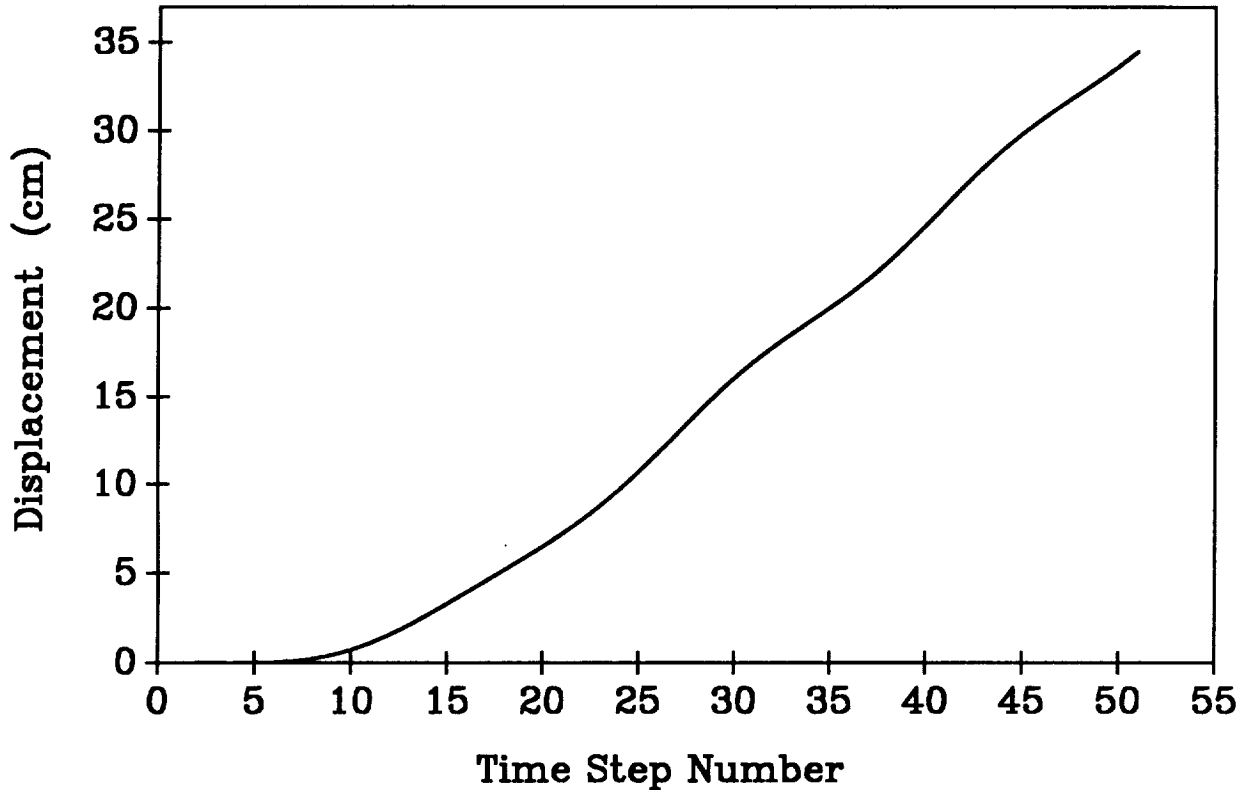


**Fig. 4 Displacement of Node 2 - Component 2**

## **OUTPUT FILES**

### **Results Translation**

CPI creates several results files which provide a direct avenue between COSMIC/NASTRAN's analysis algorithms and PATRAN's post-processing capabilities. COSMIC/NASTRAN's input file (commonly called the input data deck) provides the name of a binary file which CPI interpolates. For example, EXAMPLE.NAS (the input data deck) yields EXAMPLE.PAT (the binary file to be translated to PATRAN-compatible results files). Creation of the binary file is accomplished by inclusion of the appropriate ALTER statement in the executive control deck of COSMIC/NASTRAN's input data deck. Only filename extensions are changed by execution of COSMIC/NASTRAN. EXAMPLE.PAT is then translated by CPI into appropriate PATRAN-compatible results files. A description of each file follows.

All CPI output files are given the name 'XiiInnn.EXT' where X is either an 'S' or an 'M' depending on whether the following two digit number is either a subcase or a mode number, respectively, and EXT is the file extension named with respect to data type.

## XY-Plot

Selecting "XY-PLOT DATA" at CPI's main menu initiates a prompt screen which lists the various data blocks found in COSMIC/NASTRAN's binary output file. CPI then invites the user to specify desired data blocks containing either nodal or element data that are to be written to XYPLOT.DAT, which is the input file for P/PLOT. This file can contain one or more data sets depending on how many times the user requests that CPI write to this file. CPI writes only y-data to XYPLOT.DAT since the user defines an initial x and delta-x when executing P/PLOT. A description of XYPLOT.DAT's format is given below.

### (1) Nodal Data Blocks

The first line written for each data block contains the default title:

```
"YDATA, DATA SET: iii; NODE nnnn; COMPONENT j - "
```

and may be appended to allow for more descriptive titles. This appendage plus the default title must not exceed 80 characters. If more than 80 characters are specified, those beyond column 80 are truncated. This allows the user a suffix of anywhere from 33 to 38 characters depending on the number of digits contained in the default title.

Each line thereafter, until either a ^Z (end of file) or another title is encountered, contains nodal data for components 1, 2, 3, 4, 5, or 6, i.e., X, Y, Z,  $\theta_x$ ,  $\theta_y$ , or  $\theta_z$ , respectively, as requested from CPI's prompting.

### (2) Element Data Blocks

As with nodal data blocks, the first line written for an element data block contains a default title and takes the form:

```
"YDATA, DATA SET: iii; ELEMENT nnnn; COLUMN j - "
```

It may also be appended as described above, but again, the default title plus the appendage must not exceed 80 characters in length or truncation of characters beyond column 80 occurs. As with the nodal data case, a suffix of 33 to 38 characters is allowed.

The remaining lines associated with the current data set contain element data available for plotting. The data type is chosen by entry of a column number at CPI's prompt.

## SOFTWARE AND HARDWARE REQUIREMENTS

CPI source code was written in standard FORTRAN 77; however, some special features of VAX/VMS FORTRAN were implemented. CPI will run on any VAX machine with a VMS operating system and a FORTRAN compiler. The total length of the source code is approximately 1200 lines, which requires 104 blocks of disk space.

## REFERENCES

- (1) *NASTRAN User's Manual*, Computing Services Annex, University of Georgia, Athens, Georgia, 1986.
- (2) *NASTRAN Programmer's Manual*, Computing Services Annex, University of Georgia, Athens, Georgia, 1978.
- (3) *PATRAN Plus User Manual*, Release 2.3, PDA Engineering, Costa Mesa, California, 1988.
- (4) Schaeffer, G. H., *MSC/NASTRAN Primer*, Schaeffer Analysis Inc., Mont Vernon, New Hampshire, 1979.
- (5) *MSC/NASTRAN Demonstration Problem Manual*, The Macneal-Schwendler Corporation, Los Angeles, California, 1983.
- (6) Nyhoff, L., Leestina, S., *FORTRAN 77 for Engineers and Scientists*, Macmillan Publishing Company, New York, 1988.

## ACCURACY OF THE QUAD4 THICK SHELL ELEMENT

William. R. Case, Tiffany. D. Bowles, Alicia K. Croft\*  
and Mark. A. McGinnis  
NASA/Goddard Space Flight Center

## SUMMARY

The accuracy of the relatively new QUAD4 thick shell element is assessed via comparison with a theoretical solution for thick homogeneous and honeycomb flat simply supported plates under the action of a uniform pressure load. The theoretical thick plate solution is based on the theory developed by Reissner and includes the effects of transverse shear flexibility which are not included in the thin plate solutions based on Kirchoff plate theory. In addition, the QUAD4 is assessed using a set of finite element test problems developed by the MacNeal-Swendler Corp. (MSC). Comparison of the COSMIC QUAD4 element as well as those from MSC and Universal Analytics, Inc. (UAI) for these test problems is presented. The current COSMIC QUAD4 element is shown to have excellent comparison with both the theoretical solutions and also those from the two commercial versions of NASTRAN that it was compared to.

## INTRODUCTION

The QUAD4 thick shell element, added to NASTRAN in 1987, is one of the most important additions to the program since the original writing of the code. The deficiencies of the original QUAD1 and QUAD2 quadrilateral shell elements have been recognized for years and have been reported in the literature. At the Goddard Space Flight Center (GSFC), the quadrilateral shell element is in use in virtually all structural analyses of our spacecraft and related hardware. Typical applications are for the modelling of cylindrical shells and flat plates made of honeycomb or machined, lightweighted, metal that make up the structure of spacecraft and scientific instruments. In some cases these models require that the effects of transverse shear flexibility be included due to their thickness. The QUAD4 element includes these effects and, in addition, has an improved isoparametric membrane capability for in-plane loading.

The purpose of the study reported herein is to assess the accuracy of the QUAD4 element in modelling a variety of situations involving both solid cross-section plates as well as those constructed of honeycomb. Three goals of the study were to determine:

- a) what is the rate of convergence to the theoretical solution as the mesh is refined;

\* Currently with Swales and Associates, Inc.

- b) whether the element exhibits sensitivity to aspect ratios significantly different than 1.0;
- c) how the element behaves in a wide variety of modelling situations, such as those included in the MSC element test library (discussed below).

The first two questions were addressed in the same manner as several other studies reported by one of the authors in prior NASTRAN colloquia (references 1 and 2). The procedure used in those studies, and followed here also, is to isolate the effects of mesh refinement and aspect ratio. That is, the mesh refinement study is done using elements with an aspect ratio of 1.0. Then, once a fine enough mesh has been reached such that the errors are small, the effects of aspect ratio can be investigated by keeping the mesh the same (i.e. same number of elements) and varying the overall dimensions of the problem, thus resulting in each element aspect ratio changing. Obviously, in order to accomplish this latter step there must be a theoretical solution (or some other equally acceptable comparison solution) to the problem with which to compare the finite element model results. This is needed since, at each step, a problem of different dimensions (and therefore different theoretical solution) is being modelled.

The above tests are important in that they show the rate of convergence toward the theoretical solution as the mesh is refined. Those tests, however, are not sufficient to completely test the accuracy of a finite element since they do not test irregular geometries, or a variety of loadings or material properties. The MSC has developed a comprehensive set of problems for testing finite elements in a variety of situations (reference 3). The library of problems consists of 15 test problems for the QUAD4 element that cover all of the parameters mentioned above. A test of the COSMIC QUAD4 using these elements was reported at the 17th NASTRAN Users Colloquium in 1987 by Victoria Tischler of the Air Force Wright Aeronautical Laboratories (AFSC) at Wright Patterson Air Force Base, Ohio, but was not included in the formal proceedings. Due to the fact that it was not included in the formal proceedings, and also due to the fact that errors in the QUAD4 code for nonhomogeneous plates (to be discussed later) have been corrected, the results of our testing of the latest version of the element with the MSC library are include herein.

#### RESULTS OF MESH AND ASPECT RATIO STUDY

For the mesh and aspect ratio study a theoretical comparison solution is highly desirable. Since the effects of transverse shear flexibility are included in the QUAD4 element formulation, a theoretical solution for moderately thick plates, based on Reissner (or Mindlin) thick plate theory is also desirable. Such a solution is given in references 4 and 5 for rectangular simply supported thick plates under the action of a pressure load. Thus, this problem was used for the mesh and aspect ratio portions of the

study. Figure 1 defines the geometry, coordinate system, boundary conditions and loading for the rectangular plate. The thickness indicates a moderately thick plate of length to thickness ratio of .20. The effect of transverse shear flexibility is only approximately 1% on the maximum displacement but is important in discerning the quality of the convergence of the finite element results to the exact theoretical solution. By exact is meant the theoretical basis for the QUAD4 element, which is expressed in the Reissner thick plate theory. Figure 2 shows the finite element mesh geometry used in the mesh and aspect ratio studies. Due to symmetry only one quarter of the plate was modelled. The 4 x 4 mesh shown on figure 2 is an example only; the mesh was varied during the mesh study.

Figures 3a - 3c show characteristics of the theoretical solution. As indicated in figure 3a the central displacement solution is represented as an infinite series of hyperbolic functions. A FORTRAN computer program was written to compute the theoretical solutions for displacements (using the series shown) as well as stresses (solution not shown). As  $m$  gets large, where  $m$  is the number of terms included in the series, the hyperbolic functions tend to overflow the exponent range of the computer. This does not indicate a problem with the series shown, as the hyperbolic functions appear in both the numerator and denominator and their ratio is numerically stable. However, in separately evaluating the numerator and denominator the overflow problem was encountered. In order to circumvent this problem, the hyperbolic functions were rewritten in terms of exponentials allowing the programmed equations, in terms of ratios of numerator and denominator terms, to be evaluated without overflow problems.

Figures 3b and 3c show the stiffness parameters needed in the theoretical solution for the homogeneous (i.e. solid) plate and the honeycomb plate. For the honeycomb plate, two different core stiffnesses were investigated. The stiffer one is representative of aluminum honeycomb construction that has been used at the GSFC. The more flexible one was chosen because it represents a core flexibility that is quite low and was expected to be a more critical test of the QUAD4's shear flexibility formulation.

The results of the mesh study, showing the convergence of the QUAD4 solutions to the theoretical, are presented in tabular form in tables 1 - 2 and in graphical form in figures 4 - 7. Both formats show % error in displacement at the center of the plate as a function of mesh refinement. Results are included for COSMIC 88, MSC 65C and UAI 10.0 NASTRAN. In the tables results for COSMIC version 87 is also indicated as will be discussed below. The tables merely give exact numbers (along with the theoretical displacements) and the figures contain the same error information, but in graphic form.

Figures 4 and 5 and table 1 are the results for the homogeneous plate. The difference between the results in figures 4 and 5 (and that in the two parts of table 1) is that figure 4 (and the top half of table 1) is for a solution in which shear flexibility is included and figure 5 (and the bottom half of table 1) is without shear flexibility. These two situations were investigated to test the MID3 option on the PSHELL NASTRAN bulk data deck card which allows the effects of shear flexibility to be ignored if MID3 is left blank. As seen

in figures 4 and 5 the NASTRAN results converge very rapidly with mesh refinement for COSMIC 88, MSC 65C and UAI 10.0. Table 1 contains the same information along with results for COSMIC 87, the first COSMIC version to contain the QUAD4 element. As seen, all versions converge to less than 0.5% error for a mesh size of 8 x 8 with the results without shear flexibility converging a little more rapidly.

Figures 6 and 7 and table 2 are the results for the honeycomb plate. Figure 6 (and the top half of table 2) are for the honeycomb plate with the stiffer core and figure 7 (and the bottom half of table 2) are for the more flexible core. As seen in figures 6 and 7 the NASTRAN results for COSMIC 88 and the two commercial NASTRAN versions converge very rapidly for the two honeycomb plates as they did for the homogenous plate. Table 2 contains the same information along with the results for COSMIC 87. As indicated, the errors in the first version containing the QUAD4 were extremely large for the honeycomb plate but, as reported above, were quite good for the homogenous plate. When this was discovered it was immediately reported to COSMIC. They found the problem in a program controlled adjustable parameter (which is used to avoid the infamous shear locking phenomena in earlier thick shell finite elements based on Reissner plate theory) and sent us a fix within two days. After modifying the subroutine containing the error, the results became that which is reported under the COSMIC 88 heading (the same fix was included by COSMIC in the 88 release).

In order to test the QUAD4's sensitivity to aspect ratio, the model with a 12 x 12 mesh was run in which the plate side dimension in the x direction was varied. This causes the element aspect ratio to vary while maintaining a constant mesh in an attempt to remove mesh refinement errors from significantly affecting the results. As seen in tables 1 and 2, the QUAD4 results with a 12 x 12 mesh (and aspect ratio of 1.0) have very little error. The results of the aspect ratio study are presented in figures 8 - 10 and tables 3 - 5. Tables 3 - 5 give % error in the displacement at the center of the plate versus aspect ratio for a model with a mesh of 12 x 12 QUAD4 elements (over one quarter of the plate). As mentioned above, the aspect ratio was varied by changing the dimension of the plate along the x axis. Thus, the results for the aspect ratio of 10 are for a plate (and all QUAD4 elements) that is 10 times as long in the x direction as in the y direction. Due to this the theoretical solution changes with aspect ratio. Figure 8 and table 3 are for the homogenous plate (with transverse shear flexibility) while figure 9 and table 4 are for the stiff core honeycomb plate and figure 10 and table 5 are for the more flexible core honeycomb plate. Investigation of the % error in the tables, as well as in figures 8 - 10 show that the QUAD4 has essentially no aspect ratio sensitivity over the range investigated.

Based on the above results, the COSMIC QUAD4 element is seen to give very accurate results for the displacements in the problem investigated, both in comparison to the exact theory and in comparison to the two commercial versions of NASTRAN that we have at the GSFC. Although the results are not presented herein, similarly accurate results were obtained for the shear and moment stress resultants as well.

## RESULTS OF TESTING USING THE MSC ELEMENT TEST LIBRARY

As mentioned earlier, the mesh and aspect ratio studies, while a very useful tool in the evaluation of an element, do not test all of the important variables that affect accuracy in a finite element solution. The MSC element test library mentioned above represents a rather exhaustive series of tests that include many of the element related parameters which affect the accuracy of a finite element solution. Reference 3 gives a detailed description of the test problems along with theoretical answers and the results of the testing on several MSC elements. The reader should consult reference 3 for a complete description of the various problems in the test series. The portion of this series of element tests that relate to the QUAD4 element was run by the authors on the QUAD4 elements contained in COSMIC 88, UAI 9.8+ (not version 10.0 as for the mesh and aspect ratio study) and MSC 65C. As the MSC does in their report, the results are presented in detail and also in a summary form in which the element is given a letter grade of A through F based on the magnitude of the error. Table 6 shows the summary results for the 15 tests in the series ranging from a simple patch test to modelling of beams (using the QUAD4 element through the depth) and various plates and shells. The meaning of the letter grades is given at the bottom of the table. As pointed out in reference 3, a failing grade for an element in one test is not a reason to dismiss the element. For one thing, the test scores would improve with mesh refinement; the mesh used in most of the problems was quite coarse. Of importance in this discussion is not the actual grades listed in table 6 but the comparison of the COSMIC grades with those from the other two programs. As seen in table 6, the COSMIC QUAD4 element is as good as, or better than, those of the commercial programs. Although not shown in table 6, the old QUAD2 element (included in reference 3) has a D or F grade in 9 of the 15 problems. This is the reason for the longstanding need for an improved shell element and the QUAD4 element added to COSMIC NASTRAN clearly fills that need. Detailed results for each of the problems in the test series are contained in tables 7 - 12 and are included for completeness.

## CONCLUSIONS

The COSMIC QUAD4 general purpose flat shell element has been shown to be an excellent element and significantly enhances the usefulness of COSMIC NASTRAN. The element has been shown to compare excellently with those available in two commercial versions of NASTRAN that are currently being used at the GSFC. The addition of an improved triangular shell element, anticipated in the near future, is highly desirable as a companion element to the QUAD4 in general analyses of complicated shell like structures.

## REFERENCES

1. Case, W. R. and Mason, J. B., "NASTRAN Finite Element Idealization Study", Sixth NASTRAN User's Colloquium, pg 383, Cleveland, OH, October, 1977.
2. Case, W. R. and Vandegrift, R. E., "Accuracy of Three Dimensional Solid Finite Elements", Twelfth NASTRAN Users Colloquium, pg 26, Orlando, FL, May, 1984
3. MacNeal, R. H. and Harder, R. L. "A Proposed Standard Set of Problems to Test Finite Element Accuracy", MSC/NASTRAN Application Note, MSC/NASTRAN Application Manual, Section 5, March 1984
4. Reissner, E., "On Bending of Elastic Plates", Quarterly of Applied Math, Vol V, No. 5, pg 55, 1947
5. Salerno, V. L. and Goldberg, M. A., "Effect of Shear Deformations on the Bending of Rectangular Plates", Journal of Applied Mechanics, pg 54, March 1960

## List of Symbols

$a, b$  = plate dimensions

$t$  = plate thickness

$p$  = pressure load

$D, C_n, C_s$  = plate rigidities (see Figures 3b,3c)

$E$  = Young's Modulus

$\nu$  = Poisson's Ratio

$G_c$  = honeycomb core shear modulus

$AR, AR_e$  = aspect ratio (ratio of planar dimensions of plate or element)

$w$  = plate displacement

$N_x, N_y$  = number of elements in model of plate in  $x, y$  directions respectively



**TABLE 2**  
**MESH STUDY**  
**THICK HONEYCOMB PLATE**  
**ELEMENT ASPECT RATIO 1.0**

Theoretical Displacements  
 $G_z = 1.517 \times 10^8 \text{ N/m}^2$ :  $2.422 \times 10^{-3} \text{ m}$   
 $(9.535 \times 10^{-2} \text{ in.})$   
 $G_z = 1.379 \times 10^7 \text{ N/m}^2$ :  $3.102 \times 10^{-3} \text{ m}$   
 $(1.221 \times 10^{-1} \text{ in.})$

Mesh	Cosmic 87	% Error		MSC Ver. 65C
		Cosmic 88	UAI Ver. 10.0	
$G_z = 1.517 \times 10^8 \text{ N/m}^2$ (22000. psi)				
1x1	747.3	-16.31	-7.21	-17.98
2x2	589.9	-1.17	4.87	3.26
4x4	311.4	-0.25	1.46	1.19
8x8	103.3	-0.06	0.37	0.31
12x12	47.9	-0.03	0.16	0.14
$G_z = 1.379 \times 10^7 \text{ N/m}^2$ (2000. psi)				
1x1	-6550.4	-6.71	10.31	4.92
2x2	-5127.3	0.26	5.51	4.57
4x4	-2689.0	0.09	1.42	1.22
8x8	-888.5	0.02	0.36	0.31
12x12	-412.2	0.01	0.16	0.14

**TABLE 3**  
**ASPECT RATIO STUDY**  
**THICK HOMOGENEOUS PLATE**  
**WITH TRANSVERSE SHEAR FLEXIBILITY**  
**12X12 MESH**

AR	theoretical w, m (in.)	Cosmic 88	% Error UAI Ver. 10.0	MSC Ver. 65C
1	$3.571 \times 10^{-5}$ ( $1.406 \times 10^{-3}$ )	-0.38	0.39	0.36
2	$8.865 \times 10^{-5}$ ( $3.490 \times 10^{-3}$ )	0.28	0.26	0.27
5	$11.34 \times 10^{-5}$ ( $4.465 \times 10^{-3}$ )	-0.83	-0.01	0.05
10	$11.38 \times 10^{-5}$ ( $4.482 \times 10^{-3}$ )	-0.04	-0.06	-0.02

**TABLE 4**  
**ASPECT RATIO STUDY**  
**THICK HONEYCOMB PLATE,  $Gz=1.517 \times 10^8$  N/m<sup>2</sup> (22000. psi)**  
**12X12 MESH**

AR	theoretical w, m (in.)	Cosmic 88	% Error UAI Ver. 10.0	MSC Ver. 65C
1	$2.422 \times 10^{-3}$ ( $9.535 \times 10^{-2}$ )	0.02	-0.16	-0.14
2	$5.974 \times 10^{-3}$ ( $2.352 \times 10^{-1}$ )	0.05	-0.12	-0.13
5	$7.631 \times 10^{-3}$ ( $3.004 \times 10^{-1}$ )	0.24	0.13	0.07
10	$7.660 \times 10^{-3}$ ( $3.016 \times 10^{-1}$ )	0.27	0.17	0.14

**TABLE 5**  
**ASPECT RATIO STUDY**  
**THICK HONEYCOMB PLATE,  $Gz=1.379 \times 10^7$  N/m<sup>2</sup> (2000. psi)**  
**12X12 MESH**

AR	theoretical w, m (in.)	Cosmic 88	% Error UAI Ver. 10.0	MSC Ver. 65C
1	$3.102 \times 10^{-3}$ ( $1.221 \times 10^{-1}$ )	-0.01	-0.16	-0.49
2	$7.026 \times 10^{-3}$ ( $2.766 \times 10^{-1}$ )	0.03	-0.12	0.23
5	$8.785 \times 10^{-3}$ ( $3.459 \times 10^{-1}$ )	0.20	0.01	0.06
10	$8.815 \times 10^{-3}$ ( $3.470 \times 10^{-1}$ )	0.24	0.41	0.14

**TABLE 6**  
SUMMARY OF TEST RESULTS FOR QUAD4 SHELL ELEMENTS

Test	Elem. Loading		Element Shape	COSMIC 88	UAI 9.8+	MSC 65C
	In Plane	Out of Plane				
1. Patch Test	X		Irregular	A	A	A
2. Patch Test		X	Irregular	A	A	A
3. Straight Beam, Extension	X		All	A	A	A
4. Straight Beam, Bending	X		Regular	B	B	B
5. Straight Beam, Bending	X		Irregular	F	F	F
6. Straight Beam, Bending		X	Regular	A	A	A
7. Straight Beam, Bending		X	Irregular	A	A	B
8. Straight Beam, Twist			All	B	B	B
9. Curved Beam	X		Regular	C	C	C
10. Curved Beam		X	Regular	B	B	B
11. Twisted Beam	X	X	Regular	A	A	A
12. Rectangular Plate (N=4)		X	Regular	A	A	B
13. Scordelis-Lo Roof (N=4)	X	X	Regular	B	B	B
14. Spherical Shell (N=8)	X	X	Regular	A	A	A
15. Thick-Walled Cylinder (nu=.4999)	X		Regular	B	B	F
Number of Failed Tests (D's and F's)				1	1	2

Grading for Shell Element Test Results

<u>Grade</u>	<u>Requirement</u>
A	2% ≥ Error
B	10% ≥ Error > 2%
C	20% ≥ Error > 10%
D	50% ≥ Error > 20%
F	Error ≥ 50%

**TABLE 7**  
**PATCH TEST RESULTS**

	Maxium % Error in Stress		
	Cosmic 88 Quad4	UAI Ver 9.8+ Quad4	MSC Ver. 65C Quad 4
Constant-Stress Loading	0.00	0.00	0.00
Constant-Curvature Loading	0.00	0.00	0.00

**TABLE 8**  
RESULTS FOR STRAIGHT CANTILEVERED BEAM

Tip Loading Direction	Normalized Tip Displacement* in Direction of Loading		
	Cosmic 88 Quad4	UAI Ver. 9.8+ Quad4	MSC Ver. 65C Quad 4
(a) Rectangular Elements			
Extension	0.996	0.996	0.995
In-plane Shear	0.904	0.904	0.904
Out-of-plane Shear	0.985	0.985	0.986
Twist	0.958	0.957	0.941
(b) Trapezoidal Elements			
Extension	1.00	0.992	0.996
In-plane Shear	0.071	0.071	0.071
Out-of-plane Shear	0.980	0.979	0.968
Twist	0.937	0.934	0.951
(c) Parallelogram Elements			
Extension	0.992	0.992	0.996
In-plane Shear	0.080	0.080	0.080
Out-of-plane Shear	0.986	0.986	0.977
Twist	0.895	0.892	0.945

\*: Normalizing displacement values listed in Ref. 3. It is usually a theoretical value.

**TABLE 9**  
**RESULTS FOR CURVED BEAM**

	Normalized Tip Displacement* in Direction of Loading		
Tip Loading	Cosmic	UAI	MSC
Direction	88 Quad4	Ver. 9.8+ Quad4	Ver. 65C Quad 4
In-plane Shear	0.834	0.833	0.833
Out-of-plane Shear	0.971	0.971	0.951

**RESULTS FOR TWISTED BEAM**

	Normalized Tip Displacement* in Direction of Loading		
Tip Loading	Cosmic	UAI	MSC
Direction	88 Quad4	Ver. 9.8+ Quad4	Ver. 65C Quad 4
In-plane Shear	0.995	0.995	0.993
Out-of-plane Shear	0.984	0.984	0.985

\*: Normalizing displacement values listed in Ref. 3. It is usually a theoretical value.

**TABLE 10**  
**RESULTS FOR RECTANGULAR PLATE**

Normalized Lateral Deflection at Center\*

	Uniform Load			Concentrated Load		
	Cosmic 88	UAI V. 9.8+	MSC V. 65C	Cosmic 88	UAI V. 9.8+	MSC 65C
Nodes/ Edge	Simple Supports					
	(a) Aspect Ratio = 1.0					
2	1.01	1.05	0.981	1.05	1.04	1.02
4	1.01	1.02	1.00	1.02	1.02	1.02
6	1.01	1.01	1.00	1.01	1.01	1.01
8	1.00	1.01	1.00	1.01	1.01	1.01
	(b) Aspect Ratio = 5.0					
2	0.986	0.983	1.05	0.999	0.989	0.811
4	0.988	0.984	0.991	1.02	1.01	0.932
6	0.995	0.995	0.997	1.03	1.02	0.973
8	0.997	0.997	0.998	1.03	1.02	0.989
	Clamped Supports					
	(a) Aspect Ratio = 1.0					
2	1.052	1.046	1.008	0.971	0.963	0.994
4	1.038	1.034	1.032	1.020	1.015	1.010
6	1.024	1.022	1.023	1.027	1.018	1.012
8	1.017	1.016	1.016	1.013	1.012	1.010
	(b) Aspect Ratio = 5.0					
2	1.121	1.112	1.314	0.689	0.663	0.519
4	1.023	1.019	1.016	0.987	0.974	0.863
6	1.013	1.010	1.017	1.028	1.019	0.940
8	1.014	1.013	1.017	1.034	1.027	0.972

\*: Normalizing displacement values listed in Ref. 3. It is usually a theoretical value.

**TABLE 11**  
**RESULTS FOR THICK-WALLED CYLINDER**

Normalized Radial Displacement\*  
at Inner Boundary

Poisson's Ratio	Cosmic 88 Quad4	UAI Ver. 9.8+ Quad4	MSC Ver. 65C Quad4
0.4900	1.027	1.027	0.864
0.4990	1.032	1.032	0.359
0.4999	1.033	1.033	0.053

\*: Normalizing displacement values listed in Ref. 3. It is usually a theoretical value.

**TABLE 12**  
**RESULTS FOR SCORDELIS-LO ROOF**

No. of Spaces per Edge	Normalized Vertical Deflection* at Midpoint of Free Edge		
	Cosmic 88 Quad4	UAI Ver. 9.8+ Quad4	MSC Ver. 65C Quad4
2	1.450	1.450	1.376
4	1.070	1.070	1.050
6	1.030	1.030	1.018
8	1.019	1.019	1.008
10	1.015	1.015	1.004

**RESULTS FOR SPHERICAL SHELL**

No. of Spaces per Edge	Normalized Vertical Deflection* at Midpoint of Free Edge		
	Cosmic 88 Quad4	UAI Ver. 9.8+ Quad4	MSC Ver. 65C Quad4
2	1.020	1.011	0.972
4	1.043	1.040	1.024
6	1.023	1.020	1.013
8	1.010	1.009	1.005
10	1.004	1.003	1.001
12	1.000	0.999	0.998
16	0.998	0.997	0.997

\*: Normalizing displacement values listed in Ref. 3. It is usually a theoretical value.

Fig. 1  
Test Problem

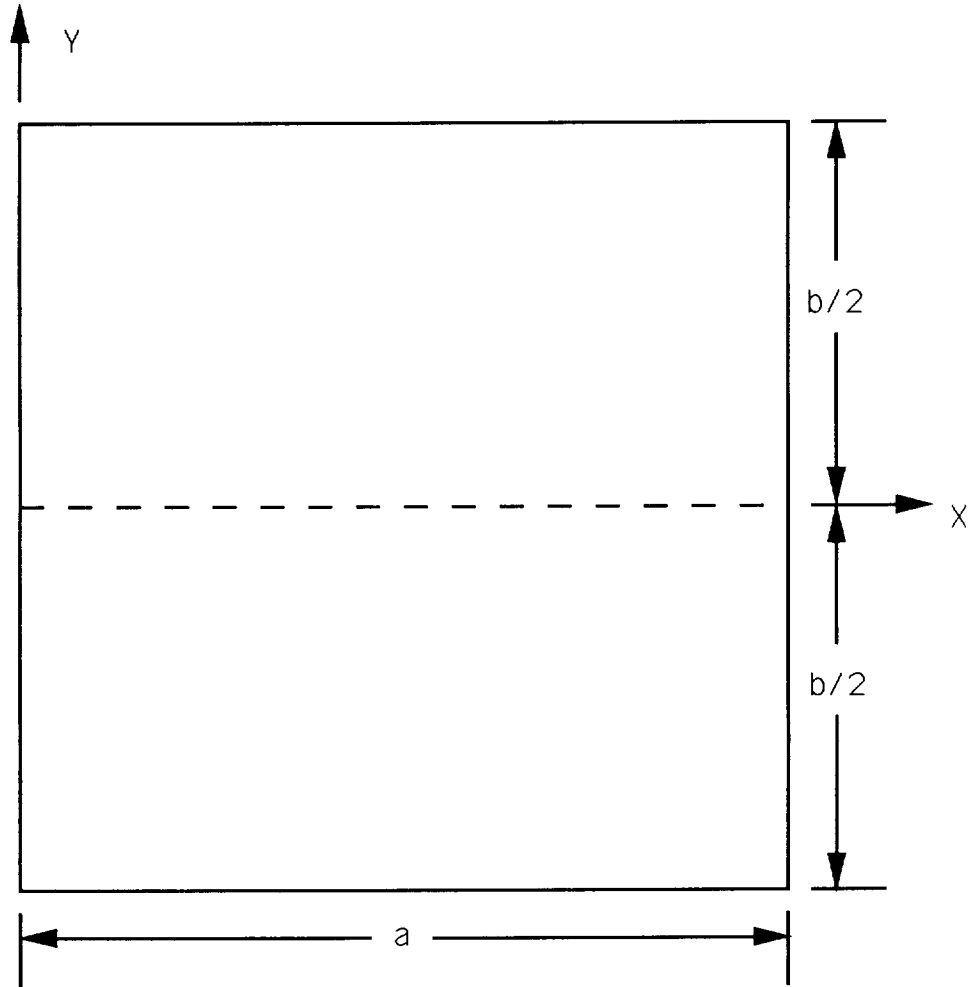


Plate Size:  $a=1.016$  m (40. in.)\*  $b=1.016$ m (40.in.)

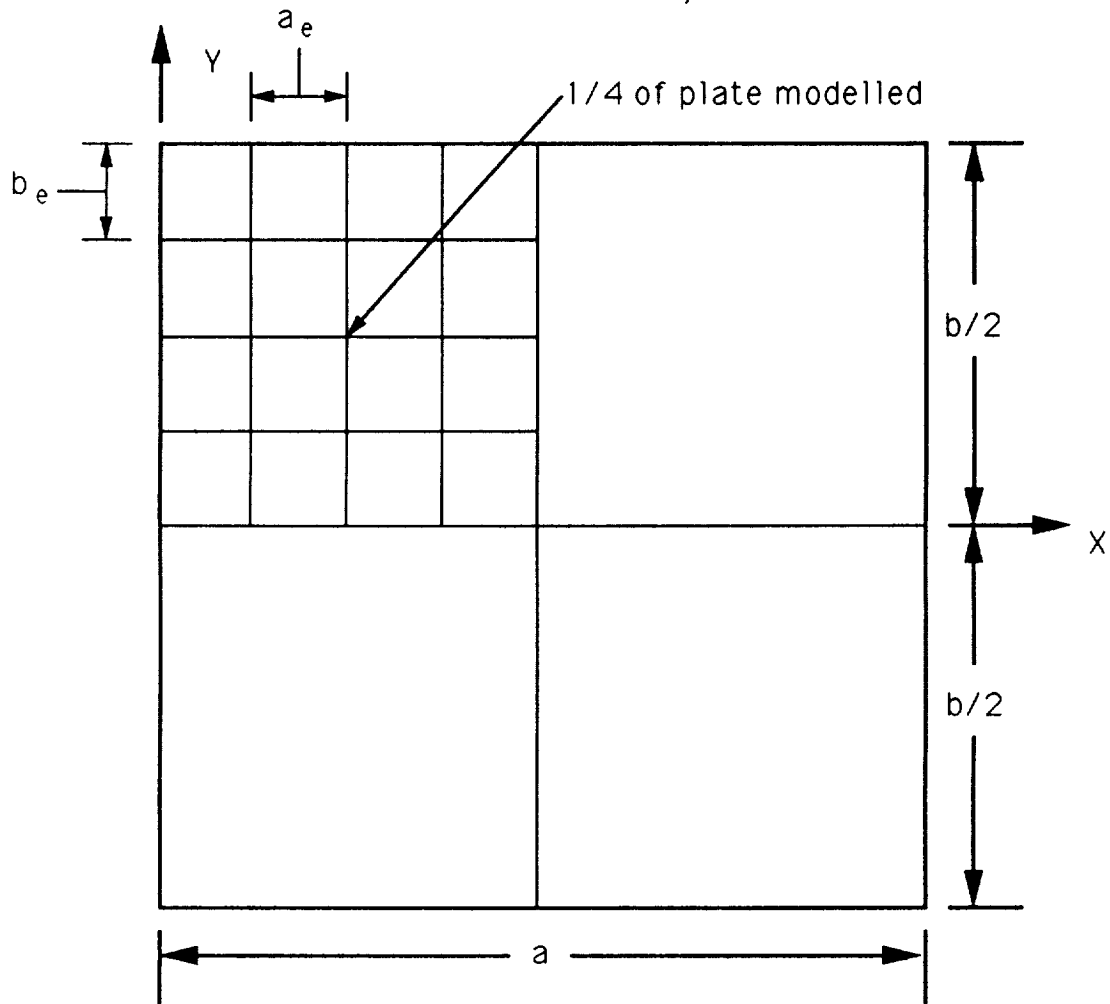
Boundary Conditions: simply supported on all edges

Loading: pressure load,  $p=6895$ .  $N/m^2$  (1.0 psi) +Z direction

Thickness:  $t=0.0508$  m (2.0 in.)

\*: Variable in aspect ratio studies

Fig. 2  
Mesh Geometry



$AR_e = a_e/b_e =$  element aspect ratio

$N_x = a/2a_e =$  number of elements in X direction in 1/4 of plate

$N_y = b/2b_e =$  number of elements in Y direction in 1/4 of plate

Fig. 3a

Theoretical Solution - Central Displacement

Central Displacement

$$w(x=\frac{a}{2}, y=0) = \frac{4p}{aD} \sum_{m=1,3,5,\dots} \left[ 1 + C_5 \cosh(\mu y) + \mu y C_6 \sinh(\mu y) + \mu^2 D \left( \frac{1}{C_s} - \frac{1+\nu}{C_n} \right) \right] \frac{\sin \mu x}{\mu^5}$$

where,

$$C_5 = -\frac{1}{\cosh \alpha_m} \left[ 1 + \mu^2 D \left( \frac{1}{C_s} - \frac{1+\nu}{C_n} \right) + \frac{1}{2} \alpha_m \tanh(\alpha_m) \right]$$

$$C_6 = \frac{1}{2 \cosh \alpha_m}$$

$$\alpha_m = \frac{m\pi b}{2a}, \quad \mu = \frac{m\pi}{a}$$

Fig. 3b

Theoretical Solution - Homogeneous Plate Parameters

Homogeneous Plate

$$D = \frac{Et^3}{12(1-\nu^2)}$$

$$C_n = \frac{5}{6} \frac{Et}{\nu}$$

$$C_s = \frac{5}{6} Gt, \quad G = \frac{E}{2(1+\nu)}$$

$$E = 6.89 \times 10^{10} \text{ N/m}^2 \quad (10.0 \times 10^6 \text{ lb/in}^2)$$

$$\nu = 0.33$$

Fig. 3c

Theoretical Solution - Honeycomb Plate Parameters

Honeycomb Plate

$$D = \frac{E_f t_f (t_c + t_{f/2})^2}{4(1-\nu^2)}$$

$$C_n = \infty$$

$$C_s = t_c G_c$$

$$E_f = 6.89 \times 10^{10} \text{ N/m}^2$$

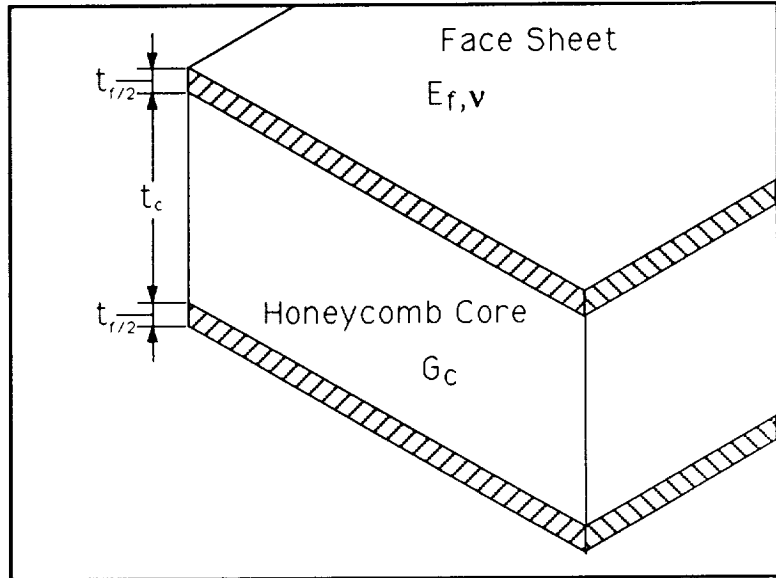
$$(10 \times 10^6 \text{ lb/in}^2)$$

$$\nu = 0.33$$

$$G_c = 1.379 \times 10^7 \text{ N/m}^2 \text{ (2000. lb/in}^2)$$

or

$$1.517 \times 10^8 \text{ N/m}^2 \text{ (22000. lb/in}^2)$$



Core Detail

**Fig. 4**  
**Error in Displacement at Center of Plate**  
**Mesh Size Study**  
Homogeneous Plate with Transverse Shear Flexibility  
Element Aspect Ratio 1.0

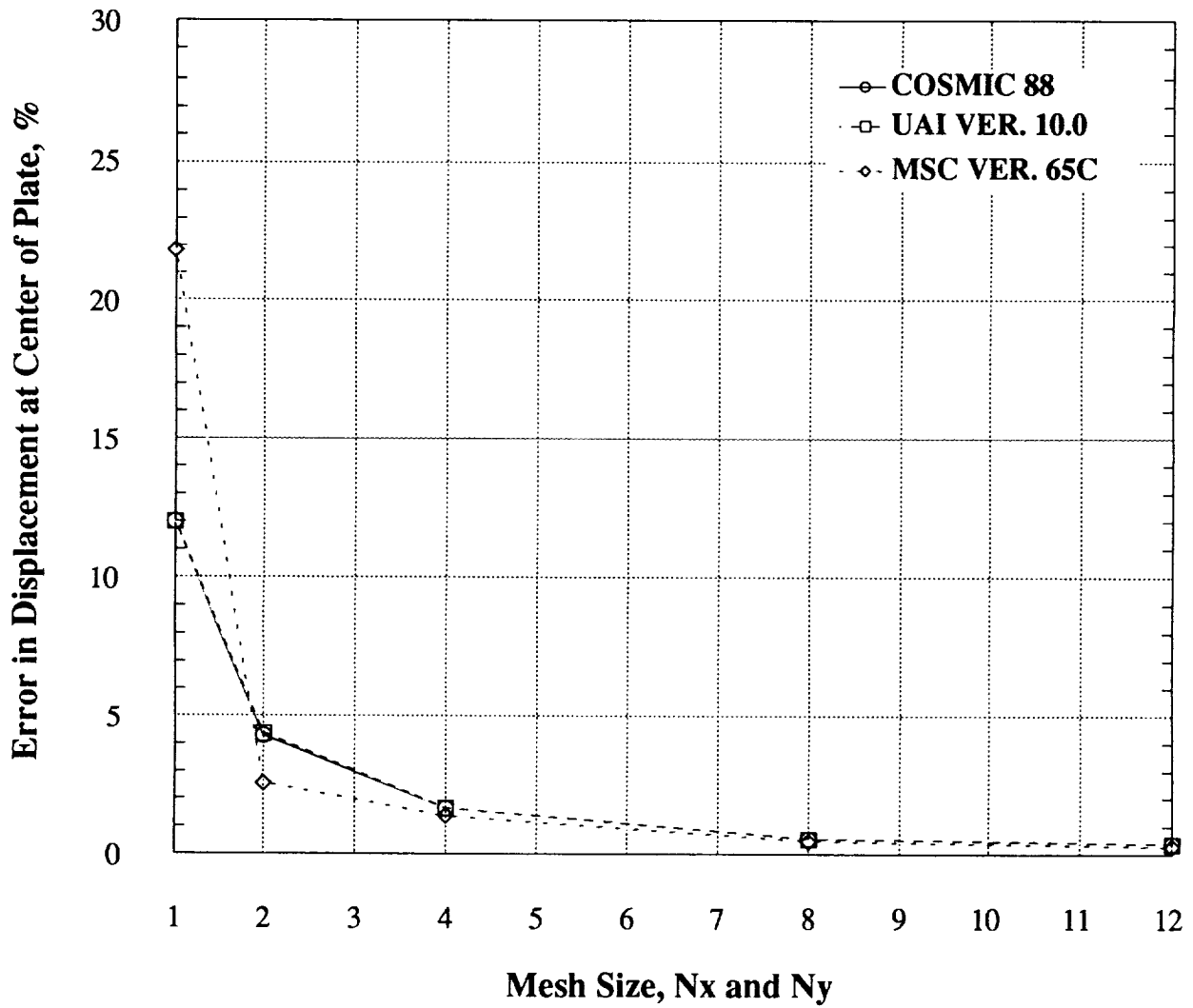


**Fig. 5**  
**Error in Displacement at Center of Plate**  
**Mesh Size Study**  
Homogeneous Plate without Transverse Shear Stiffness  
Element Aspect Ratio 1.0

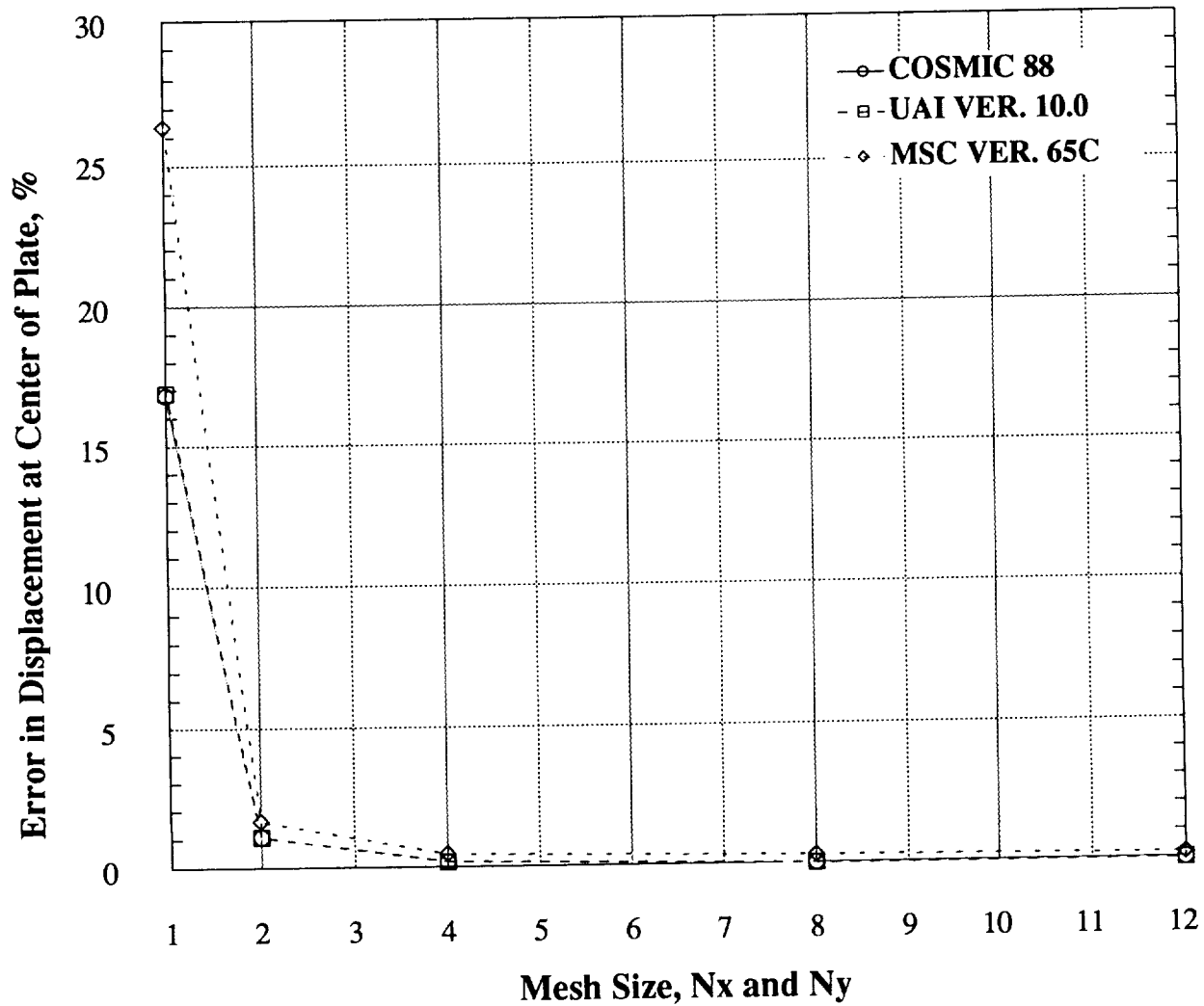


**Fig. 6**  
**Error in Displacement at Center of Plate**  
Mesh Size Study  
Stiff Honeycomb Plate  
Element Aspect Ratio 1.0

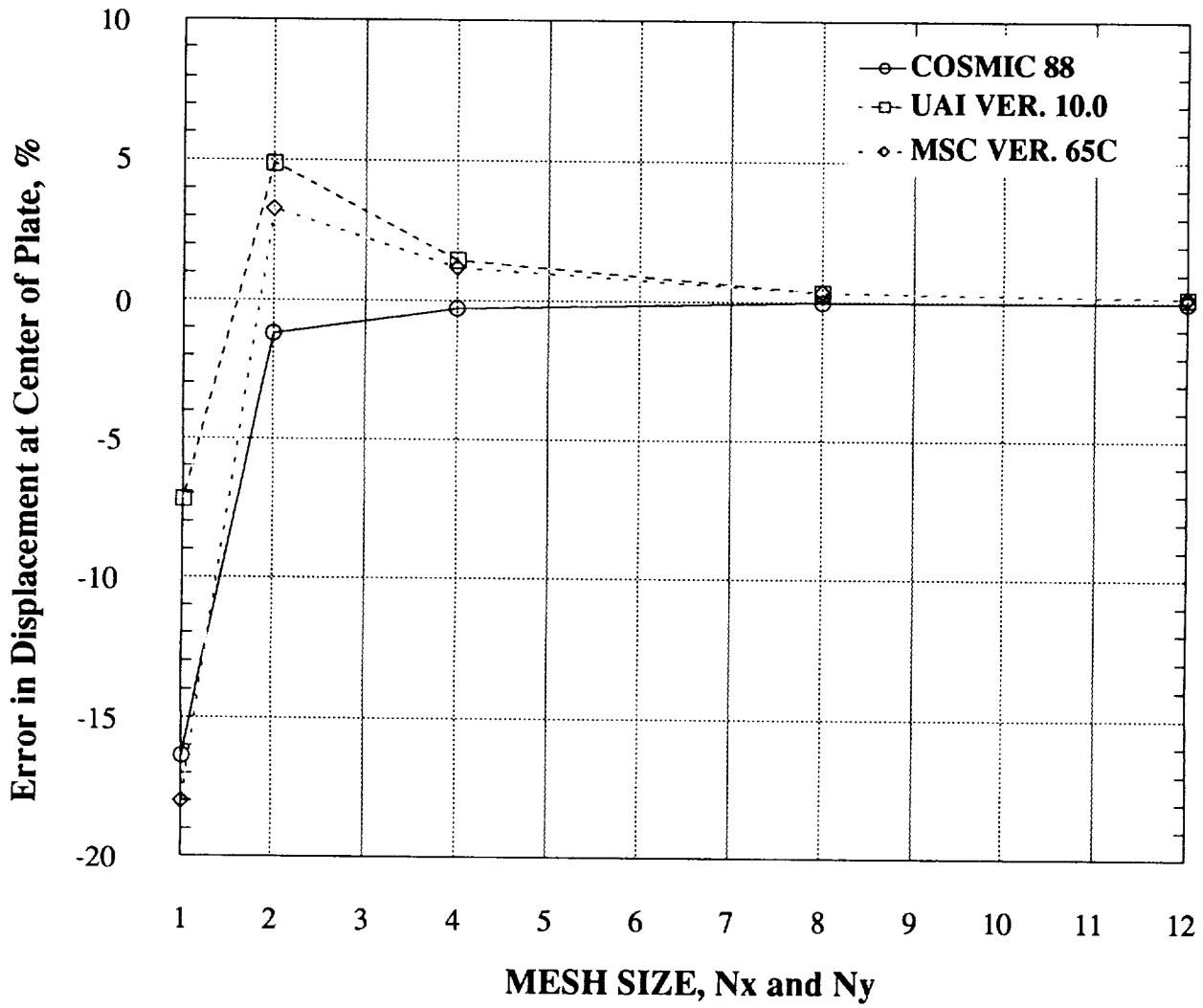


**Fig. 7**  
**Error in Displacement at Center of Plate**  
**Mesh Size Study**  
**Flexible Honeycomb Plate**  
**Element Aspect Ratio 1.0**

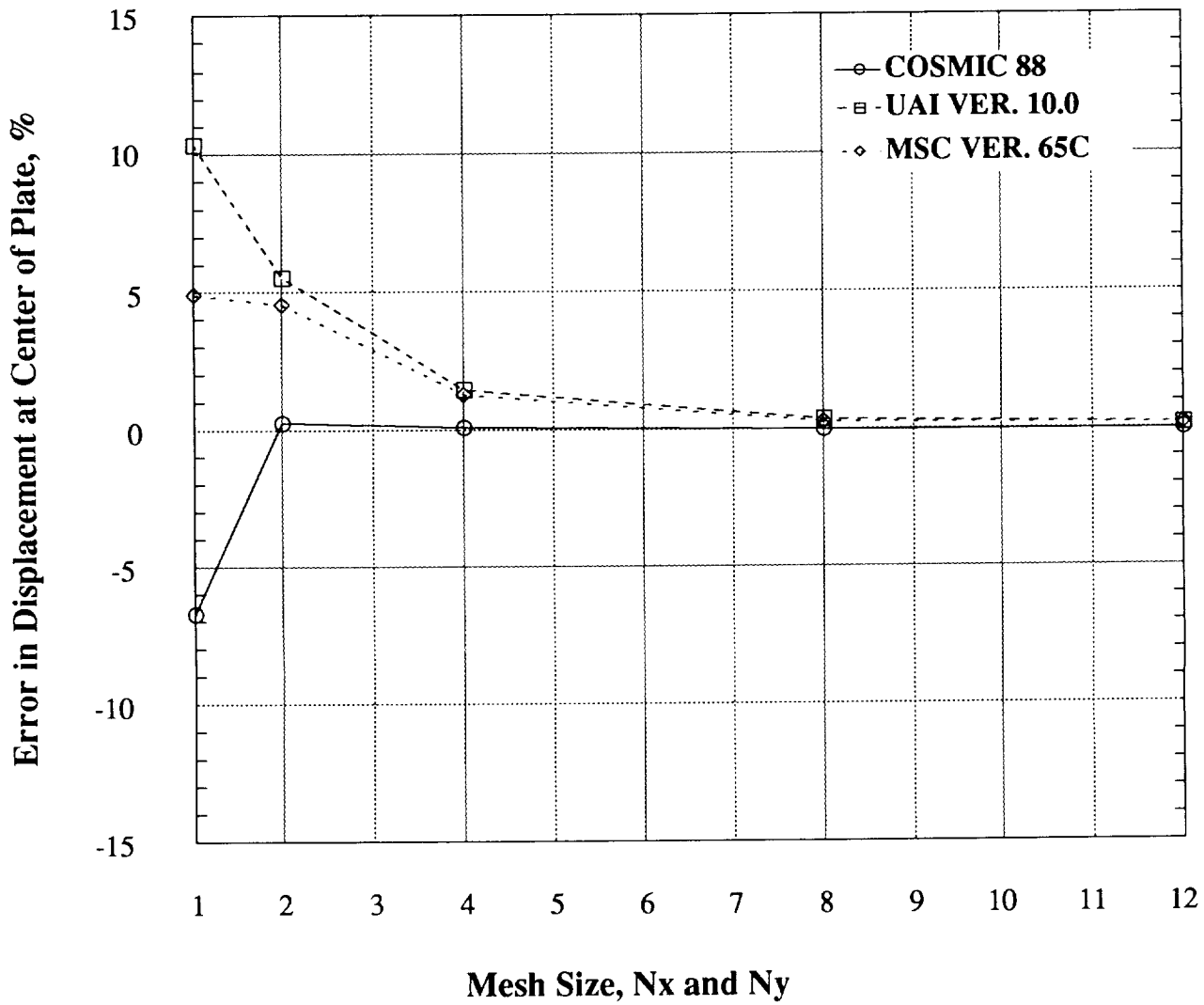


**Fig. 8**  
**Error in Displacement at Center of Plate**  
**Aspect Ratio Study**  
**Homogeneous Plate**  
**12 x 12 Mesh**

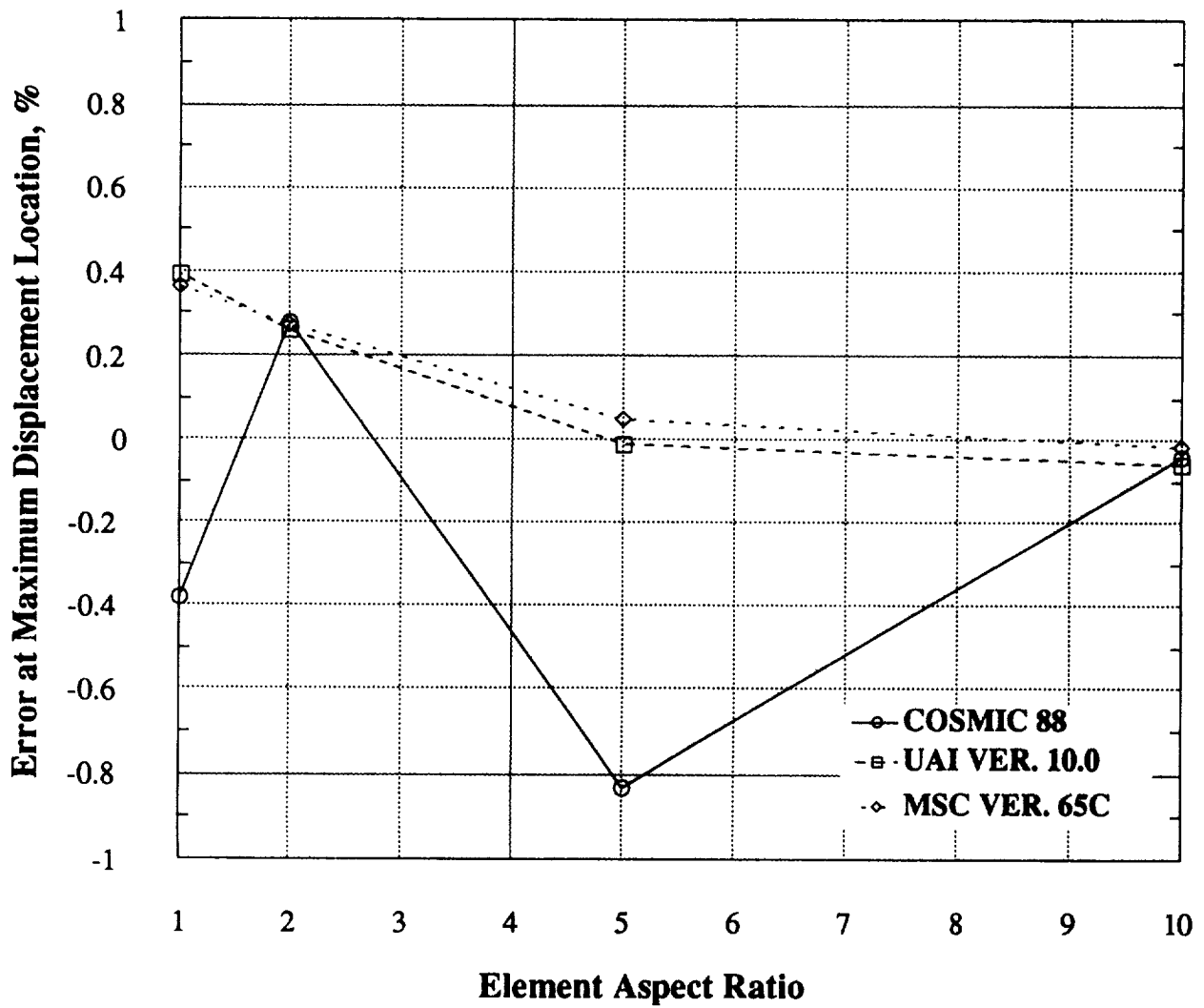


**Fig. 9**  
**Error in Displacement at Center of Plate**  
Aspect Ratio Study  
Stiff Honeycomb Plate  
12 x 12 Mesh

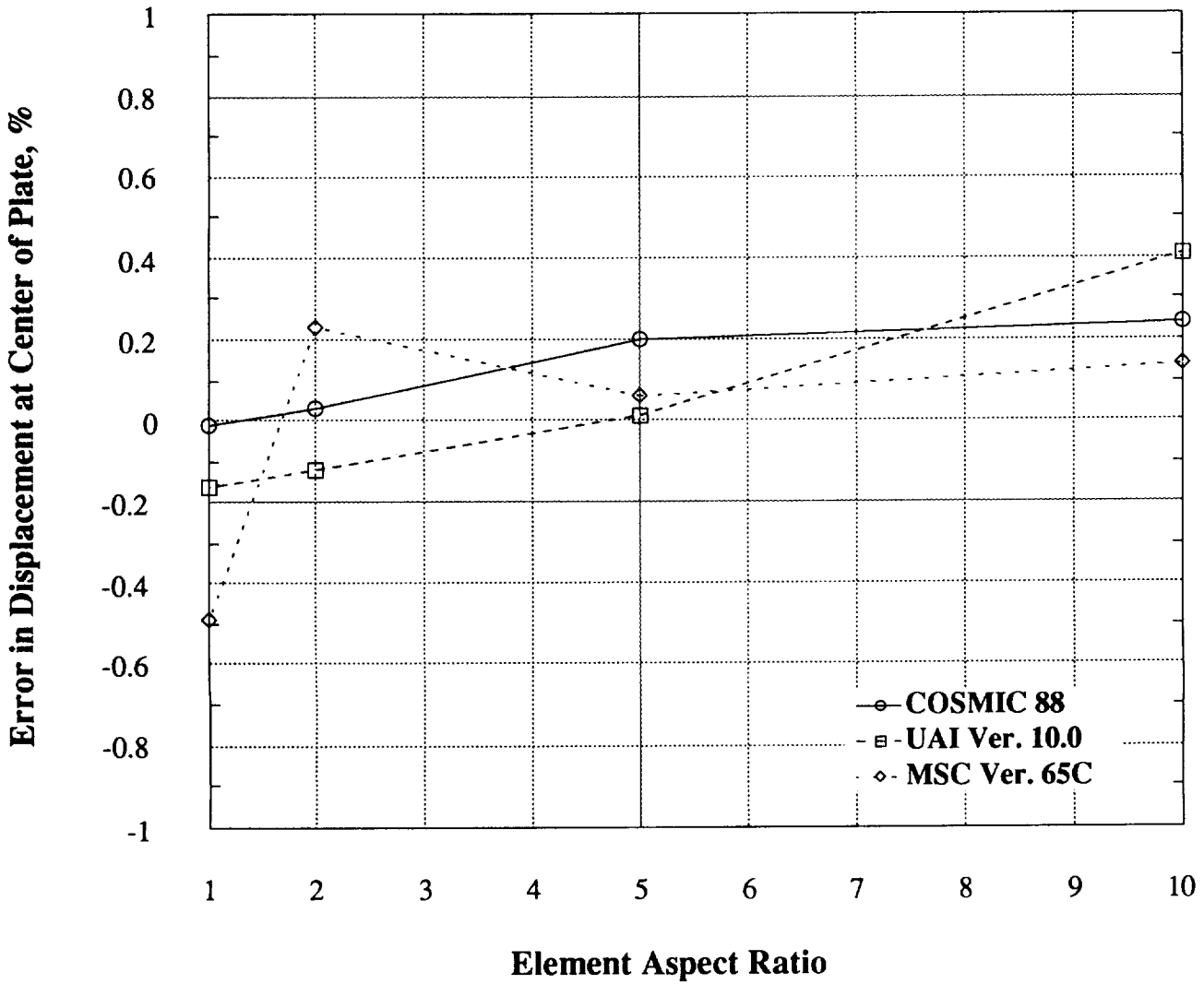
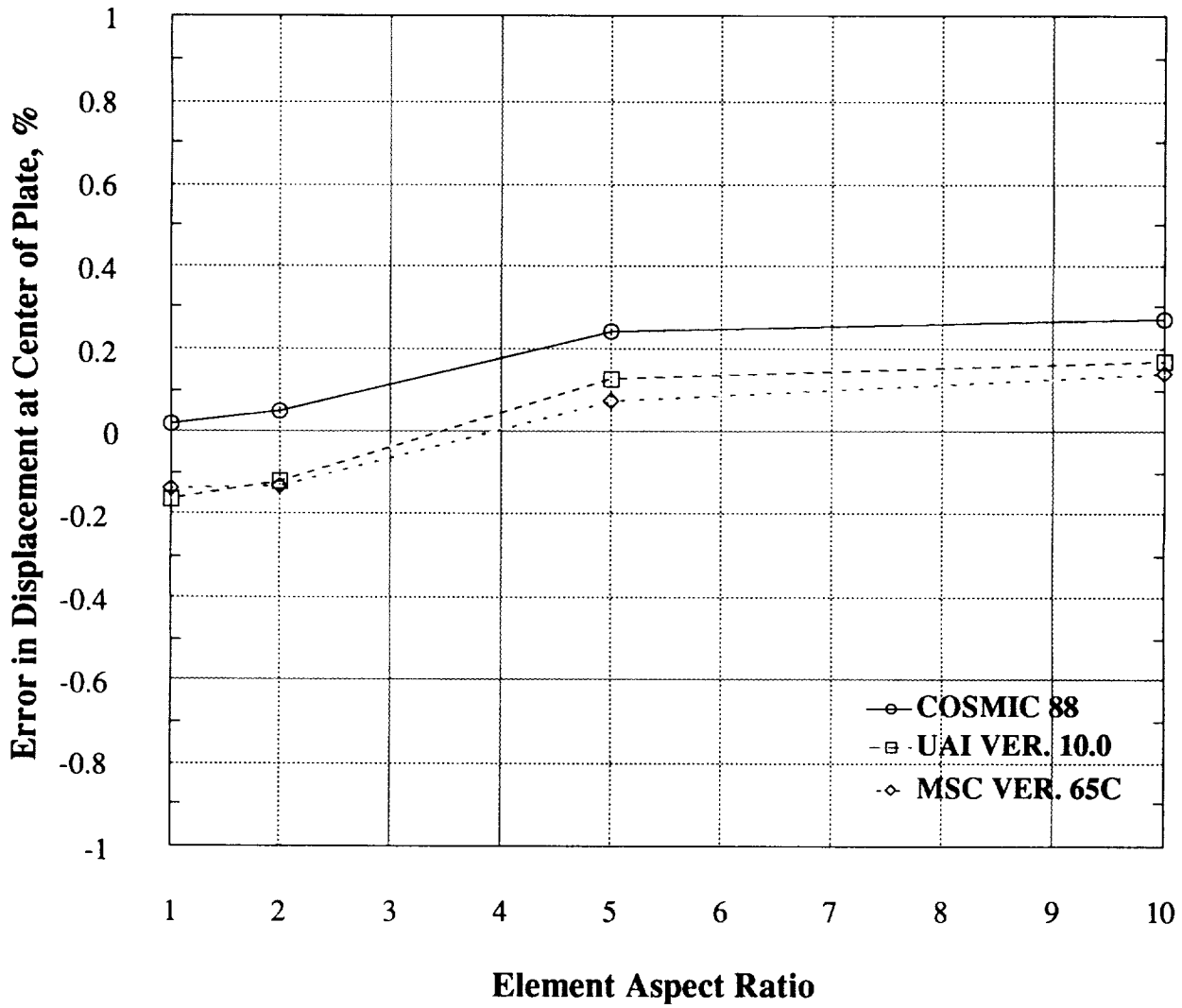


**Fig. 10**  
**Error in Displacement at Center of Plate**  
Aspect Ratio Study  
Flexible Honeycomb Plate  
12 x 12 Mesh



## EIGENVALUE COMPUTATIONS WITH THE QUAD4 CONSISTENT-MASS MATRIX

Thomas A. Butler  
Los Alamos National Laboratory

## SUMMARY

The NASTRAN user has the option of using either a lumped-mass matrix or a consistent- (coupled-) mass matrix with the QUAD4 shell finite element. At the Sixteenth NASTRAN Users' Colloquium (1988), Melvyn Marcus and associates of the David Taylor Research Center summarized a study comparing the results of the QUAD4 element with results of other NASTRAN shell elements for a cylindrical-shell modal analysis. Results of this study, in which both the lumped- and consistent-mass matrix formulations were used, implied that the consistent-mass matrix yielded poor results. In an effort to further evaluate the consistent-mass matrix, a study was performed using both a cylindrical-shell geometry and a flat-plate geometry. Modal parameters were extracted for several modes for both geometries leading to some significant conclusions. First, there do not appear to be any fundamental errors associated with the consistent-mass matrix. However, its accuracy is quite different for the two different geometries studied. The consistent-mass matrix yields better results for the flat-plate geometry and the lumped-mass matrix seems to be the better choice for cylindrical-shell geometries.

## INTRODUCTION

At the 1988 NASTRAN Users' Colloquium, results of a study using the QUAD4, four-node, shell finite element for shell vibrations was presented (ref. 1). This study indicated that using the QUAD4 element with a consistent-mass matrix results in poor prediction of natural frequencies of a cylindrical shell. The errors in predicted frequencies were small for lower circumferential harmonics ( $n < 4$ ) and grew from approximately 10 per cent for the fourth circumferential harmonic to over 20 per cent for the sixth circumferential harmonic. The errors seemed to be relatively independent of the longitudinal harmonics. The authors conclude that the poor performance is probably caused by either a bad formulation of the consistent-mass matrix or, more likely, a coding error in the program. The QUAD4 element is described in reference 2.

In an effort to determine whether either of the above reasons for the poor results is correct, a study was undertaken at Los Alamos to gain more insight into the problem. Earlier studies to evaluate the performance of the element for static problems indicate that the stiffness matrix formulation is correct. Also, results reported in reference 1 for the QUAD4 element with a lumped-mass matrix indicate that the problem is not with the stiffness matrix because the error in frequency prediction is quite low (less than 4 percent even for higher circumferential harmonics). Of course, some degradation in accuracy is expected for higher harmonics because the mesh density can become a limiting factor.

As a first step in our evaluation, an independent check of the formulation and coding was performed. No problems were found with either the formulation or the coding. As a final check, the mass matrix for a single element oriented at a skew angle to the global coordinate system was calculated by hand, and then results of the code were compared. There apparently are no errors in either the formulation or the coding.

A brief review of the literature on the subject of consistent-mass matrices does lend some insight into the problem. Clough and Wilson (ref. 3) state that, if the consistent-mass formulation is used with a displacement compatible element, resulting frequencies are always larger than the true frequencies. With a lumped-mass matrix, the frequencies may be above or below the true frequencies leading to the possibility that use of the lumped-mass matrix formulation may result in more accurate frequency predictions. The NASTRAN Theoretical Manual (ref. 4) describes errors associated with both consistent- and lumped-mass matrices for the rod elements. Fortunately, in this case, the errors turn out to be opposite in sign and of equal magnitude for lower-order terms. Thus, an accurate mass matrix can be generated simply by averaging the lumped- and consistent-mass matrices. The case does not appear to be the same for shell elements. Stavrinidis et al. (ref. 5) propose improved mass matrices for several elements, including the one-dimensional bar, two-dimensional membrane, and the pure bending beam element. Their method and other methods using so-called "higher-order" mass matrices depend on the predicted frequencies being consistently high or low. With significant effort, similar methods may be applicable to the current three-dimensional shell problem. However, as will be seen later in this paper, solutions with the consistent-mass matrix for the QUAD4 element can be either high or low, depending on the geometry of the structure.

#### TEST PROBLEMS

Two test problems were chosen for this study. The first was a free-free flat plate for whose natural frequencies we have

closed-form, analytical solutions. The second was a right, circular cylinder. Closed-form solutions do not exist for this geometry, so the finite-difference code BOSOR (ref. 6) was used with a fine mesh to establish the reference frequencies and mode shapes. BOSOR results compare favorably with approximate solutions presented by Blevins (ref. 7).

The flat plate was a 10 by 10, 0.1-thick square. Its elastic modulus was  $1.0 \times 10^5$ , Poisson's ratio was 0.3, and the density was 1.0. Figure 1 shows the first three vibration modes of the plate with the theoretical frequencies.

The cylindrical shell had a radius of 300 and a length of 600. The material thickness was 3.0. Its elastic modulus, Poisson's ratio, and density were  $3.0 \times 10^6$ , 0.3, and  $2.588 \times 10^{-4}$ . The cylinder ends were simply supported without axial constraint (rigid diaphragm). Table I gives the reference frequencies calculated with BOSOR (ref. 6) for the cylindrical shell, along with the approximate solutions given by Blevins (ref. 7).

#### FINITE ELEMENT MODELS

Three different finite-element codes were used to model each of the two test problems. The finite-element code SPAR (ref. 8) was used with its E43, four-node quadrilateral element. This element is based on a mixed formulation first proposed by Pian (ref. 9). For analyzing these problems both the lumped- and coupled-mass matrices in the SPAR code were used. Because the E43 element is based on an assumed-stress function, rather than an assumed-displacement function, its coupled-mass matrix is not "consistent." That is, it is not derived from the same displacement functions used in deriving the stiffness matrix. Two types of elements were used with the ABAQUS finite-element code (ref. 10). The S8R5 element is an eight-node element that has only a consistent-mass matrix option. The S4R5 element is a four-node element that offers only a lumped-mass matrix. Finally, NASTRAN was used with the QUAD4 element with both the lumped- and the consistent-mass matrix options. In addition, the problems were analyzed with NASTRAN using a matrix that is the average of the consistent- and lumped-mass matrices.

The flat plate was modeled with three mesh densities having three, five, or seven nodes along each edge of the plate. ABAQUS was not used with the coarsest mesh because that would have resulted in a one-element mesh for the eight-node S8R5. The cylindrical shell was also modeled with three different mesh densities. These meshes had 5, 9, or 17 nodes on each edge. For the ABAQUS eight-node element, fewer total nodes were present because of the lack of the middle node. For this study, only one eighth of the shell was modeled, and symmetry conditions were used on all boundaries. Thus, only the even circumferential and odd longitudinal harmonics were determined.

All the NASTRAN solutions were obtained using the FEER eigenvalue extraction method. The mass-orthogonality test parameter was 0.0001 for the analyses.

## RESULTS

Results for the flat plate are shown in figures 2 through 4. In these figures, the horizontal axes show the number of nodes on each side of the square mesh and the vertical axis is the natural log of the absolute value of the error in predicted frequency. The error is simply the ratio of the calculated frequency to the theoretical frequency minus 1.0. For reference, a plotted  $\ln(\text{error})$  of -4.6 is approximately 1.0 per cent in error in absolute frequency determination. A plotted value of -8.0 is roughly equivalent to 0.03 per cent error.

The data points labeled "lumped," "consistent," and "average" are all for the NASTRAN QUAD4 element. Study of the results reveals some definite patterns. As might be expected, the consistent-mass matrix always outperforms the lumped-mass matrix. However, the rates of convergence seem to be approximately the same. The SPAR results that were obtained by using the coupled-mass matrix are consistently better than the NASTRAN results. However, the convergence pattern is not smooth and, for all cases, the SPAR E43 element with its coupled-mass matrix yields better answers with the intermediate, rather than the fine, mesh. This result is somewhat disturbing, although, in all cases, the errors were small. The ABAQUS S8R5 element also gives slightly better results than does the NASTRAN QUAD4 element. For the flat plate, the elements with the consistent-mass matrix formulation always overpredicted the frequencies and those with the lumped-mass matrices always underpredicted the frequencies.

Results for the cylinder are not as clear as for the flat plate. Figures 5 through 7 show the frequency-convergence characteristics for the elements that are being considered for three different modes. These involve the second, fourth, and sixth circumferential harmonics ( $n=2,4,$  and  $6$ ) and the first longitudinal harmonic ( $m=1$ ). The most striking observation is that, for the QUAD4 element, the lumped-mass matrix is now outperforming the consistent-mass matrix. This observation seems to confirm the result of Marcus (ref. 1). To illustrate the point, data from reference 1 have been added to the figures. Here, the definition of the ordinate axis has to be qualified. In reference 1, a 13 node by 37-node mesh was used in modeling one half of a cylinder. This becomes a 7-node by 19-node mesh when an eighth of the cylinder is considered, as is the case for this study. Because, for the modes presented, only the first longitudinal harmonic is

present, we can loosely define this as a 7 by 7 mesh and plot it as such on our figures.

Only for the lower, second harmonic (fig. 5) does the ABAQUS S8R5 element outperform the NASTRAN lumped-mass element. For all three modes, the QUAD4 with the lumped-mass matrix yields the best results. Its deviation from the QUAD4 with the consistent-mass matrix increases with higher circumferential harmonics. The SPAR, E43 element with a coupled-mass matrix tends to follow the QUAD4 element closely for these modes.

Except for a few cases, the frequencies were overpredicted for consistent-, lumped-, and coupled-mass matrices for the cylindrical-shell problem. The exceptions were the QUAD4 lumped-mass matrix and the E43 coupled-mass matrix for the finest mesh for the second and third modes considered here.

Frequency is not the only parameter that should be considered for modal analyses. The other is, of course, the mode shape. One method of comparing mode shapes is to compare calculated generalized masses for the solutions using the different elements being considered. Another is to use a parameter frequently calculated when comparing calculated mode shapes with experimentally measured mode shapes. This parameter is called the mode shape correlation coefficient (MSCC) and is described in reference 11. It essentially provides a measure of the least-squares deviation of the points being compared from a straight-line correlation. Both these measures were used in comparing solutions for the  $n=8$ ,  $m=5$  mode for the cylinder being considered here. Results of these comparisons are summarized in table II, along with comparisons of the predicted frequencies. The predicted frequencies are normalized using the BOSOR code results as the baseline. The generalized masses were normalized using the theoretical value obtained by direct integration of the square of the analytically perfect mode shape multiplied by the material density. For the MSCC comparisons, mode shapes predicted by BOSOR were used as the "correct" shape.

A study of the results summarized in table II shows again that the lumped-mass matrix provides better frequency predictions than does the consistent-mass matrix for the NASTRAN QUAD4 shell element. Note that for the 9-node by 9-node mesh, the error for the consistent-mass matrix is over 30 per cent. A finer mesh (17 by 17) with the consistent-mass matrix provides better frequency approximations, but the prediction is still not as good as for the lumped-mass matrix with a coarser mesh. The generalized mass is in considerable error for both QUAD4 cases in which the consistent-mass matrix is used.

The generalized mass is a much more sensitive measure of mode shape error than the MSCC, as evidenced by data for the ABAQUS results that used the S8R5 element. Here the MSCC is quite close

to 1.0 for the 9-node by 9-node mesh, but the generalized mass is over 30 per cent in error. As the mesh is refined, the generalized mass improves, but it is still not as accurate as for the QUAD4 when a lumped-mass matrix is used. Note that the performance of the ABAQUS S4R5 element compares favorably with the NASTRAN QUAD4 element.

The SPAR E43 element, which performed nearly as well as the QUAD4 in predicting frequencies for all the shell modes considered in this study, apparently predicts both the frequency and generalized mass accurately if the coupled-mass matrix is used. However, somewhat unexpectedly, this element does not perform quite so well with a lumped-mass matrix. In this case, the frequency is predicted accurately but the mode shape has considerable error associated with it, as evidenced by the underprediction of the generalized mass.

### CONCLUSIONS

Among the elements considered in this study, the NASTRAN QUAD4 element with a lumped-mass matrix seems to be the best choice when the geometry is a cylindrical shell. A general rule seems to be that, for any element considered here, consistent-mass matrices should be avoided for this particular geometry. On the other hand, for flat-plate geometries, the consistent-mass matrix outperforms the lumped-mass matrix.

These conclusions imply that choices are difficult when modeling geometries that deviate from the simple geometries considered here. It is possible that an alternate method of deriving the mass matrix, such as the SPAR coupled-mass matrix, would generate a result that would be more generally applicable. Note that it seems to perform well for both geometries. However, for the present, if the geometry is predominantly cylindrical, the lumped-mass matrix should always be used with the NASTRAN QUAD4 element.

## REFERENCES

1. Marcus, M. S.; Everstine, G. S.; and Hurwitz, M. M.: Experiences with the QUAD4 Element for Shell Vibration. Sixteenth NASTRAN Users' Colloquium, NASA CP-2505, National Aeronautics and Space Administration, April 1988, pp. 39-43.
2. Venkayya, V. B.; and Tischler, V. A.: QUAD4 Seminar. WRDC-TR-89-3046, Wright Research and Development Center, April 1989.
3. Clough, R. W.; and Wilson, E. L.: Dynamic Finite Element Analysis of Arbitrary Thin Shells. Computers and Structures, vol. 1, 1971, pp. 33-56.
4. The NASTRAN Theoretical Manual. NASA SP-221(06), National Aeronautics and Space Administration, January 1981.
5. Stavrinidis, C.; Clinckemaele, J.; and Dubois, J: New Concepts for Finite-Element Mass Matrix Formulations. AIAA Journal, vol. 27, 1989, pp 1249-1255.
6. Bushnell, D: BOSOR 4: Program for Stress, Buckling, and Vibration of Complex Shells of Revolution. Structural Mechanics Software Series - Vol. 1, N. Perrone and W. Pilkey, Eds., University Press of Virginia, Charlottesville, Virginia, 1976.
7. Blevins, R. D.: Formulas for Natural Frequency and Mode Shapes. Robert E. Krieger Publishing Co., Malabar, Florida, 1979, pp. 293-309.
8. Whetstone, W. D.: SPAR Structural Analysis System Reference Manual. NASA Cr 145098-1, Engineering Information Systems, Inc., February 1977.
9. Pian, T. H. H.: Derivation of Element Stiffness Matrices by Assumed Stress Distributions. AIAA Journal, vol 2, 1964, pp. 1333-1336.
10. ABAQUS User's Manual, Version 4.7. Hibbitt, Karlsson, and Sorenson, Inc., 1988.
11. Ewins, D. J.: Modal Testing; Theory and Practice. Research Studies Press LTD., Letchworth, Hertfordshire, England, 1986, pp. 222-226.

**TABLE I**  
 PREDICTED FREQUENCIES (Hz) FOR CYLINDRICAL SHELL USING BOSOR (BLEVINS)  
 FOR EVEN CIRCUMFERENTIAL HARMONICS (n) AND ODD LONGITUDINAL HARMONICS (m).

$n \backslash m$	1	3	5
2	19.61 (21.82)	47.97 (48.61)	54.69 (54.83)
4	7.92 (8.27)	33.27 (33.85)	47.05 (47.30)
6	7.32 (7.59)	23.64 (24.00)	39.56 (39.83)
8	10.76 (11.68)	20.63 (20.94)	35.18 (35.47)

**TABLE II**  
 COMPARISON OF FREQUENCY, GENERALIZED MASS, AND MODE SHAPE PREDICTED  
 BY VARIOUS FINITE ELEMENT MODELS FOR CYLINDRICAL SHELL MODE  $n=8, m=5$ .

Nodes/side	Computer code/ element	Mass matrix	Normalized frequency	Mode shape correlation coef.	Normalized generalized mass
9	SPAR/E43	coupled	1.032	0.9995	1.011
9	SPAR/E43	lumped	1.046	0.9853	0.810
9	ABAQUS/S8R5	consistent	0.982	0.9998	0.677
17	ABAQUS/S8R5	consistent	1.010		0.971
9	ABAQUS/S4R5	lumped	0.987		0.995
9	NASTRAN/QUAD4	lumped	1.014	0.9991	1.010
9	NASTRAN/QUAD4	consistent	1.336		0.603
17	NASTRAN/QUAD4	consistent	1.066		0.876

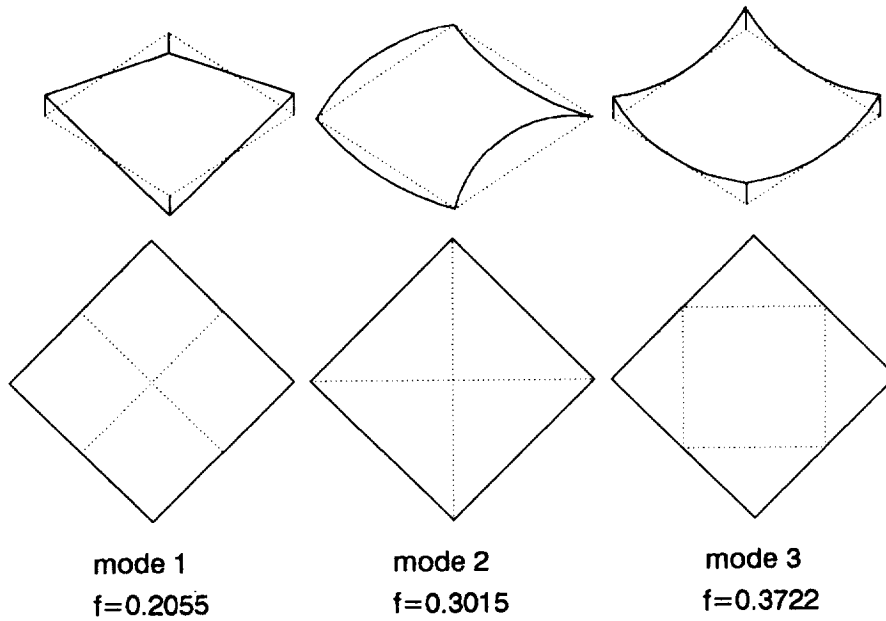


Figure 1. Mode shapes and frequencies (Hz) for flat plate.

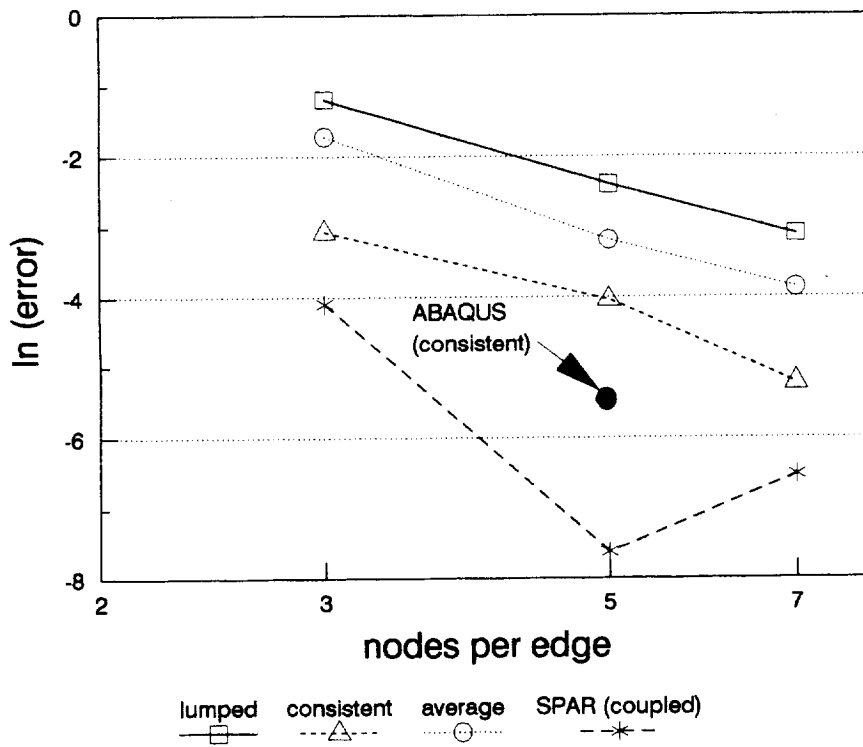


Figure 2. Frequency convergence for mode 1 of a flat plate as a function of mesh density for different finite elements.

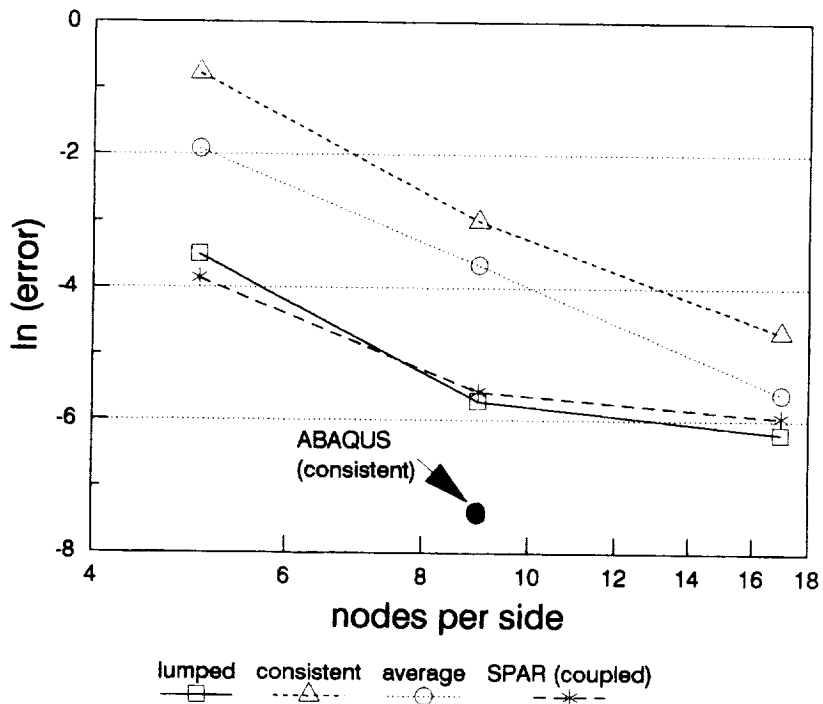


Figure 3. Frequency convergence for mode 2 of a flat plate as a function of mesh density for different finite elements.

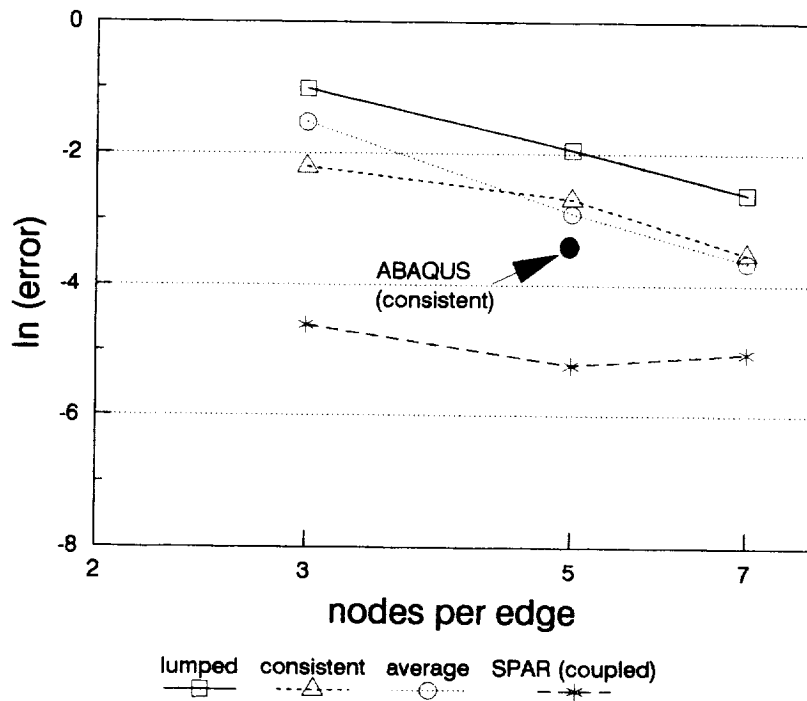


Figure 4. Frequency convergence for mode 3 of a flat plate as a function of mesh density for different finite elements.

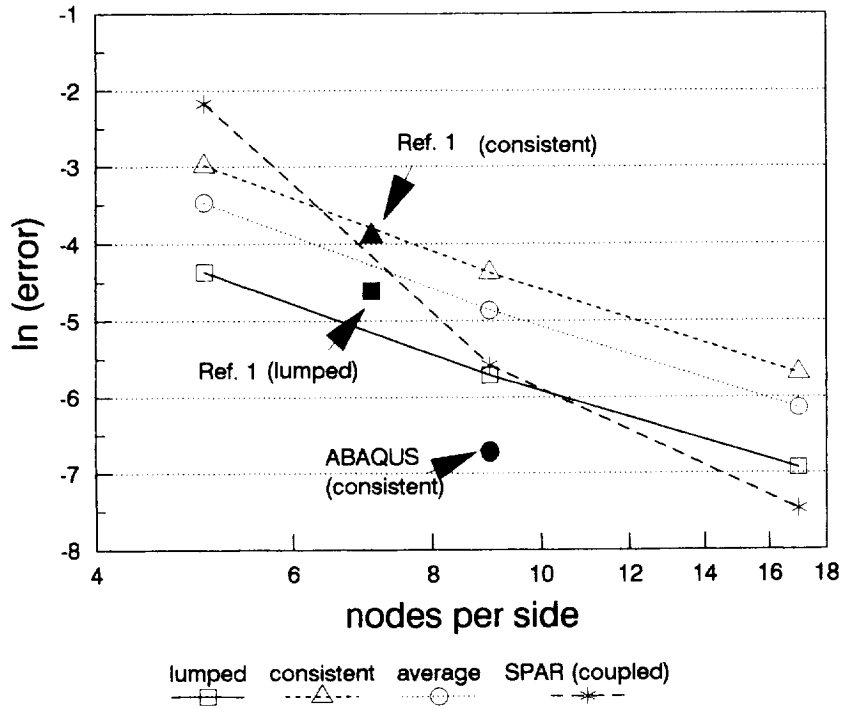


Figure 5. Frequency convergence for mode  $n=2$ ,  $m=1$  of cylindrical shell as a function of mesh density for different finite elements.

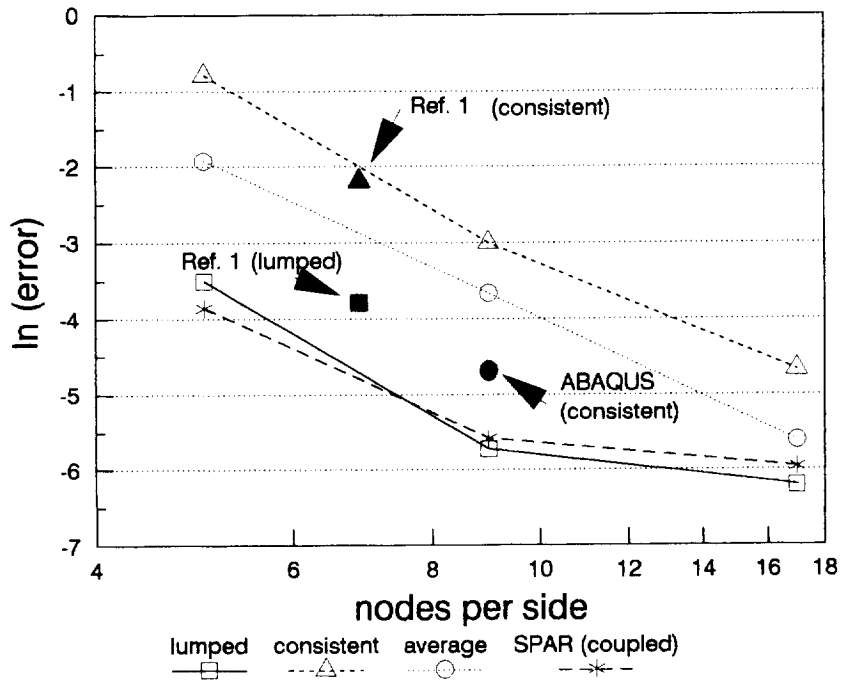


Figure 6. Frequency convergence for mode  $n=4$ ,  $m=1$  of a cylindrical shell as a function of mesh density for different finite elements.

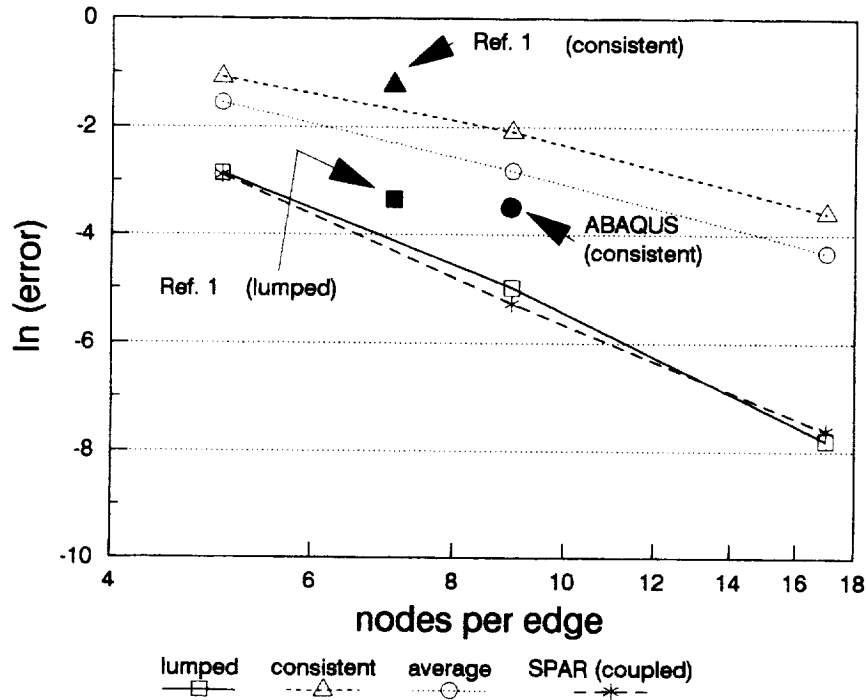


Figure 7. Frequency convergence for mode  $n=6$ ,  $n=1$  of a cylindrical shell as a function of mesh density for different finite elements.

## NASTRAN MIGRATION TO UNIX

by

Gordon C. Chan  
Horace Q. Turner  
UNISYS Corporation  
Huntsville, Alabama

## ABSTRACT

COSMIC/NASTRAN, as it is supported and maintained by COSMIC, runs on four main-frame computers - CDC, VAX, IBM and UNIVAC. COSMIC/NASTRAN on other computers, such as CRAY, AMDAHL, PRIME, CONVEX, etc., is available commercially from a number of third party organizations. All these computers, with their own one-of-a-kind operating systems, make NASTRAN machine dependent. The job control language (JCL), the file management, and the program execution procedure of these computers are vastly different, although 95 percent of NASTRAN source code was written in standard ANSI FORTRAN 77.

The advantage of the UNIX operating system is that it has no machine boundary. UNIX is becoming widely used in many workstations, mini's, super-PC's, and even some main-frame computers. NASTRAN for the UNIX operating system is definitely the way to go in the future, and makes NASTRAN available to a host of computers, big and small.

Since 1985, many NASTRAN improvements and enhancements were made to conform to the ANSI FORTRAN 77 standards. A major UNIX migration effort was incorporated into COSMIC NASTRAN 1990 release. As a pioneer work for the UNIX environment, a version of COSMIC 89 NASTRAN was officially released in October 1989 for DEC ULTRIX VAXstation 3100 (with VMS extensions). A COSMIC 90 NASTRAN version for DEC ULTRIX DECstation 3100 (with RISC) is planned for April 1990 release. Both workstations are UNIX based computers. The COSMIC 90 NASTRAN will be made available on a TK50 tape for the DEC ULTRIX workstations. Previously in 1988, an 88 NASTRAN version was tested successfully on a SiliconGraphics workstation.

## INTRODUCTION

The advantage of AT&T's UNIX operating system is that it is an "open system", hardware independent, single and multiuser system, powerful, versatile, and reliable. This "open system", which may appear under different names such as ULTRIX, XENIX, SunOS, AIX etc., is becoming the standard software today for the fast-growing market of workstation computers. Even IBM is going to adopt UNIX for its forthcoming workstations. As many more computers are designed to run under the UNIX banner, these newcomers are getting cheaper, faster, and more powerful. The

result: unprecedented price competition that's making UNIX another word for cheap computing. The migration of NASTRAN to the UNIX "open system", is definitely the way to go.

#### THE EARLY DEVELOPMENT

NASTRAN is written mainly in FORTRAN language. Only about five percent of the source codes are machine-dependent. The early stage of migration, started in 1984-1985, was a move towards ANSI FORTRAN 77, which is a standard FORTRAN compiler for all UNIX based computers. In this early stage of development, the NASTRAN UNIVAC version was moved from the 'FOR' compiler to the 'FIN' compiler, and the CDC version from FORTRAN 4 to FORTRAN 5. The VAX NASTRAN had been maintained as a separate version until the 1984 release. This release shared the machine independent source code with the other computers (IBM, CDC and UNIVAC).

#### TEST ON SiliconGraphics WORKSTATION

A NASTRAN test program, based on COSMIC/NASTRAN 88 VAX release, was converted and ran "successfully" on a SiliconGraphics workstation. Only occasionally this test program failed in some NASTRAN dynamic problems. Several UNIX job control languages (JCLs) were written to compile, link edit, and execute NASTRAN for this test program. These JCLs played an important part in the success of the SiliconGraphics pilot NASTRAN test. With further refinement and improvement (done in 1989), the JCLs, applicable to all UNIX based computers, play an important role in the NASTRAN migration to UNIX. The JCL to execute a NASTRAN job (cold start, restart or substructuring) is indeed very user friendly.

This SiliconGraphics test program was also used to identify and verify efficiency improvements of the NASTRAN source code. The UNIX utility profiler, prof, was used for timing studies of the codes needing efficiency improvement. These studies resulted in over 30 percent speed improvement of the VAX NASTRAN version. The other NASTRAN versions were also benefited.

All changes that were required to make this SiliconGraphics test program successful, were incorporated into the machine independent NASTRAN source codes.

#### VAX NASTRAN

The VAX version of NASTRAN is written entirely in FORTRAN language. Hardware-wise, VAX and many UNIX based computers are quite similar. They are virtual memory computers with 32-bit word architecture. The file management

systems are quite similar. The VAX FORTRAN version is the natural choice for the migration of NASTRAN to the UNIX system.

The NASTRAN GINO (General Input and Output file management) package of the VAX version has gone through extensive revision and improvement in 1987-1988. Many I/O processes have been shortened and streamlined. The packing and unpacking of matrix data were improved and speeded up. The UNIX based computers have therefore benefited from previous VAX improvements. (The improved VAX GINO and matrix packing/unpacking was also tested successfully on an IBM 3084 machine)

The VAX 89 NASTRAN release was compiled and linked successfully on a DEC ULTRIX VAXstation 3100 (with VMS extensions), using the UNIX JCLs from the SiliconGraphics test program. Only one subroutine, CPUTIM that obtains the CPU time from the computer system, needed modification. All 119 NASTRAN demonstration problems, plus 20 more user problems, ran successfully. This NASTRAN UNIX version was officially released on a TK50 tape in October 1989.

The DEC ULTRIX DECstation 3100 (with RISC, Reduced Instruction Set Chip) required additional modification of the NASTRAN source codes. (See next paragraph.) Occasionally this version failed in some dynamic problems, exhibiting the same symptom as that of the SiliconGraphics test program. There will be no official 89 release of this UNIX version. Presently, it is planned to have a 90 NASTRAN release for UNIX based computers with RISC processors.

#### UNIX/FORTRAN REQUIREMENTS

The ANSI FORTRAN 77 is the standard FORTRAN compiler for all UNIX based computers and workstations. However, small differences may exist among ANSI FORTRAN 77 compilers from different manufacturers. The 1990 COSMIC/NASTRAN incorporates many known specifications that are required by various ANSI FORTRAN 77 compilers. The changes involve:

- a. External declaration of bit-shifting functions (LSHIFT and RSHIFT), the logical functions (ANDF and ORF), and complement function (COMPLF), to avoid system functions of the same names.
- b. Standardization of OPEN, READ and WRITE commands for direct-access files.
- c. Removal of octal and hexadecimal constants from FORTRAN executable source code.
- d. Elimination of jumping into an inner do-loop, which was previously allowed via an ASSIGN statement.
- e. Dimension of one for all open core arrays.
- f. Alignment of all open core arrays.

The last change (f) above is the most tricky process for UNIX based computers, particularly those with RISC. Throughout the NASTRAN source code, several hundred labelled commons are used for the open core space. (NASTRAN has no dimension limit. The open-ended open core is used as scratch space for internal computations and storage). The other mainframe computers, particularly the non-virtual CDC and UNIVAC machines, require this open core space to have a unique name in a subroutine or group of subroutines, such that the open core space can be positioned strategically in the executable overlay program. To compromise among the virtual (UNIX based computers, VAX and IBM) and the non-virtual memory computers (that require program overlays), a block data routine, ZZCORE.f, was written to be used only for the UNIX based computers. All the open core labelled commons are included in this block data routine. The labelled common /XNSTRN/ must be the very first in the list, and /ZZZZZZ/ must be the very last. These first and last labelled common requirements must be true not only in the FORTRAN source code, but also in the compiled relocatable (or object) program. The user could use the UNIX command 'nm -n ZZCORE.o' to verify that /XNSTRN/ and /ZZZZZZ/ are positioned correctly. If they are not, something must be done to get the NASTRAN open core alignment correct. It is for this reason (too many labelled commons in one subroutine) that the DEC ULTRIX DECstation 3100 (RISC) uses two block data routines: ZZCORE.f for NASTRAN links 1 through 14, and ZZKORE.f for NASTRAN link 15. It is also for this reason that a C-program, SOROBJ.c, is included in the UNIX NASTRAN release tape, to sort the open core labelled commons in ZZCORE.o (a relocatable file), only if all other efforts fail to obtain the proper alignment.

#### CONCLUSION

The 90 COSMIC/NASTRAN release incorporates many changes as required by the UNIX based computers and workstations. With a set of proven user friendly UNIX JCLs, it should run successfully on many UNIX based computers presently available, or still on the vendors' drawing boards. (FORTRAN compile and link edit are required.) Of course, this 90 COSMIC/NASTRAN release will continue to operate as before on the IBM, VAX, CDC and UNIVAC mainframes. This is a version that bridges from the old world of proprietary and limited operating systems to the new UNIX world of "open system".

**OBTAINING EIGENSOLUTIONS FOR MULTIPLE FREQUENCY  
RANGES IN A SINGLE NASTRAN EXECUTION**

by

**P. R. Pamidi  
RPK Corporation  
Columbia, Maryland**

and

**W. K. Brown  
RPK Corporation  
Hayes, Virginia**

**SUMMARY**

A novel and general procedure for obtaining eigenvalues and eigenvectors for multiple frequency ranges in a single NASTRAN execution is presented. The scheme is applicable to normal modes analyses employing the FEER and Inverse Power methods of eigenvalue extraction. The procedure is illustrated by examples.

**INTRODUCTION**

NASTRAN currently offers four methods for real eigenvalue extraction. They are the Tridiagonal or Givens method, the Tridiagonal Reduction or FEER method, the Inverse Power method and the Determinant method (see Section 10 of Reference 1 for details).

The Givens method is a transformation method that computes all of the eigenvalues in a problem; in addition, eigenvectors corresponding to a specified range of frequencies or to a specified number of lowest eigenvalues can also be computed. The FEER method is also a transformation method that allows for the extraction of a specified number of eigensolutions. It requires the specification of a "shift point" or frequency around which the eigensolutions are desired. The Inverse Power and Determinant methods are both tracking methods that allow for the extraction of a specified number of eigensolutions. They both require the specification of a frequency range for which the eigensolutions are desired.

When all, or almost all, of the eigenvalues in a problem are required, the Givens method is the generally the most efficient method to use because the total effort is not highly dependent upon the number of eigenvalues that are extracted. However, when the order of the problem exceeds a few hundred, this method may require prohibitively time-consuming out-of-core operations, thereby losing its efficiency.

If an user is not interested in obtaining all of the modes in a problem, but only in a smaller number of eigensolutions around a certain frequency or within a certain frequency range, the FEER, the Inverse Power and the Determinant methods are the obvious choices. The computations in all of these methods are proportional to the number of eigensolutions extracted. The FEER method is probably the most efficient of the three. It is quite effective in obtaining eigensolutions around the selected frequency. It is also very efficient even when out-of-core operations are involved. The results obtained by the Inverse Power and Determinant methods, on the other hand, are very susceptible to the number of estimated roots specified for a given frequency range (field 5 on the EIGR bulk data card; see Reference 2). When the specified number for the estimated roots is larger than the actual number of roots in that range, these methods are apt to yield many lower frequencies outside the specified frequency range. The Determinant method is the least efficient of all of the methods and will, therefore, not be considered any further for the purpose of this paper.

### **CURRENT PROCEDURE FOR OBTAINING EIGENSOLUTIONS FOR MULTIPLE FREQUENCY RANGES**

There are practical situations in which an user may be interested in obtaining eigensolutions for multiple frequency ranges, with one frequency range quite distinct and apart from another frequency range. Complex configurations involving control systems, experimental setups and structural subsystems are examples of such situations.

None of the eigenvalue extraction methods discussed earlier can accomplish the above objective directly. So, if the user wishes to obtain eigenvalues for more than one range of frequencies in such cases as the above, he can accomplish it at present in one of two ways. The first way is for the user to make a single NASTRAN execution with a large frequency range (or a shift point in conjunction with a large number of desired roots) so as to encompass all of the frequencies in the ranges of interest. However, this will not be very cost effective if the frequency ranges of interest are widely separated. The alternative way is for the user to perform multiple NASTRAN executions, one execution for each range of frequencies, effectively utilizing the APPEND feature (see Section 9.2.2 in Reference 1 and Section 2.3.7 in Volume 2, Reference 2). However, this latter procedure involves checkpoint/restart runs and is rather cumbersome for the purpose.

### **PROPOSED PROCEDURE FOR OBTAINING EIGENSOLUTIONS FOR MULTIPLE FREQUENCY RANGES**

The above objective of obtaining eigensolutions for multiple frequency ranges can be accomplished in a single NASTRAN execution by an innovative procedure that involves the use of DMAP ALTERs in conjunction with certain specific input data requirements. This procedure involves performing a normal modes analysis employing multiple subcases and using the FEER method or the Inverse Power method (whichever is preferred). Each subcase is setup so as to obtain eigensolutions in a specified frequency range. The final results of the analysis will contain the eigensolutions obtained in all of the specified frequency ranges. This procedure is, in essence, a novel application of the APPEND feature referred to above. The important difference is that, while the APPEND feature was originally conceived to be employed in a checkpoint/restart environment, the proposed procedure accomplishes this in a single NASTRAN execution.

The DMAP ALTER package required for the above procedure is given in Appendix A. The details of the input data requirements and the output obtained from the analysis are discussed below.

### Executive Control Deck

The user should employ the DMAP ALTER package given in Appendix A either by explicitly including it or by referencing it via a READFILE card in the Executive Control Deck. Note that, for every additional subcase beyond the first subcase, the ALTER package involves a pair of OFP and READ modules.

### Case Control Deck

The user should have as many subcases in the Case Control Deck as the number of distinct frequency ranges for which he wishes to obtain eigensolutions. Each subcase must have a separate METHOD request. The METHOD request in each subcase references a distinct EIGR card in the Bulk Data Deck that either implies (in the case of the FEER method) or defines (in the case of the Inverse Power method) a distinct frequency range.

All output requests and constraint specifications must be above the subcase level. Thus, the only difference between one subcase and another must be the different METHOD that they request. Also, since the final results include eigensolutions for all of the subcases, PLOT requests should not make explicit references to subcase numbers.

### Bulk Data Deck

In addition to the required modeling (geometry, constraints, etc.) data, the Bulk Data Deck should have as many EIGR cards as the number of subcases employed (and the corresponding METHOD requests) in the Case Control setup.

When using the FEER method, the EIGR bulk data card for each METHOD request requires the specification of a shift point or frequency that indicates the center of a frequency range as well as the number of desired roots (see Reference 2). The user should specify appropriate values accordingly. The shift point specified has a significant effect on the actual eigensolutions extracted. Accordingly, depending upon the shift point specified, the actual number of roots computed may be more or less than the number of desired roots specified in the data.

When using the Inverse Power method, the EIGR bulk data card for each METHOD request requires the specification of a frequency range, the number of desired roots as well as the number of estimated roots in the specified frequency range (see Reference 2). The number of estimated roots specified has a significant effect on the actual eigensolutions extracted. However, the user, in general, will not have an a priori idea of the actual number of eigenvalues that may exist in a particular frequency range. Accordingly, the user should use his best judgment to specify this number. A number for the estimated roots that is larger than the actual number of roots in that range will, in general, yield a number of lower frequencies that are outside the specified frequency range.

It should also be noted here the eigensolutions resulting from any particular subcase will include not only the eigensolutions that are computed in that subcase, but also the eigensolutions resulting

from all previous subcases. Accordingly, regardless of which eigenvalue extraction method is employed, the number of desired roots specified on the EIGR card for a particular subcase must allow not only for the roots that will be computed by that subcase, but also include the roots computed by all of the previous subcases.

### Output from the Analysis

As mentioned earlier, the final results from the analysis will include the eigensolutions for all of the subcases specified in the Case Control Deck setup. The DMAP ALTER package given in Appendix A also generates the eigenvalue summary table and the eigenvalues for all of the subcases of the analysis. If the user so desires, he can suppress any of these intermediate results by commenting out the OFP modules corresponding to those subcases (see Appendix A). Also, for every subcase, the program indicates the number of roots from all previous subcases that are included in that subcase.

## EXAMPLES

Two examples were set up to illustrate the procedure discussed above. Details are given below. All of the runs were made on RPK's CRAY version of NASTRAN.

### Example 1

The standard NASTRAN Demonstration Problem No. D10-02-1A (see Reference 3) was selected for this example. This problem employs the Givens method for eigenvalue extraction. The cyclic frequencies obtained for this case are presented in Table 1.

This problem was then modified to use the Inverse Power method and eigensolutions for two frequency ranges (500.0 - 1000.0 hertz and 20000.0 - 30000.0 hertz) were requested using the procedure described above. The input data setup is given in Appendix B.

The cyclic frequencies obtained for this case are presented in Table 2. It can be seen that these frequencies are subsets of those in Table 1.

### Example 2

A variation of NASTRAN Demonstration Problem No. D03-08-1A (without any SUPORT data) (see Reference 3) was selected for this example. This problem also employs the Givens method for eigenvalue extraction. The cyclic frequencies obtained for this case are presented in Table 3.

This problem was then modified to use the FEER method and eigensolutions around three shift points or frequencies (100.0 hertz, 1500.0 hertz and 5300.0 hertz) were requested using the procedure described above. The input data setup is given in Appendix C.

The cyclic frequencies obtained for this case are presented in Table 4. It can be seen that these frequencies are subsets of those in Table 3.

The results of the above examples clearly demonstrate the validity and usefulness of the proposed method.

### ACKNOWLEDGMENT

The procedure described above was developed as part of RPK's continuing support of its CRAY version of NASTRAN at NASA's Marshall Space Flight Center in Huntsville, Alabama. The authors are thankful to Mr. David Christian of NASA-MSFC for triggering the study that made this work possible.

### CONCLUDING REMARKS

A novel procedure for obtaining eigenvalues and eigenvectors for multiple frequency ranges in a single NASTRAN execution is presented. The scheme is applicable to normal modes analyses employing the FEER and Inverse Power methods of eigenvalue extraction. The procedure is illustrated by examples. The procedure should be particularly helpful in large problems with widely separated frequency ranges.

### REFERENCES

1. The NASTRAN Theoretical Manual, NASA SP-221(06), January 1981.
2. The NASTRAN User's Manual, NASA SP-222(08), June 1986.
3. The NASTRAN Demonstration Problem Manual, NASA SP-224(05), December 31, 1978 Edition, Reprinted September 1983.

## APPENDIX A

### DMAP ALTERs for Obtaining Eigensolutions for Multiple Frequency Ranges in a Single NASTRAN Execution

```
$*****  
$ THE FOLLOWING ALTERS ARE FOR DISPLACEMENT RIGID FORMAT 3  
$ (NORMAL MODES ANALYSIS). SIMILAR ALTERS WILL WORK FOR  
$ OTHER RIGID FORMATS THAT INVOLVE REAL EIGENVALUE  
$ EXTRACTION.  
$  
$ NOTE THAT, FOR EVERY SUBCASE BEYOND THE FIRST SUBCASE, THE  
$ ALTERS BELOW INVOLVE A PAIR OF OFP AND READ MODULES.  
$*****  
$  
$ INSERT AFTER THE READ MODULE IN THE RIGID FORMAT  
$  
INSERT READ $ ON RPK-SUPPORTED VERSIONS  
$ USE ALTER 70 $ ON 1989 COSMIC-SUPPORTED VERSIONS  
$ USE OF ALTER 70 $ IS ALSO PERMITTED ON RPK-SUPPORTED VERSIONS  
$  
$ USE THE FOLLOWING OFP STATEMENT TO REQUEST THE EIGENVALUE  
$ SUMMARY TABLE AND THE EIGENVALUES THAT ARE AUTOMATICALLY  
$ OBTAINED BY THE RIGID FORMAT FOR THE FIRST SUBCASE  
$  
OFP      OEIGS,LAMA,,,//S,N,CARDNO $  
$  
$ COMPUTE THE EIGENSOLUTIONS FOR THE SECOND SUBCASE  
$ (THE LAST PARAMETER 2 IN THE FOLLOWING READ MODULE  
$ INDICATES THAT THE ANALYSIS IS FOR THE SECOND SUBCASE)  
$  
READ     KAA,MAA,MR,DM,EED,uset,CASECC/LAMA,PHIA,MI,OEIGS/  
         *MODES*/S,N,NEIGV/2 $  
$  
$ USE THE FOLLOWING OFP STATEMENT TO REQUEST THE EIGENVALUE  
$ SUMMARY TABLE AND THE EIGENVALUES FOR THE SECOND SUBCASE  
$ (THE RESULTS WILL INCLUDE THE RESULTS FOR THE FIRST SUBCASE)  
$  
OFP      OEIGS,LAMA,,,//S,N,CARDNO $  
$  
$ COMPUTE THE EIGENSOLUTIONS FOR THE THIRD SUBCASE  
$ (THE LAST PARAMETER 3 IN THE FOLLOWING READ MODULE  
$ INDICATES THAT THE ANALYSIS IS FOR THE THIRD SUBCASE)  
$
```

APPENDIX A  
(Continued)

READ KAA,MAA,MR,DM,EED,USET,CASECC/LAMA,PHIA,MI,OEIGS/  
\*MODES\*/S,N,NEIGV/3 \$

\$

\$ USE THE FOLLOWING OFP STATEMENT TO REQUEST THE EIGENVALUE  
\$ SUMMARY TABLE AND THE EIGENVALUES FOR THE THIRD SUBCASE  
\$ (THE RESULTS WILL INCLUDE THE RESULTS FOR THE FIRST AND  
\$ SECOND SUBCASES)

\$

OPF OEIGS,LAMA,,//S,N,CARDNO \$

.

.

.

.

.

\$

\$ COMPUTE THE EIGENSOLUTIONS FOR THE LAST SUBCASE  
\$ (THE LAST PARAMETER  $n$  IN THE FOLLOWING READ MODULE  
\$ SHOULD BE AN INTEGER VALUE CORRESPONDING TO THE LAST  
\$ SUBCASE, INDICATING THAT THE ANALYSIS IS FOR THE LAST SUBCASE)

\$

\$ THE FINAL RESULTS (WHICH INCLUDE THE RESULTS FOR ALL OF THE  
\$ SUBCASES) ARE AUTOMATICALLY OUTPUT BY THE RIGID FORMAT

\$

READ KAA,MAA,MR,DM,EED,USET,CASECC/LAMA,PHIA,MI,OEIGS/  
\*MODES\*/S,N,NEIGV/n \$

\$

CASE CASECC,/CASEXX/\*TRAN\* \$  
EQUIV CASEXX,CASECC \$  
ENDALTER \$

## APPENDIX B

### Input Data Setup for NASTRAN Demonstration Problem

No. D10-02-1A Modified to Use the Procedure Described

in the Paper

```
ID ...  
.   
.   
READFILE alters  
.   
.   
CEND  
.   
.   
SUBCASE 10  
    METHOD = 100  
SUBCASE 20  
    METHOD = 200  
.   
.   
BEGIN BULK  
.   
.   
EIGR,100,INV,500.0,1000.0,5,5,,+EIG1  
+EIG1,MAX  
EIGR,200,INV,20000.0,30000.0,10,10,,+EIG2  
+EIG2,MAX  
.   
.   
ENDDATA
```

## APPENDIX C

**Input Data Setup for NASTRAN Demonstration Problem  
No. D03-08-1A (Without Any SUPORT Data) Modified to  
Use the Procedure Described in the Paper**

```
ID ...  
. .  
READFILE alters  
. .  
CEND  
. .  
SUBCASE 11  
    METHOD = 1001  
SUBCASE 21  
    METHOD = 2001  
SUBCASE 31  
    METHOD = 3001  
. .  
BEGIN BULK  
. .  
EIGR,1001,INV,100.0,,,5,,,+EIG1  
+EIG1,MAX  
EIGR,2001,INV,1500.0,,,10,,,+EIG2  
+EIG2,MAX  
EIGR,3001,INV,5300.0,,,12,,,+EIG3  
+EIG3,MAX  
. .  
ENDDATA
```

**TABLE 1****Natural Frequencies for NASTRAN  
Demonstration No. D10-02-1A**

Mode No.	Cyclic Frequency (Hz)
1	3.996147E+01
2	2.364137E+02
3	2.504423E+02
4	7.014011E+02
5	7.034198E+02
6	1.153105E+03
7	1.375429E+03
8	1.574398E+03
9	1.956923E+03
10	2.277239E+03
11	2.291261E+03
12	2.569183E+03
13	2.783842E+03
14	2.929954E+03
15	3.003921E+03
16	3.411562E+03
17	4.786588E+03
18	6.412708E+03
19	8.291552E+03
20	1.030759E+04
21	1.371895E+04
22	1.657422E+04
23	2.009181E+04
24	2.424947E+04
25	2.913932E+04
26	3.485085E+04
27	4.136255E+04
28	4.828881E+04
29	5.437856E+04
30	6.805413E+04

**TABLE 2**

**Natural Frequencies for NASTRAN Demonstration  
No. D10-02-1A Modified to Use the Procedure  
Described in the Paper**

Computed Mode No.	Corresponding Mode No. in Table 1	Cyclic Frequency (Hz)	Subcase in Which Computed (See Appendix B)
1	2	2.364137E+02	First
2	3	2.504423E+02	First
3	4	7.014011E+02	First
4	5	7.034198E+02	First
5	22	1.657422E+04	Second
6	23	2.009181E+04	Second
7	24	2.424947E+04	Second
8	25	2.913932E+04	Second
9	26	3.485085E+04	Second

**TABLE 3****Natural Frequencies for NASTRAN  
Demonstration No. D03-08-1A  
(Without Any SUPORT Data)**

Mode No.	Cyclic Frequency (Hz)
1	7.341481E-04
2	4.168523E-04
3	6.790643E-05
4	1.505714E-04
5	2.765971E-04
6	6.434454E-04
7	2.987344E+00
8	3.372945E+00
9	2.447569E+01
10	2.682217E+01
11	6.154903E+01
12	7.034309E+01
13	1.133579E+02
14	1.174531E+02
15	1.646037E+02
16	2.902883E+02
17	2.905903E+02
18	4.508246E+02
19	4.515298E+02
20	6.945689E+02
21	6.953026E+02
22	8.685333E+02
23	9.752645E+02
24	9.752699E+02
25	1.343024E+03
26	1.344180E+03
27	1.466313E+03
28	1.569195E+03
29	1.912914E+03
30	1.918371E+03
31	2.025981E+03
32	2.446537E+03
33	2.446840E+03
34	2.458828E+03
35	2.742675E+03
36	2.971822E+03
37	3.918531E+03
38	3.918534E+03
39	4.451851E+03
40	6.261906E+03
41	8.528055E+03

**TABLE 4**

**Natural Frequencies for NASTRAN Demonstration  
No. D03-08-1A (Without Any SUPORT DATA) Modified  
to Use the Procedure Described in the Paper**

Computed Mode No.	Corresponding Mode No. in Table 3	Cyclic Frequency (Hz)	Subcase in Which Computed (See Appendix C)
1	9	2.447569E+01	First
2	10	2.682217E+01	First
3	11	6.154903E+01	First
4	12	7.034309E+01	First
5	13	1.133579E+02	First
6	14	1.174531E+02	First
7	25	1.343024E+03	Second
8	26	1.344180E+03	Second
9	27	1.466313E+03	Second
10	28	1.569195E+03	Second
11	39	4.451851E+03	Third
12	40	6.261906E+03	Third

RANDOM VIBRATION ANALYSIS  
OF SPACE FLIGHT HARDWARE USING NASTRAN

S. K. Thampi and S. N. Vidyasagar  
GE Government Services  
1050 Bay Area Blvd.  
Houston, TX 77058

During liftoff and ascent flight phases, the Space Transportation System (STS) and payloads are exposed to the random acoustic environment produced by engine exhaust plumes and aerodynamic disturbances. The analysis of payloads for randomly fluctuating loads is usually carried out using the Miles' relationship. This approximation technique computes an equivalent load factor as a function of the natural frequency of the structure, the power spectral density of the excitation, and the magnification factor at resonance. Due to the assumptions inherent in Miles' equation, random load factors are often over-estimated by this approach. In such cases, the estimates can be refined using alternate techniques such as time domain simulations or frequency domain spectral analysis. This paper describes the use of NASTRAN to compute more realistic random load factors through spectral analysis. The procedure is illustrated using Spacelab Life Sciences (SLS-1) payloads and certain unique features of this problem are described. The solutions are compared with Miles' results in order to establish trends at over or under prediction.

## INTRODUCTION

During the past decade, the U.S. Spacelab program has made significant contributions to the advancement of space exploration and research. The Spacelab is a reusable laboratory that is carried in the cargo bay of the Space Shuttle. Experiments in several different disciplines such as astronomy, life sciences, and material science are accommodated in this modular laboratory for various shuttle missions. The module also contains utilities, computers, and work areas to support the experiments. The experiment hardware is mounted in instrument racks located on either side of the module, in overhead lockers, or in the center aisle, as shown in Figure 1.

During liftoff and ascent flight events, the Shuttle and its payload are exposed to the acoustic environment produced by engine exhaust plumes and aerodynamic disturbances. Random vibrations are created by the response of the module shell to the acoustic noise inside the cargo bay. The vibrations of the shell are transmitted through the support structures (racks, mounting frames, etc.) to the payload equipment. The vibration levels that the equipment has to withstand depend on its own dynamic characteristics and its location inside the Spacelab. The equipment and its structural interfaces must be analyzed for these random loads in order to ensure the integrity and flight worthiness of the system.

The analysis of flight hardware for random loads often relies on approximate formulations like the Miles' relation (ref. 1) to generate limit load factors for structural design. Due to the assumptions inherent in Miles' equation, the random vibration criteria developed through this approach tend to be over-conservative. In such cases, the results can be refined using alternate analysis techniques like time domain simulations or frequency domain spectral analysis. This paper describes the use of NASTRAN to perform spectral analysis to establish more realistic design loads. The procedure is illustrated using the Neck Chamber Pressure System (NCPS) assembly which will be flown on the Spacelab Life Sciences (SLS-1) mission.

## ANALYSIS BASED ON MILES' EQUATION

For a lightly damped single-degree-of-freedom (SDOF) oscillator subjected to random excitation through its base motion, Miles' relation is used as follows.

$$N_r = 3 \sqrt{\frac{\pi}{2}} f_n A Q \quad (1)$$

$N_r$  is the limit random load factor (g units),  $f_n$  is the resonance frequency (Hz) of the SDOF system,  $A$  is the power spectral density ( $g^2/Hz$ ) of base acceleration at the resonance frequency, and  $Q$  is the dynamic magnification factor at

resonance. The quantity under the square root represents the mean square acceleration response and the factor 3 indicates the 3-sigma probability of occurrence, i.e., the probability of exceeding  $N_r$  is 0.26%.

The mean square response is the area under the response spectral density curve and is given by

$$\langle u^2 \rangle = \int S(\omega) |H(\omega)|^2 d\omega \quad (2)$$

where  $H(\omega)$  is the transfer function of the system,  $S(\omega)$  is the base acceleration spectral density function, and  $\omega$  is the frequency in radians. The derivation of Miles' relation is based on the following simplifying assumptions for evaluating the integral in Eqn (2).

- 1) The actual spectral density of base excitation,  $S(\omega)$ , is a slowly varying function in the vicinity of resonance. It can be conveniently approximated by a constant or white-noise spectral density,  $A = S(\omega_n)$ , for computing the mean square response.
- 2) Only the excitation energy contained within the system's bandwidth is transmitted. The rest is filtered away by the system and does not contribute to the mean square response.

These assumptions are valid in the case of lightly damped systems with damping factor  $\xi \ll 1$ . For such systems, the function  $|H(\omega)|^2$  is very sharply peaked at  $\omega = \omega_n$ , and reduces to half its peak value at a short distance,  $2\xi\omega_n$ , on either side of the peak. This distance, called the half power bandwidth, is very narrow for lightly damped systems. With the assumptions mentioned above, the integral in Eqn. 2 can be approximated by a rectangular area with base equal to the bandwidth and height equal to the product of the constant value of excitation spectral density and the peak value of transmittancy. This gives

$$\langle u^2 \rangle \simeq \frac{\Pi}{2} f_n A Q \quad (3)$$

from which Miles' relation follows.

In order to use Miles' relation for the analysis of flight hardware, the natural frequency of the equipment is first determined through analysis or test. The input random excitation spectrum for the equipment is then determined as a function of its location, its mounting configuration, and its mass. The input excitation spectrum has been established using data from previous flight or ground tests and is provided in the Spacelab Payload Accomodation Handbook (ref. 2). The spectral density at the resonance frequency of the component is found from this data. The dynamic magnification factor at resonance  $Q = 1/2 \xi$ , is indicative of the system damping and is determined experimentally. For

components mounted on isolators,  $Q$  is determined from the manufacturer's data on the isolator mounting. These values are substituted in Eqn (1) to obtain the design random load factor,  $N_r$ . As the random vibration environment occurs simultaneously with other load environments during various mission phases, the estimated values of  $N_r$  are combined with the appropriate quasi-static, thermal, pressure, and crew-induced load factors to generate design load cases for component analysis.

Due to the assumptions inherent in Miles' relation and the idealization of the component as a single-degree-of-freedom resonator, the computed random load factors will be approximate. They tend to be overly conservative, especially when the natural frequency of the system is close to the peak frequency of the excitation spectrum. When the predicted random loads are unreasonably high, they lead to difficult design problems and alternate approaches are necessary to refine the random load estimates.

## ANALYSIS BASED ON SPECTRAL ANALYSIS

The dynamic behaviour of large structural/mechanical systems can be adequately predicted only by multi-degree-of-freedom (MDOF) models. For linear MDOF systems, the dynamic characteristics are specified by a matrix of transfer functions,  $[H]$ , whose elements  $H_{jk}$  represent the ratio of steady-state response at point  $j$  to a sinusoidal excitation at point  $k$ . For displacement response

$$[H(\omega)] = [-[M] \omega^2 + i [B] \omega + [K]]^{-1} \quad (4)$$

where  $[M]$ ,  $[B]$ , and  $[K]$  represent the mass, damping, and stiffness matrices of the discrete model and  $\omega$  is the excitation frequency.

The response of linear MDOF systems subjected to random excitation can be computed using well-established spectral analysis techniques. According to the theory of random vibrations, the response of a linear system with transfer function  $[H(\omega)]$ , subjected to a stationary random load  $\{P(t)\}$ , is given by

$$[S_{uu}(\omega)] = [H(\omega)] [S_{pp}(\omega)] [H^*(\omega)]^T \quad (5)$$

where  $[S_{uu}(\omega)]$  and  $[S_{pp}(\omega)]$  are the matrices of response and excitation spectral density functions and  $*$  and  $T$  represent the complex conjugate and transpose operations, respectively. These matrices will have real auto-spectral density functions as their diagonal elements and complex cross-spectral density functions as their off-diagonal elements. By integrating the area under the response spectral density curve, the mean square response at any nodal point in the model can be obtained. The foregoing development for mean-square displacement response can be generalized to provide mean-square values for other response quantities such as velocity, acceleration, or stress. It is only

necessary to replace the transfer function matrix for displacement by the corresponding transfer function matrix for the desired response. The generalization also applies to the excitation which may be a point force, a loading condition (i.e., an ensemble of applied forces that are perfectly correlated), or enforced motion.

The analysis of flight hardware subjected to random excitation can be carried out using the spectral analysis features of NASTRAN. A finite element model of the component is created which can accurately represent all its dominant modes in the excitation frequency range. The response calculations are carried out in two separate functional modules. First, the transfer function of the system corresponding to the desired response is computed in the Frequency Response module and then, the power spectral densities and other response statistics are computed in the Random Analysis module. The direct or modal superposition approaches can be used to perform the frequency response analysis. For each excitation source,  $p_k$ , the nodal response,  $u_j$ , is determined at a series of user specified frequencies,  $\omega_i$ . The ratio of output to input represents the transfer function element,  $H_{jk}(\omega_i)$ . This is determined for each excitation source and the transfer function matrix,  $[H]$ , is assembled from the results.

In NASTRAN, random vibration analysis is treated as a data reduction procedure that is applied to the results of frequency response analysis. The inputs to the random analysis module are the frequency responses of desired output quantities due to different load sources and the auto- and cross-spectral densities of these random load sources. Each load source is referred to by a separate subcase in the case control deck and their spectral densities are specified as tabular functions of frequency in bulk data cards. If the sources are statistically uncorrelated, only the auto-spectral densities need be defined. The power spectral densities of response are calculated using Eqn (5) and the root-mean-square (rms) response is evaluated by numerically integrating the area under the spectral density curve. The results are printed and plotted for specified degrees of freedom of the model.

As mentioned earlier, the random excitation applied to the structure could be a force, an enforced motion, or some other general form of excitation. In the case of Spacelab payloads, the random excitation is specified in terms of an acceleration spectrum applied at the structural support points. The "large mass" approach may be used to simulate this loading condition. This involves lumping a fictitious large mass,  $M_a$ , at the degree of freedom in which the acceleration is to be enforced. An applied force equal to  $M_a$  times the required acceleration is also prescribed for that degree of freedom. The inertia force is made so dominant through this operation that the resulting acceleration is very close to the required value.

## ILLUSTRATIVE EXAMPLE

The development of random vibration load factors for flight hardware is illustrated in this section using the Neck Chamber Pressure System assembly (NCPS). This Life Sciences Laboratory equipment item is used to study the effect of weightlessness on human cardiovascular control mechanisms and will be flown on a future Space Shuttle mission. The NCPS assembly is composed of an experiment enclosure which houses several components including a central processing unit, a motor control unit, two motor driven bellows, and a pressure gauge (Fig. 2). The assembly is mounted in an experiment rack using two support rails which are attached to the front and rear rack posts on either side. The front panel of the enclosure is bolted to the front rack post flanges at eight locations. The whole assembly weighs 48 pounds, and the installation kit including the slides, fittings, and fasteners weighs an additional five pounds.

A finite element model of the NCPS assembly is constructed using mostly plate (CQUAD2 and CTRIA2) and bar (CBAR) elements. The model has a total of 206 grid points and 192 structural elements. The masses of internal components are lumped at the respective centers of gravity, and stiff bar elements are used to connect them to the attachment points. The fasteners are modelled using rigid elements. Eigenanalysis was performed on the model with free boundary conditions to verify that the model has six rigid body modes. The analysis is repeated, with the rack-to-component interface points appropriately constrained, in order to determine the flexible modes of the component. The first twenty frequencies of the constrained model are shown in Table 1. An inspection of the modal deformation plots and mass participation factors shows that the first system mode in X direction is 80 Hz. The power spectral density of the input excitation corresponding to this frequency is found to be 0.02 g<sup>2</sup>/Hz from Figure 3. For a conservative estimate of Q = 10 for the dynamic magnification factor, Miles' relation (Eqn 1) yields

$$N_{rx} = 15.04 \text{ g units} \quad (6)$$

Random load factors,  $N_{ry}$  and  $N_{rz}$ , are computed in a similar manner.

Random load factors can also be determined through spectral analysis. The computation of  $N_{rx}$  is described here for comparison with the Miles' approach. The transfer function of the system is first determined by applying a unit sinusoidal load in the X direction at each point where the NCPS interfaces with the rack structure. The load is applied through the DLOAD and RLOAD cards which in turn refers to DELAY, DPHASE, DAREA, and TABLED cards. For a constant phase, unit sinusoidal input, the DELAY and DPHASE cards may be omitted and a unit value specified for all frequencies on the TABLED card. The input acceleration spectrum (Fig. 3) is specified through RANDPS and TABRND cards. This random acceleration is enforced at all the interface points in the X direction using the large mass approach. A fictitious mass,  $M_a$ , about 1000 times larger than the existing grid point mass, is lumped at the interface X degree of freedom using a CMASS2 card and an equal value is specified in the

corresponding DAREA load card. This produces the desired acceleration which can be verified by plotting the acceleration spectrum at the input points and comparing it with Figure 3. If the agreement is not adequate, the value of  $M_a$  is increased until a good match is obtained.

The direct and modal solution techniques are used to carry out the response calculations. The relative efficiency of the two approaches depends on several factors including the number of modes retained in the analysis and the number of response frequencies. The selection of these parameters always represents a compromise between accuracy and efficiency. The frequencies chosen for response computations should have good resolution in the vicinity of system resonances in order to obtain reliable estimates of rms response. A total of 150 frequencies in the 0 to 500 Hz range are used for this analysis. The specification of damping properties in the direct and modal formulations are somewhat different. In the direct formulation, structural damping proportional to the stiffness matrix terms is specified both on the material data cards and as an overall uniform damping factor on the PARAM G data card. In the modal formulation, the damping factor is specified as a tabular function of frequency through the SDAMPING and TABDMP1 cards to represent the variation of structural damping for different modes. A damping factor of 0.1 is used for this analysis in order to be consistent with  $Q = 10$  used in Miles' relation.

The set of output points at which the response power spectrum and rms values are to be recovered must be chosen judiciously. The selection can be based on the same criteria used for choosing an ASET (analysis set of dynamic degrees of freedom); namely, the points should be uniformly dispersed throughout the structure and should include all large mass items. A set of 12 output points were chosen for the NCPS and the rms acceleration response at these points is computed (Table 2). When these values are averaged and the 3-sigma probability of occurrence criteria is applied, one obtains

$$N_{rx} = 10.67 \text{ g units} \quad (7)$$

This is almost 30% less than the value predicted using Miles' relation.

The rms response calculated using the direct and modal solution techniques is summarized in Table 2. For the same number of response frequencies, the modal solution required 350 seconds of CPU time with 20 modes included, 450 seconds with 40 modes, 600 seconds with 60 modes, whereas the direct solution required 13160 seconds. The response spectrum at selected output points on the model is shown in figures 4, 5, and 6. The solution obtained with 20 modes is clearly inadequate while the plots obtained using 60 modes and the direct approach are virtually indistinguishable. The spectra characteristically peak at 80 Hz which corresponds to the first X mode of vibration. The effects of higher modes can also be seen in the spectral plots.

## CONCLUDING REMARKS

An alternate method of estimating random vibration load factors for design and analysis of Spacelab payloads is presented. This method, based on spectral analysis, yields more refined random load estimates at the expense of being computationally more intensive than the Miles' approach. The computational effort can be reduced by using the modal formulation rather than the direct formulation for analysis. Significant reductions can be obtained in the random load estimates using this method. While the actual reduction depends upon the payload configuration being analyzed, reductions of 20 to 30% are typical. This method could be used to resolve difficult design problems owing to unreasonably high random load predictions by the Miles' relation.

## REFERENCES

1. Harris, C. M. and Crede, C. E., "Shock and Vibration Handbook," 2nd Edition, McGraw Hill Book Company, Inc., New York, 1976, pp.24-28.
2. Spacelab Payload Accomodation Handbook: Appendix B, SLP/2104-2, NASA Marshall Space Flight Center, October 1989.

TABLE I. EIGENVALUE ANALYSIS SUMMARY

MODE NO.	EIGENVALUE	RADIAN FREQUENCY	CYCLIC FREQUENCY
1	5.606682E+04	2.367843E+02	3.768539E+01
2	8.630755E+04	2.937815E+02	4.675677E+01
3	9.900016E+04	3.146429E+02	5.007697E+01
4	1.228704E+05	3.505287E+02	5.578837E+01
5	1.483150E+05	3.851169E+02	6.129326E+01
6	1.896878E+05	4.355316E+02	6.931701E+01
7	2.301971E+05	4.797886E+02	7.636072E+01
8	2.535269E+05	5.035146E+02	8.013683E+01
9	3.989269E+05	6.316066E+02	1.005233E+02
10	4.230480E+05	6.504214E+02	1.035178E+02
11	4.433938E+05	6.658782E+02	1.059778E+02
12	4.683294E+05	6.846459E+02	1.089170E+02
13	5.100052E+05	7.141465E+02	1.136599E+02
14	5.928444E+05	7.699639E+02	1.225435E+02
15	7.732380E+05	8.793395E+02	1.399512E+02
16	7.972504E+05	8.928888E+02	1.421077E+02
17	8.693909E+05	9.324113E+02	1.483979E+02
18	9.891926E+05	9.945816E+02	1.582926E+02
19	1.104014E+06	1.050721E+03	1.672274E+02
20	1.231224E+06	1.109605E+03	1.765992E+02
21	1.492994E+06	1.221881E+03	1.944685E+02

TABLE II RMS ACCELERATION RESPONSE SUMMARY

GRID POINT	LOCATION	MODAL SOLUTION			DIRECT SOLUTION (g)
		20 MODES (g)	40 MODES (g)	60 MODES (g)	
5059	Rear Left Side Panel	2.07	3.50	3.52	3.52
5080	Rear Right Side Panel	2.06	3.97	3.99	3.98
5056	Front Left Side Panel	2.47	2.47	2.49	2.50
5077	Front Right Side Panel	2.47	2.47	2.49	2.50
5076	Top Left Rear Panel	2.08	4.53	4.58	4.58
5073	Top Left Front Panel	2.24	2.48	2.87	2.88
5094	Top Right Front Panel	2.24	2.48	2.87	2.88
5097	Top Right Rear Panel	2.08	4.89	4.91	4.91
5193	M/C Unit	2.07	4.33	4.46	4.46
5204	CPU Unit	2.81	3.89	3.95	3.95
5205	M/C Mount	2.12	4.03	4.04	4.03
5042	Front Panel	2.47	2.47	2.49	2.50
Average		2.26	3.46	3.55	3.56

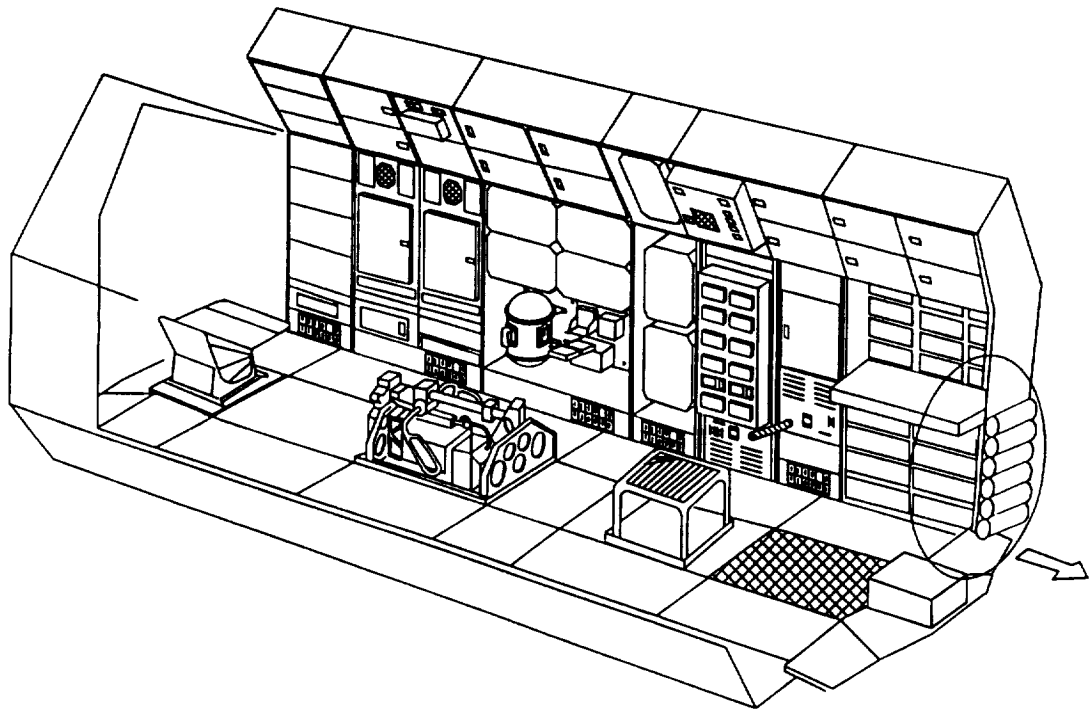
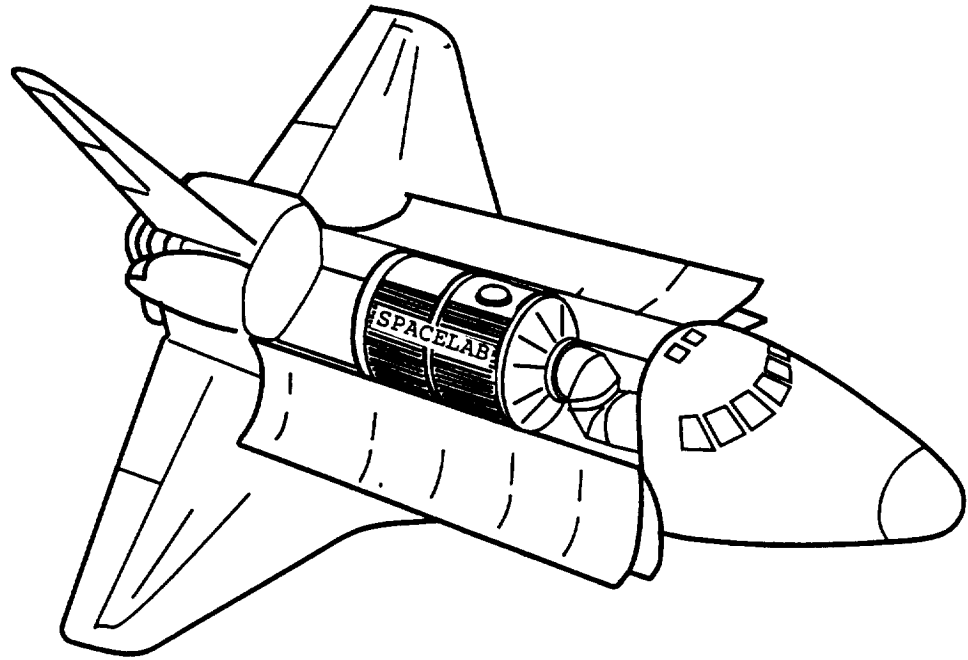


FIG. 1. TYPICAL SPACELAB CONFIGURATION

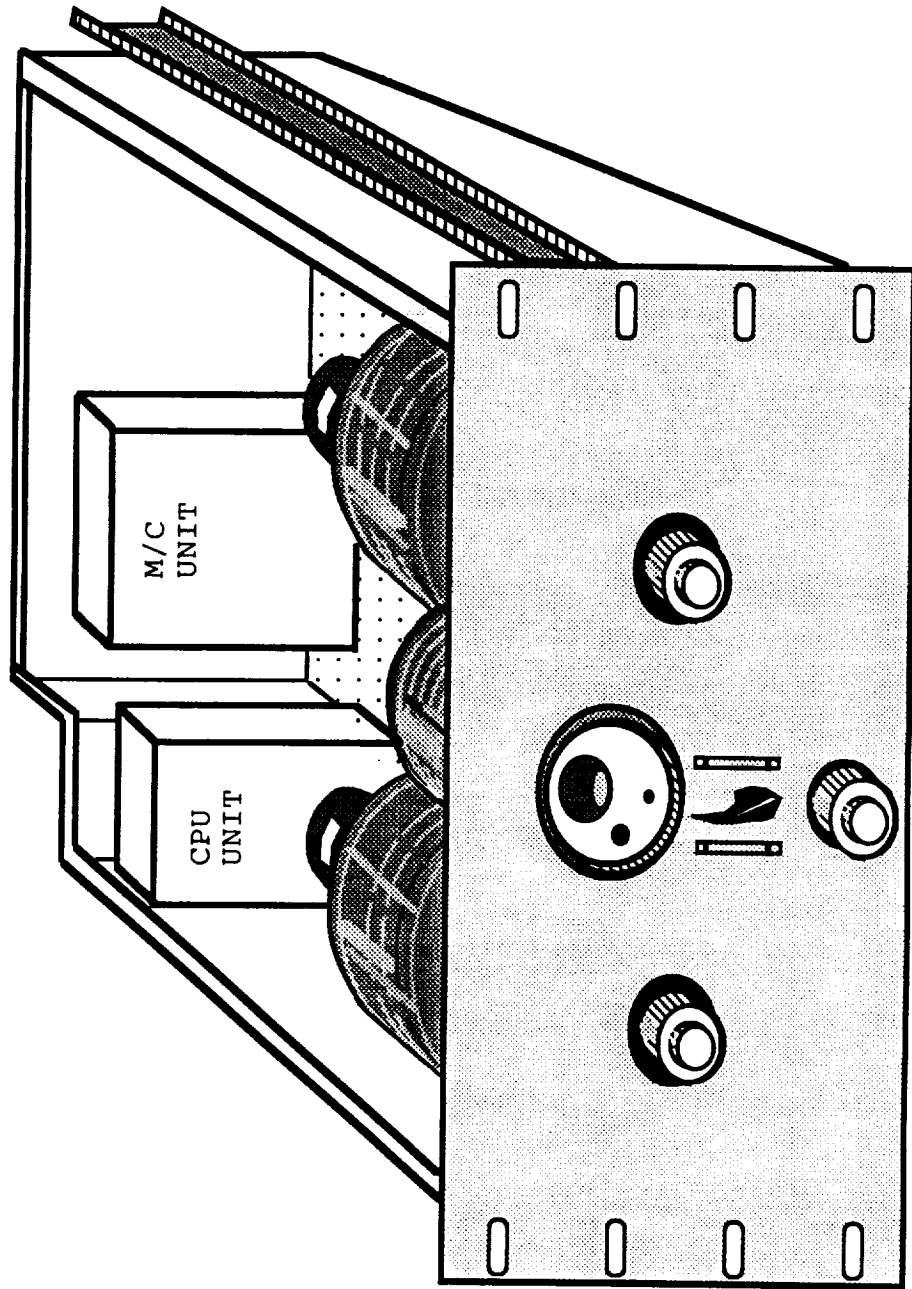


FIG. 2. SCHEMATIC OF THE NECK CHAMBER PRESSURE SYSTEM ASSEMBLY

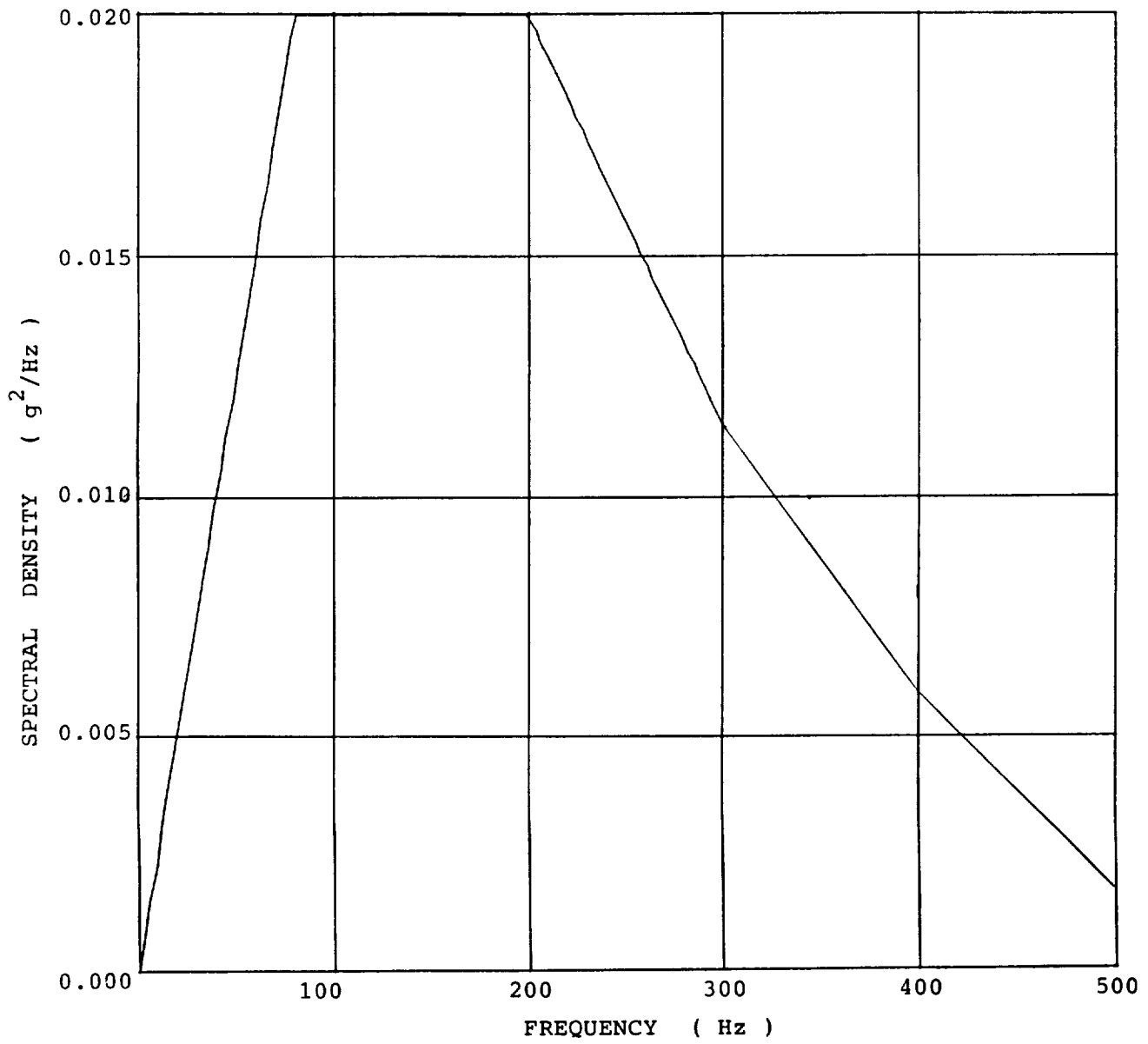


FIG. 3. INPUT ACCELERATION SPECTRUM

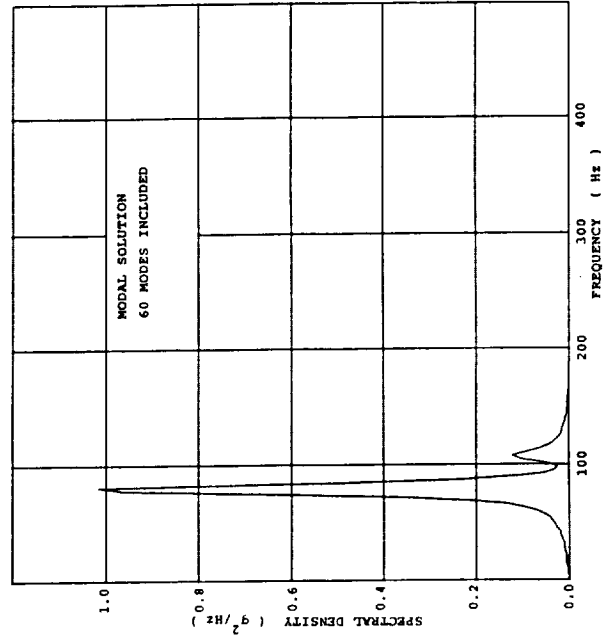
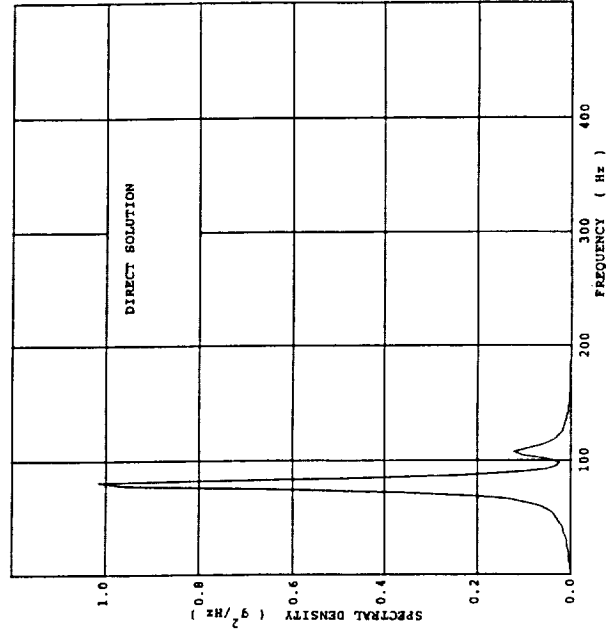
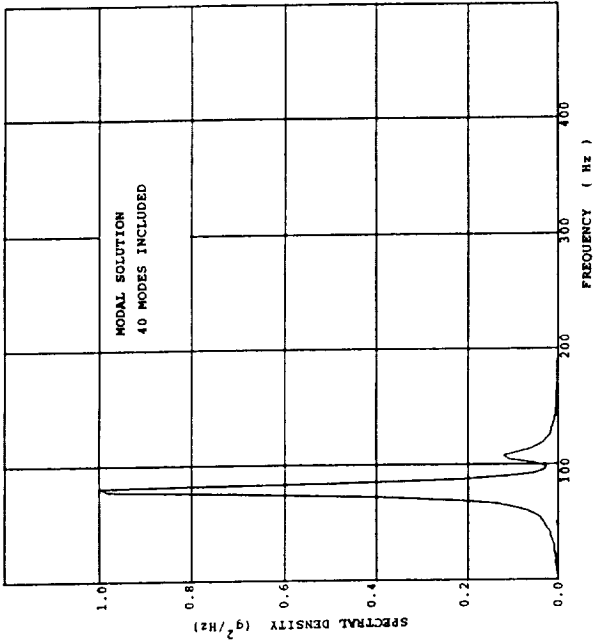
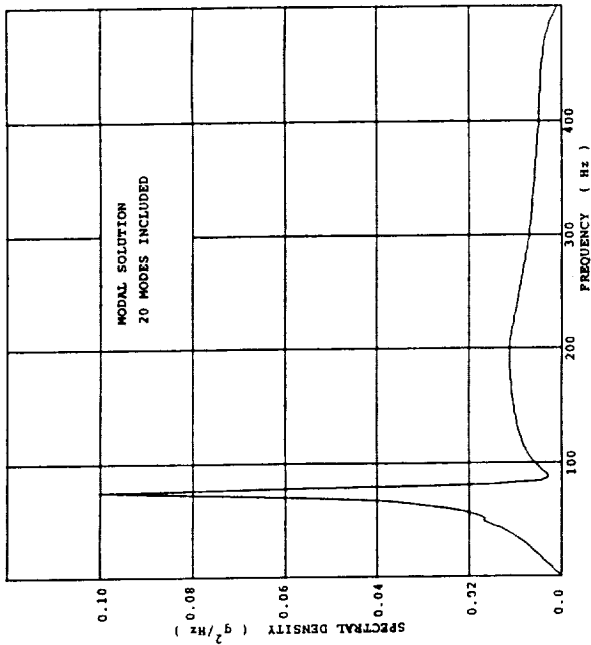


FIG. 4. ACCELERATION RESPONSE SPECTRUM AT GRID POINT 5073

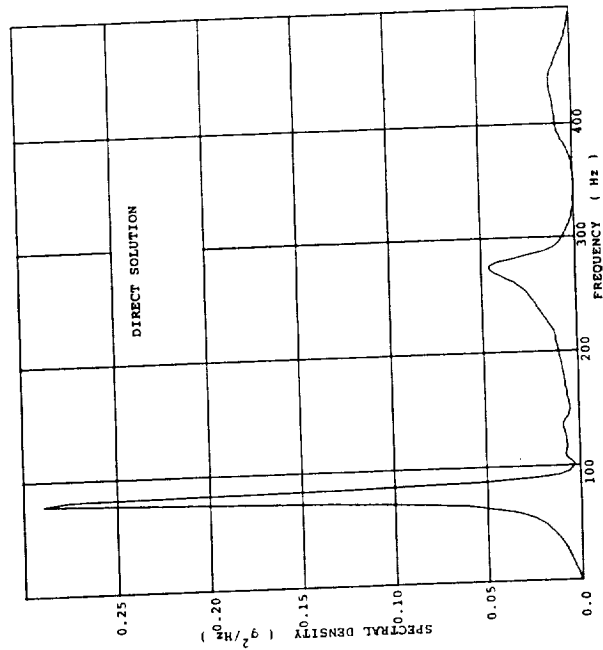
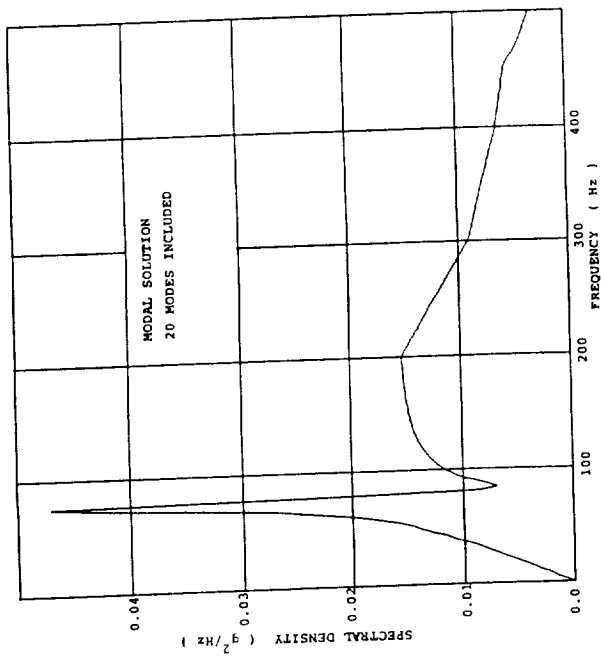
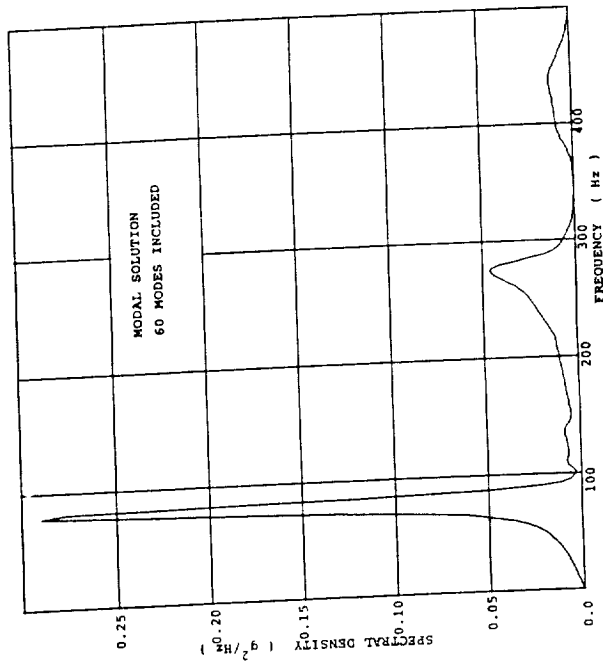
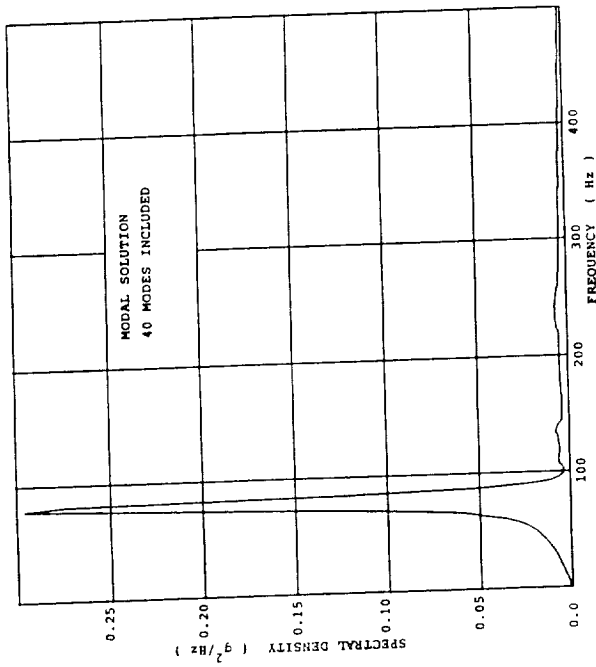


FIG. 5. ACCELERATION RESPONSE SPECTRUM AT GRID POINT 5205

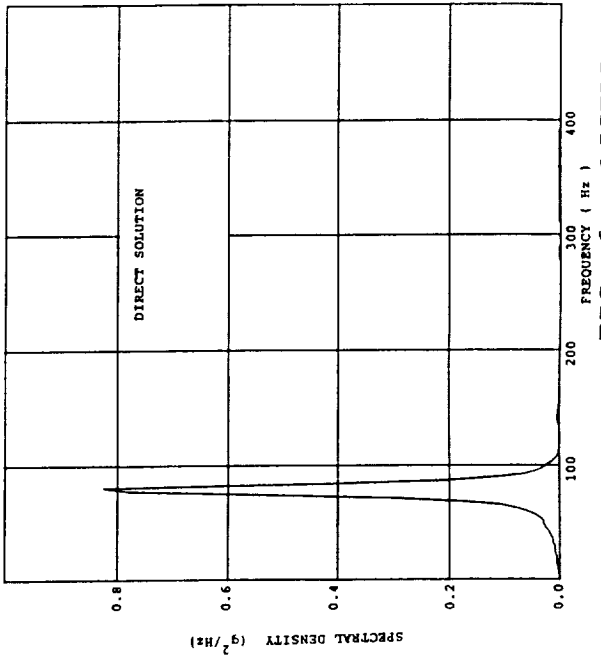
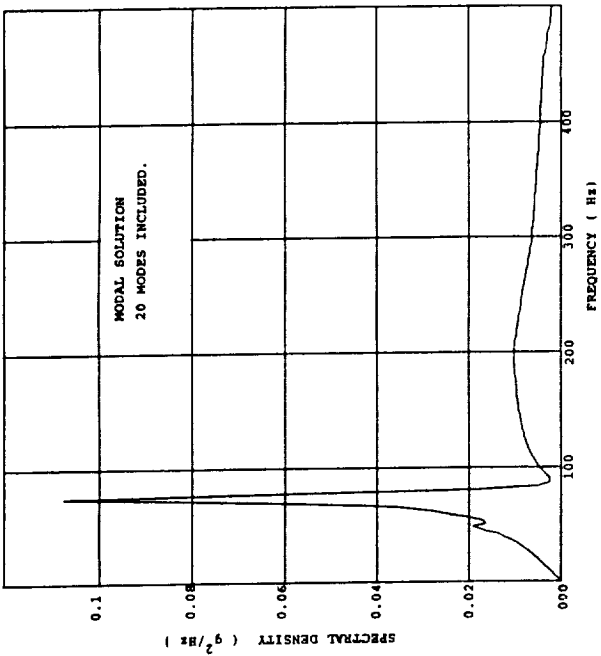
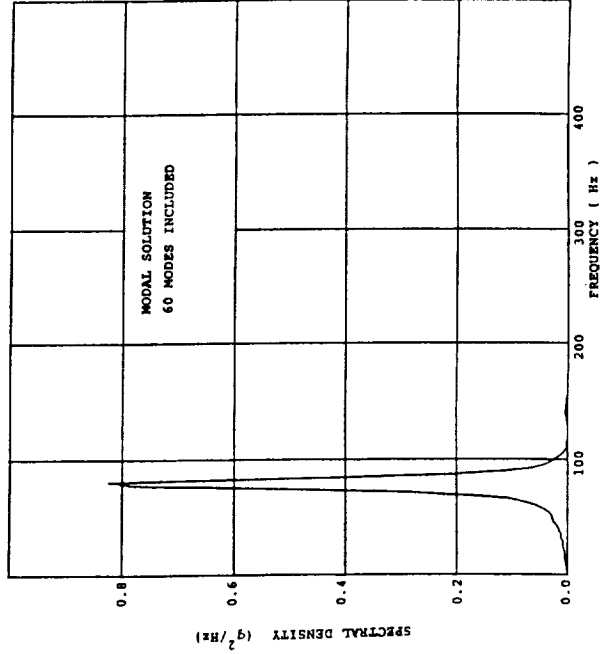
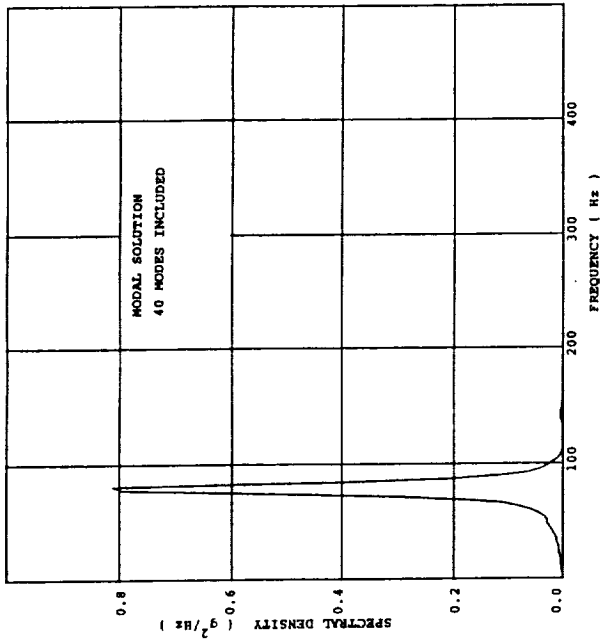


FIG. 6. ACCELERATION RESPONSE SPECTRUM AT GRID POINT 5059

N90-24646

19-39

375 380

SB.

## OBTAINING AN EQUIVALENT BEAM

THOMAS G. BUTLER

BUTLER ANALYSES

In modeling a complex structure I was faced with a component that would have logical appeal if it were modeled as a beam. It was a mast of a robot controlled gantry crane. The structure up to this point already had a large number of degrees of freedom, so the idea of conserving grid points by modeling the mast as a beam was attractive. I decided to make a separate problem of the mast and model it in three dimensions with plates then extract the equivalent beam properties by setting up the loading to simulate beam like deformations and constraints. The results could then be used to represent the mast as a beam in the full model. This seemed to be a straight forward approach, but it was sufficiently challenging that it merited publishing a paper on this topic.

The endeavor is to obtain the area  $A$ , the area moments of inertia  $I_1$  and  $I_2$ , and torsional area moment of inertia  $J$  of a prismatic beam that would be an equivalent of the crane mast over its full length. The detailed model involved about 4500 unconstrained degrees of freedom. The mast structure was essentially a hollow steel tube of square section with a cylindrical indentation along its length on one surface only. Complications that made it difficult to estimate equivalent properties analytically were the placement of two types of interior partial shear stiffeners at regular intervals along its length. These two different types of shear stiffeners alternated on opposite sides from each other most of the length. This posed no difficulty to model

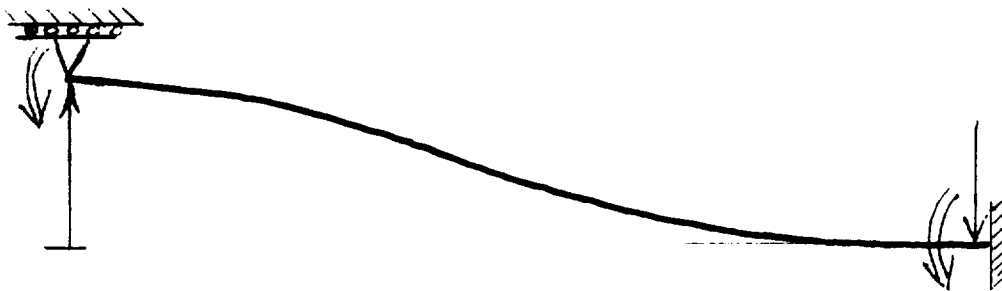
## OBTAINING AN EQUIVALENT BEAM

elastically in a three dimensional model. The interesting phase is the loading of the 3-D model in order to simulate beam action.

To put the problem in perspective, review for the moment, the definition of beam stiffness.

DEFINITION: Beam stiffness is the array of forces produced at the six degrees of freedom on both ends when a single degree of freedom at one end is deformed a unit amount while enforcing all other eleven degrees of freedom at both ends to be zero.

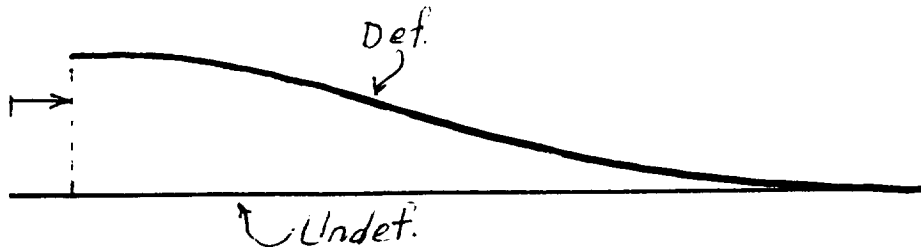
But the Bernoulli Euler formulation of the beam as used in finite element analysis programs does not faithfully follow this prescription of stiffness to the letter. For example, when one end is displaced a unit transversely, action is assumed to occur in - plane only. Diagrammatically the boundary conditions of the centroid of the B.E. formulation are indicated in the sketch.



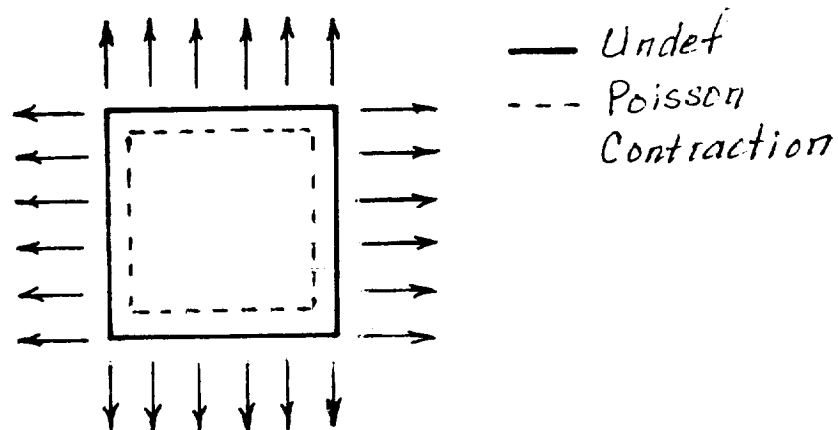
Note that the length remains invariant, because its transversely deformed end is not constrained in the axial direction. In effect, with this B.E. approach, the end position contracts when

## OBTAINING AN EQUIVALENT BEAM

bending deformation occurs. This is shown in exaggerated fashion in the sketch.

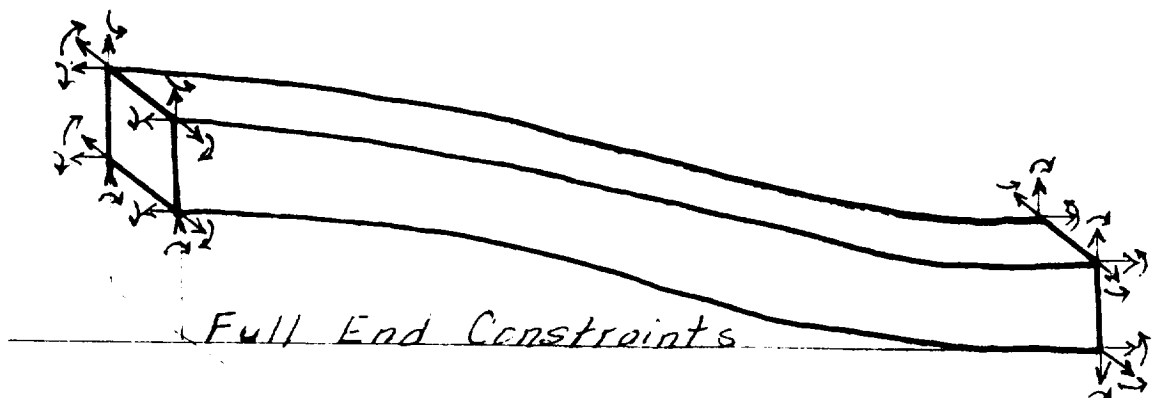
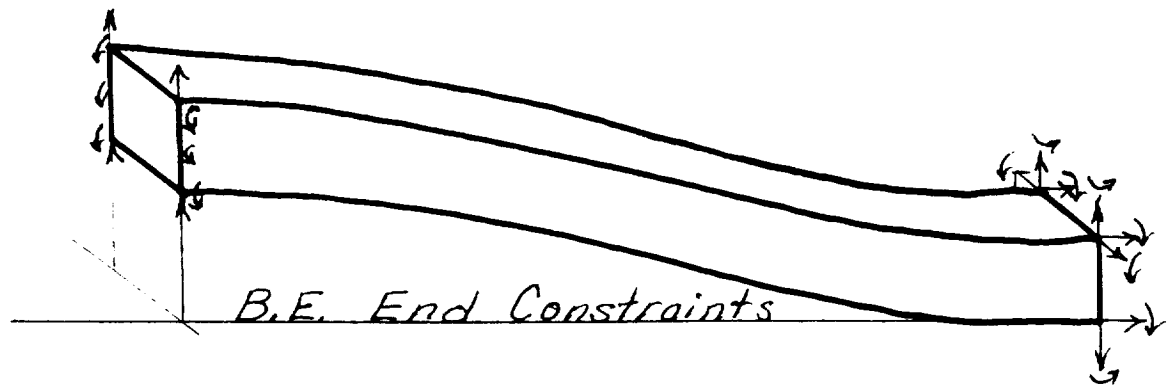


If the length is not allowed to deform, Poisson deformation does not occur and therefore needs no constraining force to inhibit Poisson deformation. But if the true definition of beam stiffness were adhered to in the finite element beam, the axial positions of the ends would be held to zero displacement and the beam would lengthen as transverse deformation occurs. Such axial stretching would result in Poisson contraction in both transverse directions. But if transverse translational deformations were held to zero, as the definition of stiffness demands, such constraints would exert forces to prevent Poisson contraction. For instance, the transverse forces at the end of a solid beam of square section with a full set of constraints applied would appear as sketched.



## OBTAINING AN EQUIVALENT BEAM

The dilemma now is to try to define what kind of equivalence should be sought. If A, I1, I2, and J were obtained with true stiffness constraints, would it be proper to operate as an equivalent beam according to those entries on the property card, so as to exclude bending/axial coupling even though such action was present during the sample run? Or would it be more proper to use only B.E. conditions to get the properties that will be used as a B.E. beam? If the latter were chosen, the question arises as to how faithfully we would be representing equivalence to the true structure. Having some doubts as to how to proceed, I modeled the constraints in two different ways; with full end constraints and with B.E. end constraints and compared the results. The sketch shows the constraints imposed for the two models. One of the things to consider in the B.E. simulation is that the theory requires planes to remain plane in bending.





## OBTAINING AN EQUIVALENT BEAM

### COMPARISON OF PROPERTIES DERIVED FROM MODELS OF DIFFERENT CONSTRAINTS VS MANUAL CALCULATIONS

SOURCE	A	I1	I2	J
FULL CONSTRAINTS	36.72	2,444.47	2,605.14	INVALID
B.E. CONSTRAINTS	36.66	728.63	853.62	600.19
MANUAL	35.96	2,541.82	3,517.62	4,710.60

This exercise had some unexpected results. The whole purpose of the exercise was to get an equivalent beam by using a full 3-D model instead of making an analytical estimate because of the uncertainty in being able to represent the effect of the partial shear panels correctly. One expects that the effect of the shear panels is to stiffen the steel tube, but the 3-D results showed less stiffness than the manual check which neglected the panels. Why?

In going back to examine the axial displacements in the 3-D model using the B.E. constraints, it indicated that the end faces tilted instead of remaining perpendicular to the undeformed centroidal axis as the B.E. theory requires. The total burden of meeting the requirement of zero slope at the displaced end was put on the QUAD4 elements which formed the side panels of the steel tube. That is; the open ended tube had two surfaces that could carry such bending and two surfaces unable to carry in-plane shear about their normals. Even those that picked up such bending couldn't transmit this moment to the QUAD's on the

## OBTAINING AN EQUIVALENT BEAM

perpendicular surface, so an inadequate moment developed to produce a net slope of zero at the centroid. By letting the end points displace axially they were in no position to create couples to satisfy the moments for zero slope. That is why the model with the B.E. constraints produced inadequately stiff sectional properties in bending and torsion.

Going back to the model with fully constrained ends, the explanation as to why this model was also inadequate for simulating an equivalent beam was this. Even though it did develop couples which formed the resisting moment for zero end slope by holding the axial displacements to zero; it still felt the deficiency of moments about the normals of side panels. In effect membrane action on corner displacements alone was not sufficient to represent the true structure without the help of the existing -- but unrepresented -- in plane shear from moments about the normals of the panels.

In the case of torsion the fully constrained model was invalid because it developed local equilibrium at the end undergoing unit rotation. The unit rotation about the axial direction for every end grid point was inhibited by the translational d.o.f.'s being held to zero. The deformation became a scalloped pattern instead of a uniformly rotated face. Representation of torsion with the B.E. model was also inadequate because it required, but didn't get, the assistance of the panels on all four sides to carry the rotation about their normals.

Does this mean that if no attempt were made to model the mast as an equivalent beam, but a full 3-D model were used, that the 3-D model would be invalid? Not at all. What it shows is that the 3-D model is ineffective in trying to conform to the

## OBTAINING AN EQUIVALENT BEAM

requirements of an equivalent beam representation. If a full 3-D plate model were used in the complete representation of the crane structure, good results would be obtained.

Since the attempt is to economize on the size of the model, a better way to achieve the same results is to use sub-structuring and condense the mast to equivalent end boundary and intermediate mass points.

The spirit in which this paper is presented is to publish failures as well as successes to help analysts avoid retracing the ground that has already been plowed.

10-39  
275381  
208

Low Velocity Impact Analysis with NASTRAN

Daniel A. Trowbridge  
Analex Corporation  
Fairview Park, Ohio 44126

Joseph E. Grady and Robert A. Aiello  
NASA Lewis Research Center  
Cleveland, Ohio 44135

ABSTRACT

A nonlinear elastic force-displacement relationship is used to calculate the transient impact force and local deformation at the point of contact between impactor and target. The nonlinear analysis and transfer function capabilities of NASTRAN are used to define a finite element model that behaves globally linearly elastic, and locally nonlinear elastic to model the local contact behavior.

Results are presented for two different structures: a uniform cylindrical rod impacted longitudinally; and an orthotropic plate impacted transversely. Calculated impact force and transient structural response of the targets are shown to compare well with results measured in experimental tests.

INTRODUCTION

Aerospace structures are subjected to impact loading from a variety of sources, including dropped tools, runway debris, and munitions. In some advanced materials, even low velocity impact can cause significant structural damage. Therefore, development of accurate means of calculating structural response due to impact loading can be of critical importance. In this paper, a computational technique is developed to predict the dynamic response of a structure to low velocity elastic impact.

Structural damage due to impact invariably initiates in the immediate vicinity of the impact. Therefore, it is important that the local stress field in the region of contact be calculated accurately. Hertz [1] derived an elasticity-based force-displacement relationship that describes contact between two elastic bodies. The Hertzian contact law is given by:

$$F = K \alpha^n \tag{1}$$

where

- F = elastic contact force
- K = contact stiffness
- n = exponent

and

$$\begin{aligned}\alpha &= \text{relative displacement (indentation) between impactor and target} \\ &= u_i - u_t \quad (i = \text{impactor}, t = \text{target})\end{aligned}$$

The exponent  $n$  was shown in reference [1] to have the value of  $3/2$ . In dynamic applications such as this;  $F$ ,  $u$ , and  $\alpha$  are all time-varying.

During low velocity impact, where impact damage is confined to the area immediately around the point of contact, areas of the structure remote from the impact may still deform in a linear elastic manner. An efficient finite element model, therefore, would combine a linear elastic model of the global structure with a non-linearly elastic behavior at the point of contact. The nonlinear force-displacement relationship in equation (1) is incorporated into a linear elastic finite element model (MSC/NASTRAN transient solution 27, COSMIC/NASTRAN transient solution 9) by using a NASTRAN transfer function definition and nonlinear analysis capability. In the following section, the Hertz contact law is discussed in addition to a method of incorporating it into NASTRAN. Impact loading of two different structures is then analyzed. The first problem is a one-dimensional rod of uniform cross section impacted longitudinally. The second is an orthotropic plate under transverse impact.

### CONTACT LAW

In reference [2] Hertz derived the force-displacement relationship for two spherical isotropic elastic bodies of radius  $r_1$ , and  $r_2$  in contact:

$$F = K \alpha^{3/2} \quad (2)$$

where

$$K = \frac{4}{3} \sqrt{\frac{r_1 r_2}{r_1 + r_2}} \frac{k_1 k_2}{k_1 + k_2} \quad (3)$$

is the contact stiffness and

$$k_i = \frac{E_i}{1 - \nu_i^2} \quad i = 1, 2 \quad (4)$$

where  $E_i$  and  $\nu_i$  are the Young's modulus and poisson's ratio, respectively, and the subscripts 1 and 2 refer to each of the spheres. When a spherical impactor contacts a flat target, (3) simplifies to

$$K = \frac{4}{3} \sqrt{r_i} \frac{k_i k_t}{k_i + k_t} \quad (5)$$

where  $i$  and  $t$  represent the impactor and target respectively and the  $k_t$  and  $k_i$  are given by:

$$k_t = \frac{E_t}{1 - \nu_t^2} \quad (6)$$

$$k_i = \frac{E_i}{1 - \nu_i^2} \quad (7)$$

In equation (2),  $\alpha$  is the local indentation at the contact point, shown schematically in figure 1. We have:

$$\alpha = u_i - u_t \quad (8)$$

where  $\alpha$  is the relative local displacement between impactor and target at the point of contact.

### NASTRAN Implementation

The non-linear local behavior was incorporated into the NASTRAN finite element model as follows:

The impactor is modeled as a lumped mass just touching the target at  $t=0$  and with an initial velocity towards the target. The difference between the displacement of this lumped mass and the displacement of the target is the indentation,  $\alpha$ . The modeling of the contact between impactor and target is performed by utilizing the transfer function card, TF, and the nonlinear force card, NOLIN3. The TF card acts as a dynamic multipoint constraint, relating the displacement, velocity and acceleration of several independent degrees of freedom to a dependant degree of freedom. In the work discussed here, only displacement relationships were used. On the TF card coefficients of the following equation are specified [3].

$$(B_0 + B_1p + B_2p^2)u_{dep} + \sum_{j=1}^n (A_0^j + A_1^j p + A_2^j p^2)u_{ind}^j = 0 \quad (9)$$

where

$B_0, B_1, B_2$  = the coefficients for the dependant degree of freedom

$A_0^j, A_1^j, A_2^j$  = the coefficients for the independent degrees of freedom

$u_{dep}$  = the displacement of the dependant degree of freedom

$u_{ind}^j$  = the displacements of the independent degrees of freedom

$n$  = the number of independent degrees of freedom

$p$  = the differential operator  $\frac{\partial}{\partial t}$ , and  $p^2 = \frac{\partial^2}{\partial t^2}$

For this analysis, the equation would appear:

$$(1.0)u_{\text{extra point}} + \left[ (-1.0)u_{\text{impactor}} + (1.0)u_{\text{target}} \right] = 0 \quad (10)$$

that is

$$\begin{aligned} n &= 2 \\ B_1, B_2, A_1^j, A_2^j &= 0.0 \quad (j = 1, n) \\ B_0 &= 1.0 \\ A_0^1 &= -1.0 \\ A_0^2 &= 1.0 \end{aligned}$$

The resulting equation defines the indentation at every time step and assigns the value to an EPOINT. The EPOINT, or extra point, is used as a nonstructural variable that provides a place to store the value of the indentation. The EPOINT is provided as input to the NOLIN3 card.

The NOLIN3 card is the means of applying the time-dependent nonlinear load based on the indentation. The NOLIN3 card has the form:

$$P(t) = \begin{cases} S(x(t))^A, & x(t) > 0 \\ 0 & , x(t) \leq 0 \end{cases} \quad (11)$$

where

- $P(t)$  = is the resulting nonlinear force
- $S$  = is a scale factor
- $x(t)$  = is the displacement or velocity of a degree of freedom
- $A$  = is an amplification factor

In modeling of the impact, we define  $x(t)$  to be the displacement of the EPOINT,  $S$  to be the Hertzian stiffness, and  $A$  to be  $3/2$ , as given in equation (2). Recall that the displacement of the EPOINT is really the indentation as obtained from the TF card. The resulting function then has the form:

$$P(t) = \begin{cases} K(\alpha(t))^{3/2}, & \alpha(t) > 0 \\ 0 & , \alpha(t) \leq 0 \end{cases} \quad (12)$$

Note that when  $\alpha$  is less than or equal to zero (ie. the target and the impactor are out of contact) then the force is also zero. Two NOLIN3 cards are used, one to apply the impact force to the target and the other to apply the same force to the impactor in the opposite direction of its initial velocity. This methodology allows the impactor to slow with increasing impact force and eventually to unload the target as the impactor begins to travel in the opposite direction, away from the target.

## RESULTS

### One Dimensional Rod

The first problem analyzed is the longitudinal impact of a steel ball on a long aluminum rod of constant cross section. Geometry and material properties of the impactor and target are given in figure 1. The problem was modeled using 144 1-D rod elements with each grid point having a single longitudinal degree of freedom. Two more degrees of freedom were used to model the impact dynamics, resulting in a total of 147 degrees of freedom. A single lumped mass with an initial velocity was used to represent the impactor. The Hertzian force-displacement relationship in equation (1) was prescribed using the NASTRAN NOLIN3 card, as shown in the example input deck in the appendix.

The calculated impact force history compares well with experimentally determined values [4], as shown in figure 2. The calculated strain response at the midpoint of the target bar is compared with measured values in figure 3. The sign reversal of the second pulse is caused by the reflected tensile stress wave generated by the incident compressive wave reaching the free end of the bar [5].

Some insight into the timing and the location of the impact-induced structural failure can be gained by tracking the distribution of energy in the impactor and the target, as shown in figure 4. The energy balance can be expressed as:

$$U_t = KE_i + SE_i + KE_t + SE_t \quad (13)$$

where

$U_t$  = total energy in system

$$KE_i = \text{impactor kinetic energy} = \frac{1}{2} m v_i^2 \quad (14)$$

$$SE_i = \text{impactor strain energy} = \int F(\alpha) d\alpha = \frac{2}{5} K \alpha^{5/2} \quad (15)$$

$$KE_t = \text{target kinetic energy} \quad (16)$$

$$= \sum_{j=1}^{n-1} \frac{1}{2} m_j \left[ \frac{V_j + V_{j+1}}{2} \right]^2 \quad (n = \text{number of elements})$$

$$SE_t = \text{strain energy of target} \quad (17)$$

$$= \sum_{j=1}^{n-1} \frac{1}{2} k_j (\delta_j - \delta_{j+1})^2 \quad (n = \text{number of elements})$$

The total energy in the system,  $U_t$ , is divided between the kinetic energy and the strain energy of the target and impactor in a time-varying manner. Because damping effects are not considered, the total system energy is constant and equal to the initial kinetic energy of the impactor. The strain energy of the impactor is non-zero only during the contact interval ( $0 < tC/L < 0.4$ , where  $t$  = time,  $L$  = the length of the bar, and  $C$  = the wave speed in the bar) and peaks when the contact force is greatest, approximately halfway through the contact interval. The kinetic energy of the impactor decreases rapidly as the impactor slows during contact with the target. Eventually, at  $tC/L = 0.25$ , the impactor velocity (and therefore its kinetic energy) decreases to zero and the elastic rebound begins. The kinetic energy of the impactor never returns to its initial level because approximately 80% of the energy has been transferred to the target in the form of strain energy and kinetic energy. The strain and kinetic energies in the target both increase rapidly during the contact with the impactor and remain constant after contact has ended ( $tC/L > 0.4$ ). Both strain and kinetic energies maintain equal and constant values until the compressive stress wave generated by the impact reaches the far end of the free-free bar ( $tC/L = 1.0$ ). A tensile stress wave is generated when the compressive pulse reflects from the stress free boundary [5]. The superposition of the incident and reflected pulses momentarily leaves the bar stress-free which causes the strain energy to decrease to zero. The kinetic energy simultaneously increases, maintaining a conservation of total energy. The reflection process is repeated at  $tC/L = 2.0$ , when the reflected pulse returns to the other end of the bar. Similar energy dissipation diagrams may prove useful in analyzing dynamic failure of more complex structures.

### Composite Plate

The low velocity transverse impact of a composite plate made from Scotchply 1003 prepreg [6] is now analyzed. The problem is depicted schematically in figure 5, and is described in detail in references [7,8]. A modified Hertzian contact stiffness has been proposed [9] for application to composite materials. Specifically, equation (6) is replaced by

$$k_t = E_{33t} \quad (18)$$

where  $E_{33t}$  is the transverse modulus of the plate. Plate membrane and bending stiffness material properties were calculated using the COBSTRAN (Composite Blade Structural Analyzer) computer code [10] which calculates elastic moduli of composite materials from known constituent properties and laminate ply orientations.

A uniform square mesh of QUAD4 elements was used to model the 15.24 cm × 15.24 cm (6 in × 6 in) target plate. A mesh convergence study was performed to establish the degree of mesh refinement necessary to arrive at a numerically converged solution. Three different meshes were considered, 25 × 25, 49 × 49, and 61 × 61 elements. Of these, the latter two produced essentially the same strain response for a given impact velocity and were therefore considered to be converged solutions. The results presented here were therefore calculated using the 49 × 49 element model. Five degrees of freedom ( $u_x$ ,  $u_y$ ,  $u_z$ ,  $\theta_x$  and  $\theta_y$ ) were used at each nodal point, giving the model a total of 11510 degrees of freedom. The problem was solved on a Cray XMP in 52 CPU minutes.

The impactor used in the tests [7,8] was a uniform 2.54 cm (1 in) long, blunt-ended steel rod of radius 0.047625 cm ( $3/16$  in). In the analysis a contact radius of 0.047625 cm ( $3/16$  in) was assumed in the Hertzian contact stiffness calculations. The calculated impact force history is shown in figure 6. Although no direct measurement of the impact force was obtained experimentally, the contact time was measured [8] and found to be 204 microseconds. This is in good agreement with the calculated result. Figure 6 also shows that a secondary impact occurs during the latter half of the contact interval ( $t = 175 \mu\text{sec}$ ), probably due to the vibration of the target plate during contact with the projectile.

The resulting displacement response of the plate is shown in figure 7, where it has been assumed that no damage occurs in the target during contact with the impactor. This assumption is valid based on the available test data. Ultrasonic C-scans of the specimens after impact indicate that this level of impactor kinetic energy (10 Joules) is very near the threshold energy level required to cause damage [8] in specimens of this layup. As a result, very little damage occurs at this impactor velocity. The anisotropic bending stiffness of the target (figure 5) is evident from the elliptical displacement contours, as the flexural disturbance travels faster in the stiffer direction (figure 7).

The strain response at gage A is compared to the calculated response in figure 8. The two curves are similar in amplitude and duration but the calculated strain appears to lag the measured values by approximately 25 microseconds. This may be due to the difficulty in establishing experimentally the precise time at which contact occurs based on strain gage readings taken at some distance from the point of contact. The comparison shown in figure 9 for gage B likewise shows a time shift of approximately 25 microseconds between the measured and the calculated response. The amplitude and duration of the calculated strain response correlate quite well with the measured signal.

## SUMMARY

A simple means of modeling low velocity, non-damaging impact using NASTRAN was demonstrated. A nonlinear elastic contact model was included in the finite element analysis using NASTRAN transfer function definitions and nonlinear analysis capabilities. The same contact law was used to define the force-indentation relationship for two different impactor/target combinations. Results in both cases showed that the impact force and resulting transient structural response of the target compared well with experimentally measured values.

## ACKNOWLEDGEMENT

The support of the Naval Weapons Center at China Lake, CA. is gratefully acknowledged. Mr. Andrew Victor was the technical monitor.

## REFERENCES

- [1] Timoshenko, S. P. and Goodier, J. N., Theory of Elasticity, McGraw-Hill, 1970.
- [2] Goldsmith, W., Impact: The Theory and Physical Behavior of Colliding Solids, Edward Arnold Publishing, London, 1960.
- [3] MacNeal, R. H., ed., The NASTRAN Theoretical Manual, 1972.
- [4] Grady, J. E., "Dimensional Analysis for Compliant Impactors", NASA Technical Memorandum, 1990
- [5] Graff, K. F., Wave Motion in Elastic Solids, Ohio State University Press, 1975
- [6] "Scotchply Reinforced Plastic Type 1003 Technical Data Sheet", Structural Products, Industrial Specialties Division/3M.
- [7] Takeda, N., Sierakowski, R. L. and Malvern, L. E., "Wave Propagation Experiments on Ballistically Impacted Composite Laminates", *J. Composite Materials*, V. 15, March 1981, pp. 157-174.
- [8] Takeda, N., Sierakowski, R. L. and Malvern, L. E., "Studies of Impacted Glass Fiber-Reinforced Composite Laminates", *SAMPE Quarterly*, January 1981, pp. 9-17.
- [9] Sun, C. T., "Analytical Method for Evaluation of Impact Damage Energy of Laminated Composites", *ASTM STP617*, 1977, p. 427.
- [10] Aiello, Robert A., Composite Blade Structural Analyzer (COBSTRAN) User's Manual, NASA Technical Memorandum 101461, April 1989.

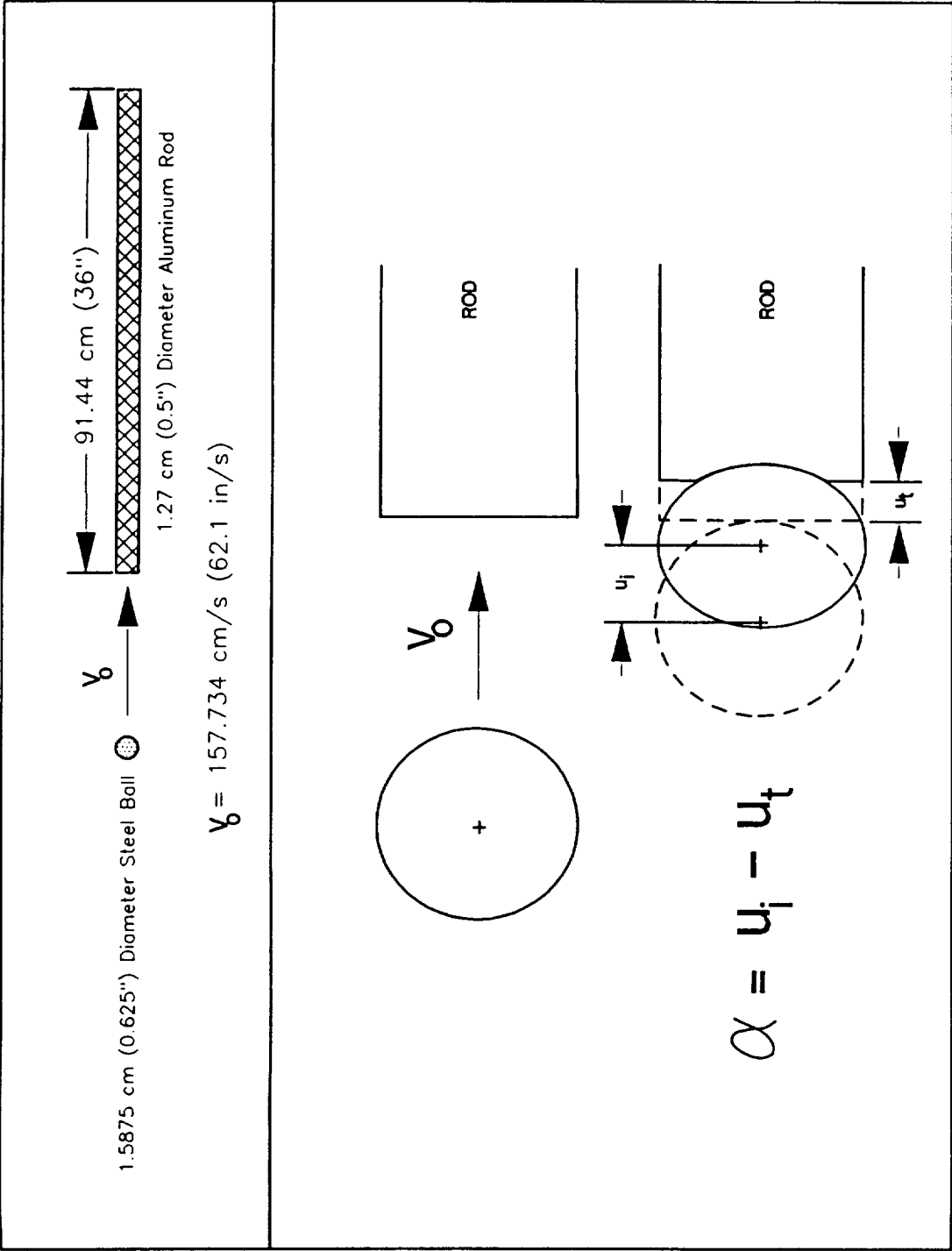


Figure 1: Longitudinal Bar Impact Problem

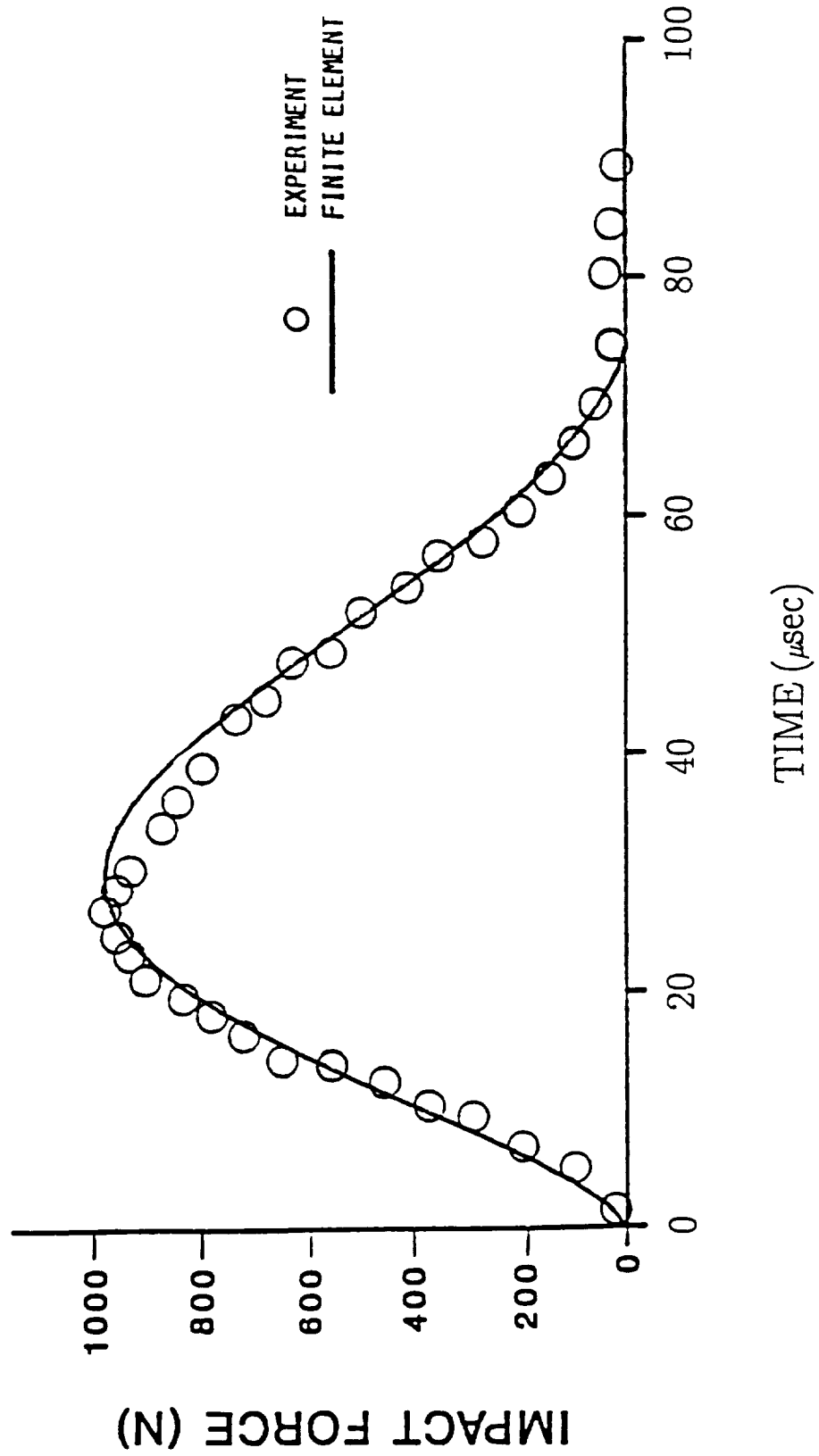


Figure 2: Impact Force for Bar Problem

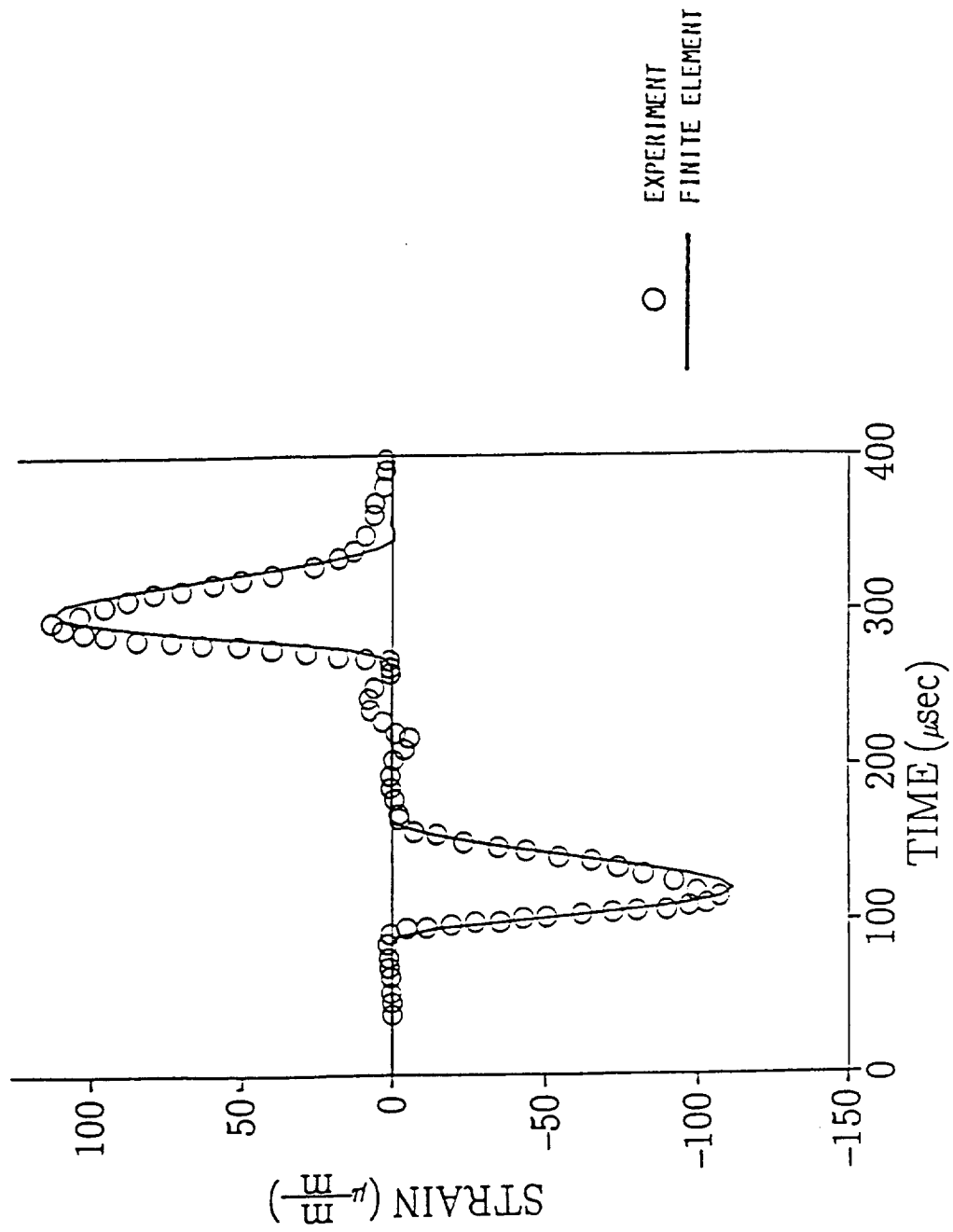


Figure 3: Strain Response at Midpoint of Impacted Bar

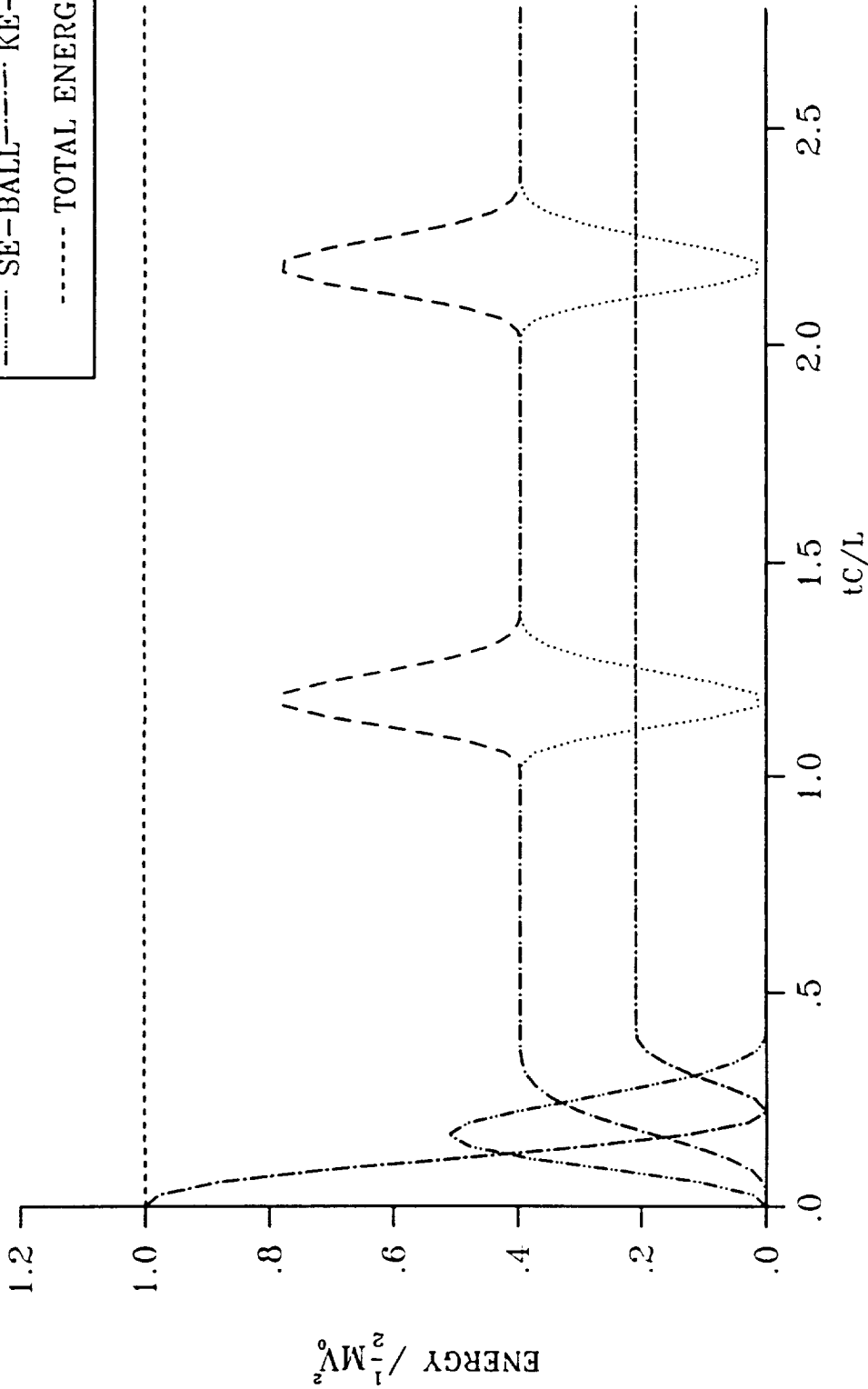
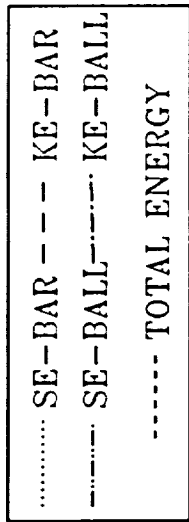


Figure 4: Energy Distribution for Longitudinal Bar Impact Problem

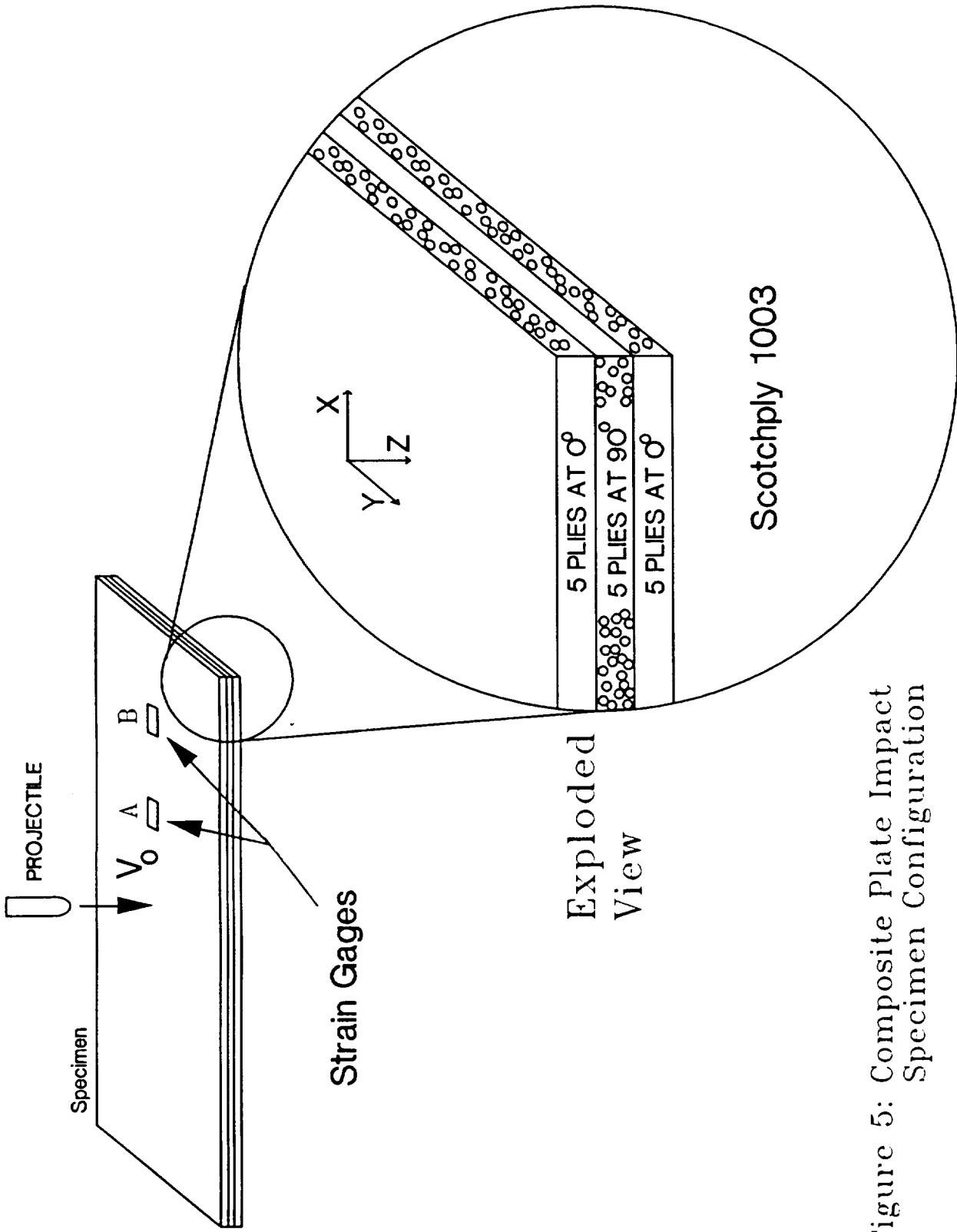


Figure 5: Composite Plate Impact Specimen Configuration

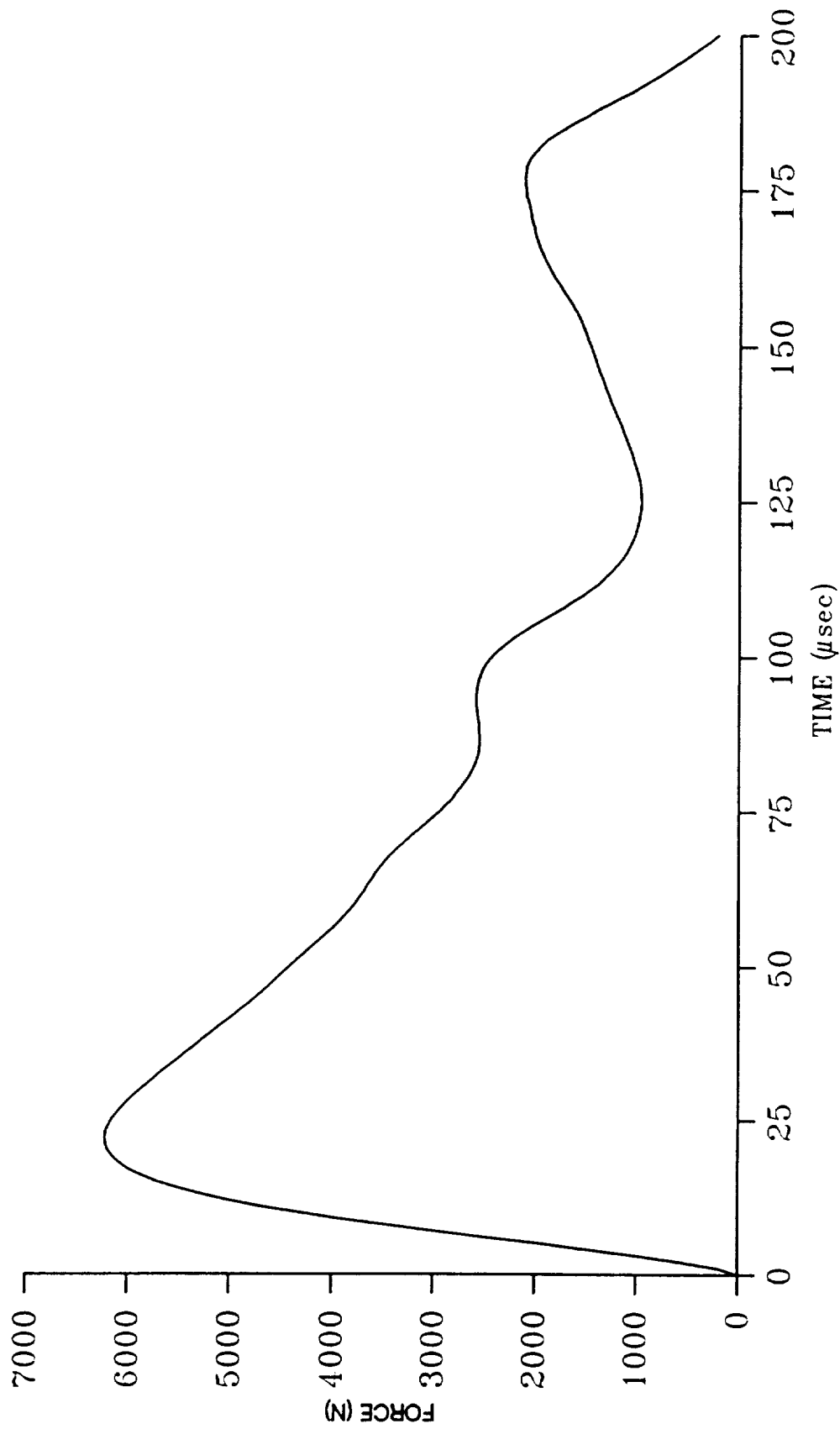


Figure 6: Calculated Force History for Transverse Impact of Composite Plate

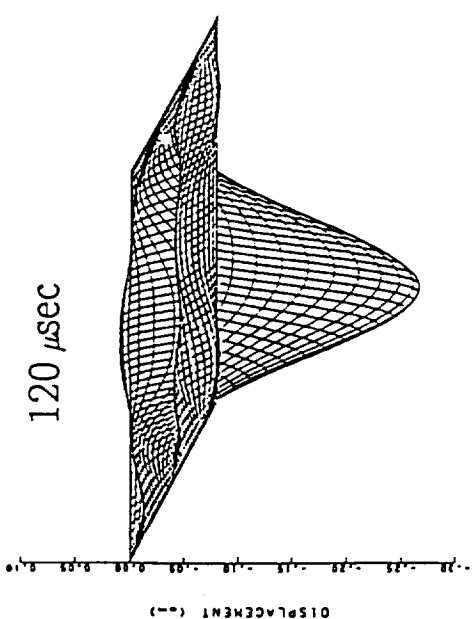
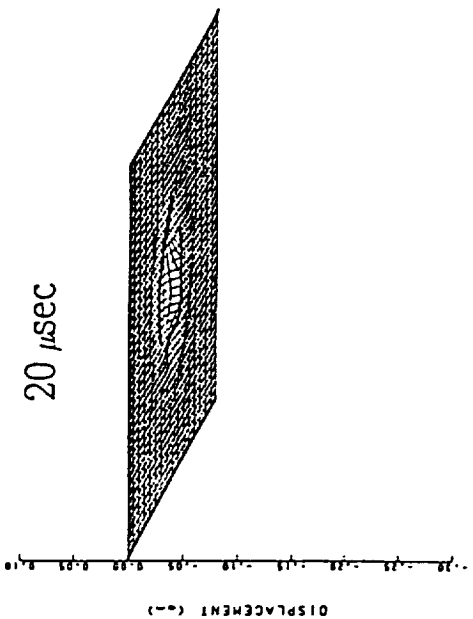
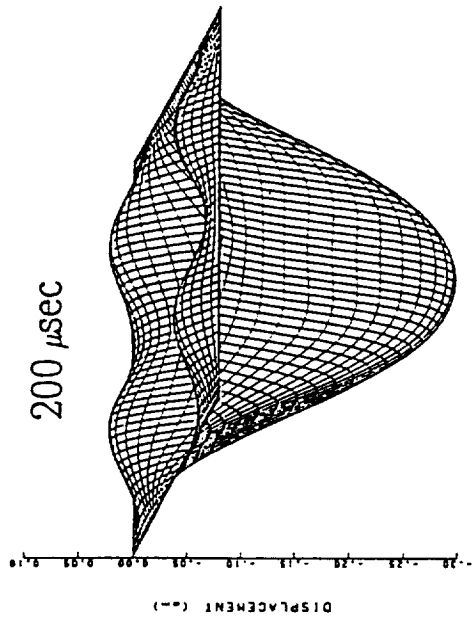
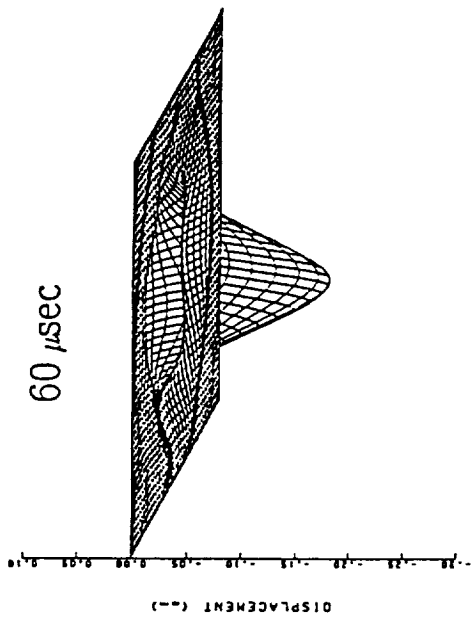


Figure 7: Calculated Displacement Response for Composite Plate

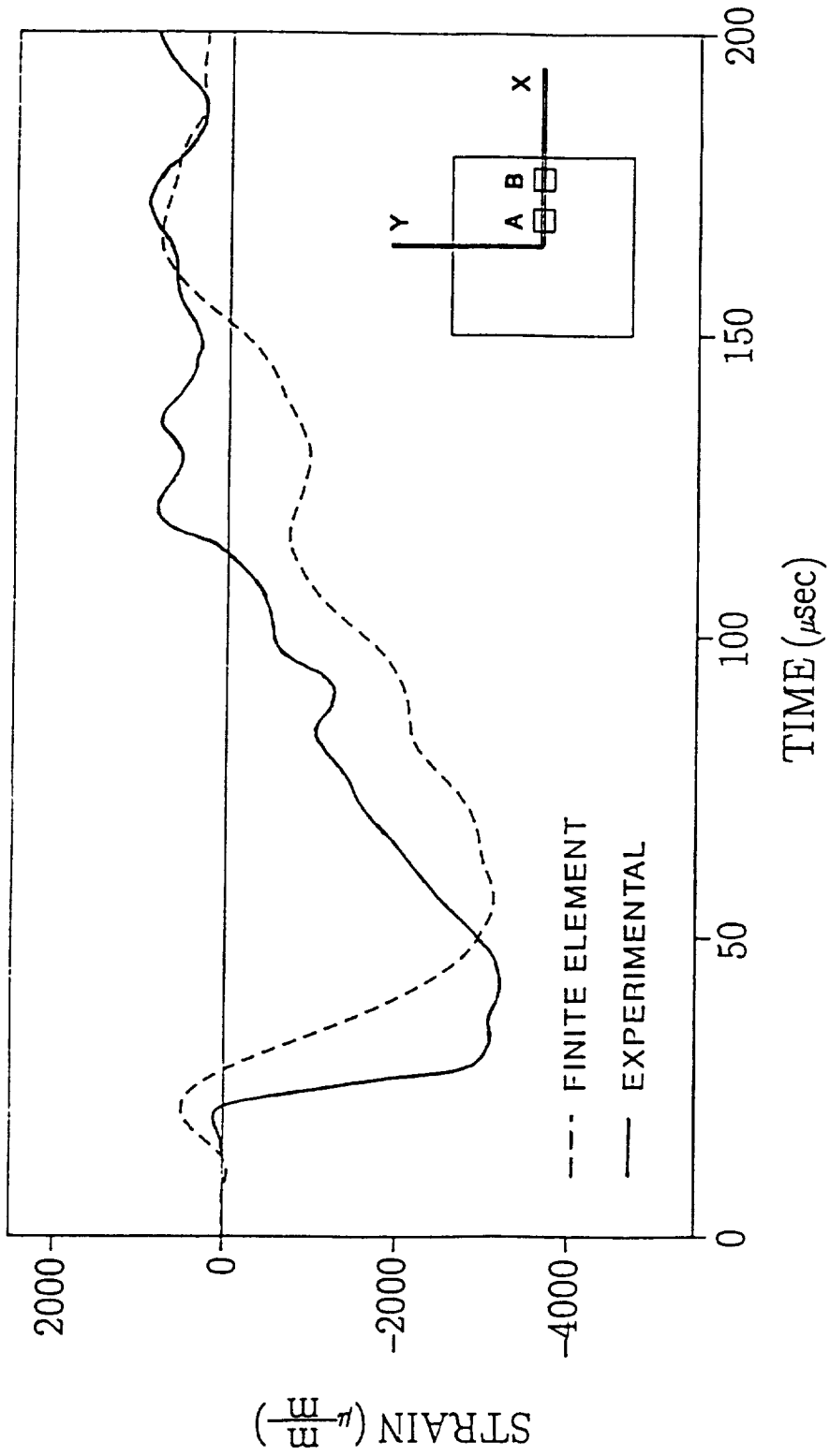


Figure 8: Strain Response at Gage Location "A"

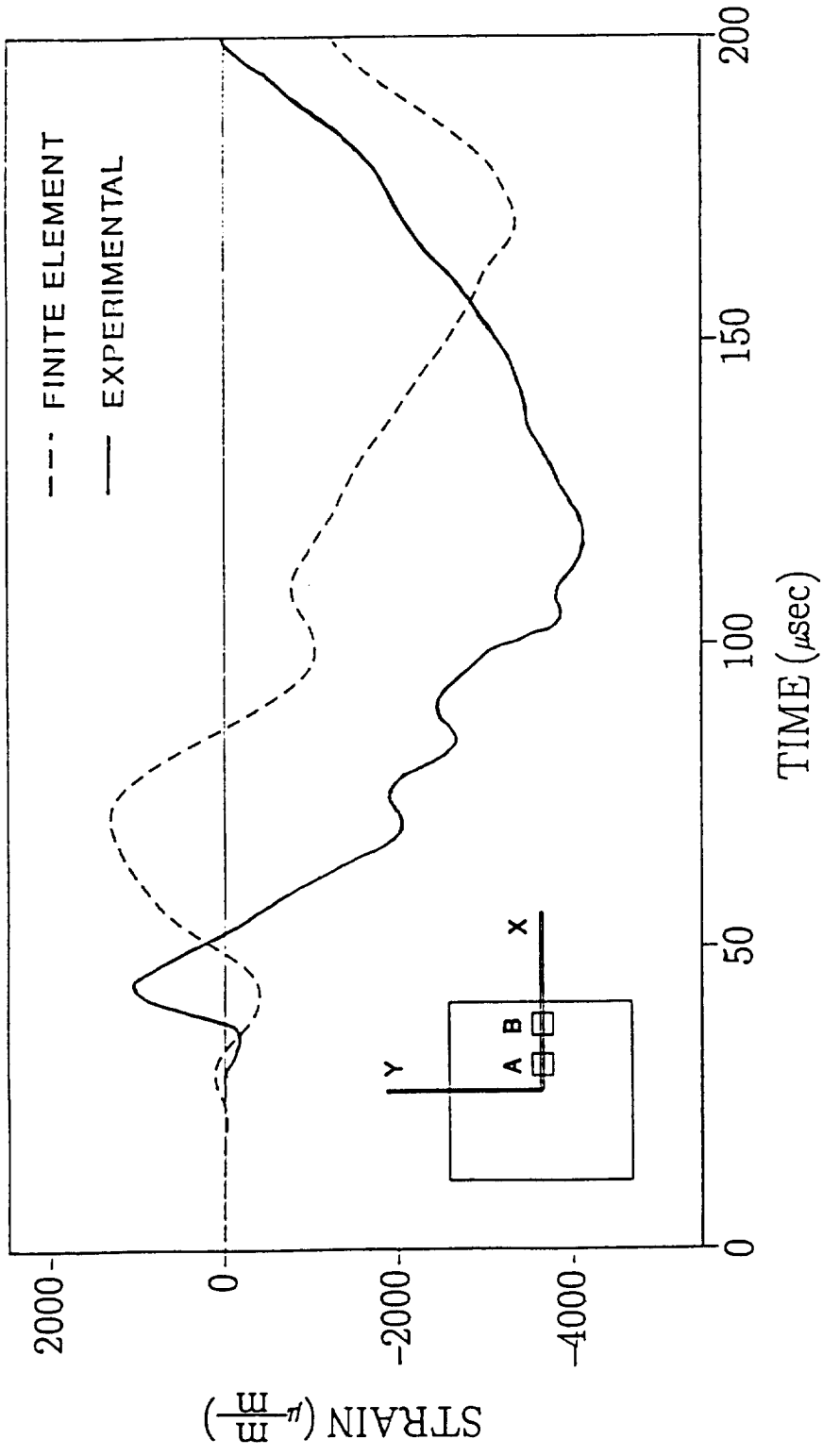


Figure 9: Strain Response at Gage Location "B"

# APPENDIX

```

ID TRANS,LOAD
APP DISP
TIME 60
SOL 9
CEND
  TITLE = COSMIC: TRANSIENT RESPONSE ANALYSIS: HERTZIAN IMPACT FF
SUBTITLE = 36" AL. ROD 5/8 STEEL BALL V0=62.1 IN/S
  LABEL = ROD          * <----- IMPACT
$      NONLINEAR LOAD
NONLINEAR = 5
$      INITIAL CONDITIONS SET
IC = 1
TFL=111
SPC = 4
TSTEP = 7
$      OUTPUT STUFF
SET 30 = 1,72,73,999,1001
NLLOAD = 30
STRESS(PRINT) = 30
DISP(PRINT) = 30
BEGIN BULK
$ .....
$      EXTRA POINT = INDENTATION
EPOINT,1001
GRID,999,,-0.3125,0.0,0.0
GRID,1,0.0,0.0,0.0
=(144),*(1),*(0.25),=
CROD,1,1,1,2
=(143),*(1),*(1),*(1)
$      LUMP MASS OF IMPACTOR
CONM2,200,999,0,9.587-5,0.0,0.0,0.0, +CON2-2
+CON2-2,3.745-6,,3.745-6,,3.745-6
$      MATERIAL PROPERTIES
PROD,1,11,0.196,6.14-3,0.25
MAT1,11,10.0+6,,0.33,2.5-4,,,+MAT1-1
+MAT1-1,35.0E6,36.0E6,27.0E6
$      BOUNDARY CONDITIONS
SPC1,4,23456,1,THRU,145
$      REMOVE DEGREES OF FREEDOM FROM IMPACTOR
SPC1,4,23456,999
$      TRANSFER FUNCTION TO DEFINE INDENTATION
TF,111,1001,0,+1.0,0.0,0.0,0.0,+,TF-1
+TF-1,999,1,-1.0,0.0,0.0,0.0,+,TF-2
+TF-2,1,1,1.0,0.0,0.0
$      TIMING
TSTEP,7,2500,2.0-7,25
$      LOAD DEPENDENT ON DISPLACEMENT OF IMPACTOR
NOLIN3,5,1,1,6.24+6,1001,1,1.5
$      SLOW DOWN IMPACTOR
NOLIN3,5,999,1,-6.24+6,1001,1,1.5
$      INITIAL CONDITIONS: IMPACTOR VELOCITY = 62.1 IN/SEC
TIC,1,999,1,0.0,62.1
ENDDATA

```

```

ID IMPACT,PLATE
APP DISP
TIME 120
SOL 27
CEND
  TITLE = IMPACT OF PLATE 49X49 : CENTERED ELEMENT
  SUBTITLE = TRANSIENT ANALYSIS: FIXED-FIXED: NO SYMMETRY
  SPC = 1
  IC = 3
  NONLINEAR = 5
  TSTEP = 1
  TFL = 111
  SET 15 = 999,2525,2526,2625,2626
  NLLOAD = 15
  SET 20 = 2525,3325,4125
  STRESS = 20
BEGIN BULK
$ **** EXTRA POINT TO HOLD INDENTATION *****
EPOINT,10001
$ **** IMPACTOR *** 3/8 IN DIAMETER *****
GRID,999,,0.0,0.0,-0.1875
CONM2,200,999,0,8.096-5,0.0,0.0,0.0,, +CON2-2
+CON2-2,7.459-6,,7.459-6,,,1.423-6
$ * * * * * GRIDS AND CQUAD4 ELEMENTS DEFINING THE PLATE GO HERE ...
$ MATERIAL PROPERTIES... MAT2 CARDS GENERATED BY COBSTRAN
PSHELL,1,101,0.15,201,1.0
MAT2,101,4.3E+06,2.9E+05,-1.7E-03,2.8E+06,-3.4E-02,5.7E+05,1.8E-04,+A101
+A101,5.8E-06,8.9E-06,5.0E-13
MAT2,201,5.7E+06,2.9E+05,-1.9E-04,1.4E+06,-3.8E-03,5.7E+05
$ BOUNDARY CONDITIONS
SPC1, 1, 123456, 101, THRU, 150
SPC1, 1, 123456, 5001, THRU, 5050
SPC1, 1, 123456, 101
=,=,=.100
=48
SPC1, 1, 123456, 150
=,=,=.100
=48
SPC1, 1, 12456, 999
GRDSET,.....6
$ TIME STEP INFO
TSTEP, 1,2000, 1.0-7, 10
$ LOAD DEPENDENT ON RELATIVE DISPLACEMENT OF IMPACTOR
NOLIN3, 5,2525, 3,+1.945+5, 10001, 0, 1.5
NOLIN3, 5,2526, 3,+1.945+5, 10001, 0, 1.5
NOLIN3, 5,2625, 3,+1.945+5, 10001, 0, 1.5
NOLIN3, 5,2626, 3,+1.945+5, 10001, 0, 1.5
$ SLOW DOWN IMPACTOR
NOLIN3, 5, 999, 3,-7.779+5, 10001, 0, 1.5
$ TRANSFER FUNCTION TO CALCULATE INDENTATION
TF,111,10001,0,+1.0,00.0,00.0...+TF-1
+TF-1,999,3,-1.0,00.0,00.0...+TF-2
+TF-2,2525,3,+0.25,00.0,00.0...+TF-3
+TF-3,2526,3,+0.25,00.0,00.0...+TF-4
+TF-4,2625,3,+0.25,00.0,00.0...+TF-5
+TF-5,2626,3,+0.25,00.0,00.0
$ INITIAL CONDITIONS: IMPACTOR VELOCITY = 1470 IN/SEC (122.5 FT/SEC)
TIC,3,999,3,0.0,1470.0
ENDDATA

```

TRANSITIONING OF POWER FLOW IN  
BEAM MODELS WITH BENDS

by

Stephen A. Hambric  
Applied Mathematics Division (184)  
David Taylor Research Center  
Bethesda, MD 20084-5000

27-002  
N90-24648

ABSTRACT

*The propagation of power flow through a dynamically loaded beam model with 90 degree bends is investigated using NASTRAN and McPOW. The transitioning of power flow types (axial, torsional, and flexural) is observed throughout the structure. To get accurate calculations of the torsional response of beams using NASTRAN, torsional inertia effects had to be added to the mass matrix calculation section of the program. Also, mass effects were included in the calculation of BAR forces to improve the continuity of power flow between elements. The importance of including all types of power flow in an analysis, rather than only flexural power, is indicated by the example. Trying to interpret power flow results that only consider flexural components in even a moderately complex problem will result in incorrect conclusions concerning the total power flow field.*

INTRODUCTION

Methods for calculating power flows in dynamically loaded finite element models using NASTRAN (Rigid Format 8 - Direct Frequency Response) and McPOW (Mechanical POWER) were developed previously.<sup>1</sup> The power flow equations for beam elements derived in that paper included all forms of dynamic energy propagation: flexural, longitudinal (or axial), and torsional. The flexural waves were split into shear and moment components.

The majority of procedures employed in other studies (see the list of references in Hambric<sup>1</sup>) only consider flexural vibration in their calculations of power flow. This can be dangerous if an analyst is investigating the energy propagation characteristics of a complex structure. Though flexural vibration is in most cases the dominant response in a dynamically excited beam, different kinds of propagation will occur in structures with even a small degree of complexity, such as a simple beam model with 90-degree bends.

Such a model is tested here using a frequency range spanning several resonances and types of motion. Plots showing the contributions of the different forms of power flow to the total power travelling through the system are shown, and illustrate the importance of all types of energy propagation to the power flow method.

To improve the accuracy of both the finite element solution and the power flow solution of the problem, a few modifications were made to NASTRAN and McPOW. First, to show the importance of torsional power flow, a capability to calculate dynamic torsional forces and corresponding angular velocities is required. Therefore, torsional inertias were added to the coupled mass matrix formulation of the BAR element. Also, since the beam element force calculation algorithm in NASTRAN considers only stiffness effects, mass and damping effects had to be added to McPOW to modify the element forces.

## METHODOLOGY

The procedure for solving for the power flow field in a finite element model using NASTRAN and McPOW is:

1. Run Rigid Format 8 (Direct Frequency Response) on a NASTRAN data deck (using the ALTER statements shown in Ref. 1 to output force and velocity data blocks to the OUTPUT2 file). Coupled mass formulations should always be used.
2. Run McPOW using the binary data in the OUTPUT2 file as input.

### General Methods

A typical power flow cycle is shown in Fig. 1. The figure shows an arbitrary structure mounted to a connecting structure by a spring and damper coupling. A dynamic load is applied, and energy flows into the structure at the load point. The input power then flows through the structure along multiple flow paths denoted by arrows whose lengths represent power flow magnitudes. As the energy flows toward the mounting, it is dissipated by material damping and sound radiation into a surrounding medium, and the flow arrows shorten. The flow and dissipation processes continue until the remaining energy exits the structure through the mounting and flows into the connecting structure. Though only one power entry point and one exit point are shown in this drawing, multiple loads and mountings may exist. A classic text which describes the flow of structure-borne sound is the book by Cremer, Heckl, and Ungar.<sup>2</sup>

The structural dynamics problem may be solved using NASTRAN. The structure may be modeled with various element types; mountings are modeled with scalar spring, damping, and mass elements. Constraints and loads are directly applied. The steady-state response for the model is solved for a given excitation frequency, and the power flow variables are calculated.

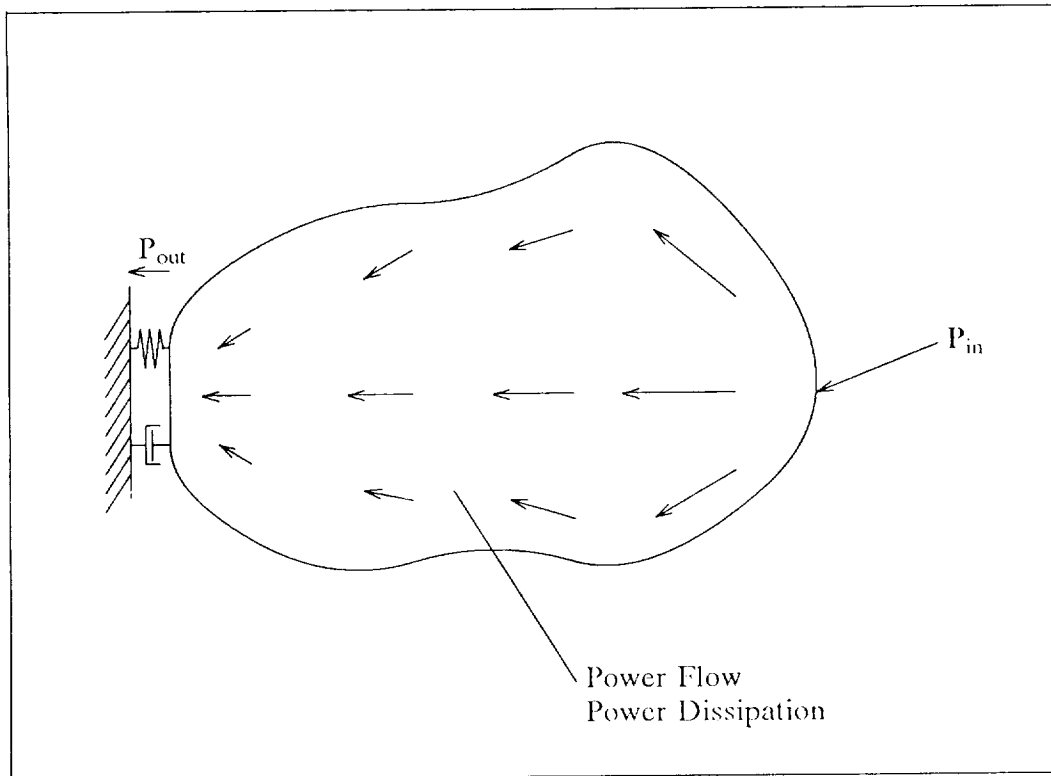


Fig. 1. Sample Power Flow Diagram.

Power is defined as the time-averaged product of a force with the in-phase component of velocity in the direction of the force. For time-harmonic analysis, where complex numbers are used, this calculation may be visualized as taking the dot product of the force and velocity phasors. (There is no factor 1/2 in the following power equations if the assumption that forces and velocities are "effective" values rather than amplitudes is made. With this assumption, consistency is maintained, and there is no mixing of effective and peak quantities in this formulation.)

Multiplying one complex number by the in-phase part of another complex number is the same operation as multiplying the first number by the complex conjugate of the other number and taking the real part of the result. Therefore a general formula for power flow in a structure is

$$\text{Power} = \text{Real} [Fv^*], \quad (1)$$

where

$F$  = force, and  
 $v^*$  = complex conjugate of velocity.

## Power Flow Equations

The equations for power flows in BAR elements are repeated here. A diagram of the BAR element and its NASTRAN force output conventions is shown in Fig. 2, where Plane 1 is vertical and Plane 2 is horizontal.

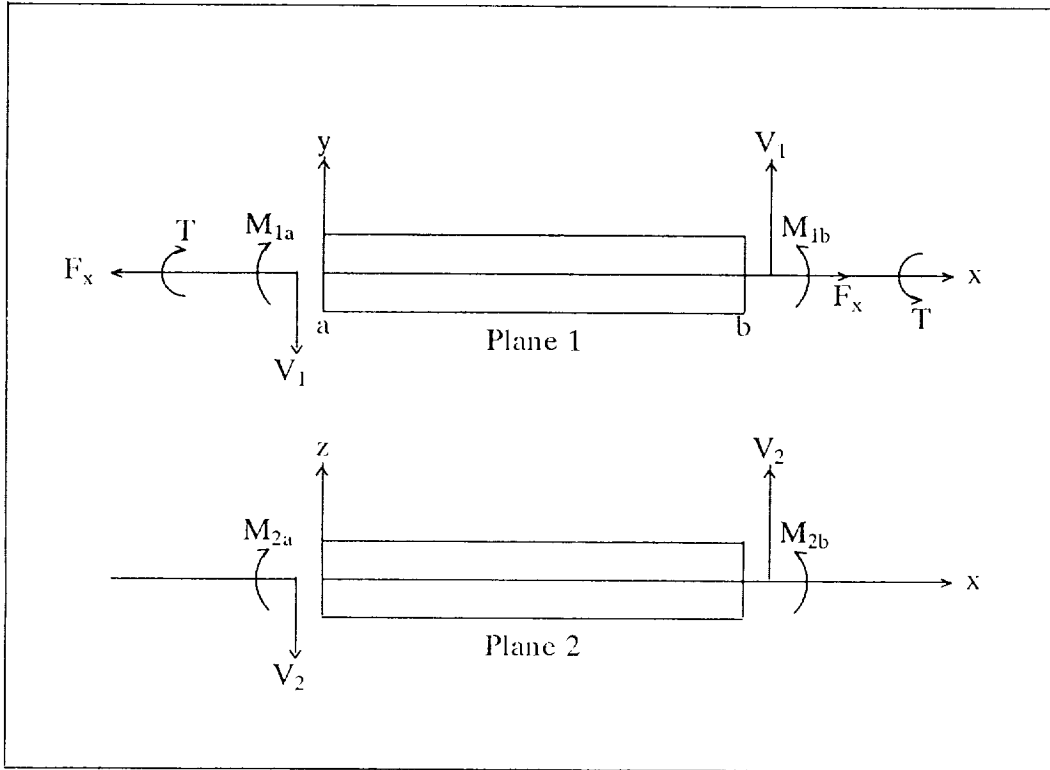


Fig. 2. The BAR Element

Since a beam is a one-dimensional element, energy flows in only one direction: in the local \$x\$ direction, or along the length of the beam. The total power flow for a beam element is

$$P_x = \text{Real} [ - (F_x v_x^* + V_1 v_y^* + V_2 v_z^* + T \dot{\theta}_x^* - M_2 \dot{\theta}_y^* + M_1 \dot{\theta}_z^*) ], \quad (2)$$

where

- $F_x$  = axial force,
- $V_1$  = shear force in \$y\$ direction,
- $V_2$  = shear force in \$z\$ direction,
- $T$  = torsion about \$x\$,
- $M_2$  = bending moment about \$y\$,
- $M_1$  = bending moment about \$z\$,
- $v_i$  = translational velocities in direction \$i\$, and

$\dot{\theta}_i$  = rotational velocities about axis i.

The negative sign on the result comes from force and displacement direction conventions for the element. The negative sign on the  $M_2$  term reflects the NASTRAN force output convention. In Fig. 2,  $M_2$  is shown as positive in the opposite sense to  $\dot{\theta}_y$ . Therefore,  $M_2\dot{\theta}_y^*$  is opposite in sign to the other power flow components.

### **NASTRAN Modifications**

#### *Torsional Inertias*

NASTRAN currently does not consider torsional inertias in its beam element formulation. Therefore, all torsional results (angular displacements and torques) are based on stiffness only, and are essentially those of a static problem solution. To remedy this, torsional inertias were added to the coupled mass formulation. At the point in NASTRAN where the basic element mass matrix is formed, no consideration is given to beam offsets or beam orientation; all mass coefficients (as well as stiffness) are calculated in the local beam coordinate system.

The torsional mass moment of inertia of a beam is  $\rho L J_x/2$ , where  $\rho$  is the mass density,  $L$  is the beam length, and  $J_x$  is the polar area moment of inertia. In the standard consistent mass matrix for a beam,<sup>3</sup> this value is broken up into 2/3 and 1/3 components; 2/3 of the value is placed at the diagonal, and 1/3 is placed at the coupled degree of freedom (the node on the other end of the beam). The same fractions are used for the translational, or axial masses. In NASTRAN, however, the coupled mass formulation uses an average of lumped and consistent formulations to reduce error. This average changes the components to 5/6 and 1/6 of the total value. Since these values are currently used for the axial masses in NASTRAN, they were also used for the torsional inertias.

#### *Element Force Calculations*

NASTRAN element forces are currently calculated by multiplying element stiffness matrices by element displacement vectors. Both damping and mass effects are ignored. The damping in a stiffness element is actually in the form of a loss factor, which generates a complex stiffness matrix. All stiffness terms are multiplied by  $1.0 + i\eta$ . For most dynamic analyses, neglecting the  $i\eta$  term is acceptable since it is generally small. For a power flow analysis of a highly reverberant structure, however, ignoring the loss factor is disastrous. In a highly reverberant structure, the force and velocity at a given point are close to 90 degrees out of phase. Since power flow is defined as the dot product of these two components, a small change in the phase of the force has large effects on the calculated element powers.

Neglecting the element mass matrices, whose components are several orders of magnitude less than those of the stiffness matrices, has less drastic

effects on the power flow solution, since at low frequencies the masses will have little effect on the force calculations (the element mass matrix is multiplied by  $-\omega^2$  to take the second time derivative of the corresponding displacements). However, when high frequency analyses are performed on a model, the  $-\omega^2$  multiplying factor becomes more significant, and neglecting the mass contributions will cause some error in the force calculations. Errors in element forces cause errors in element power flows.

Including these missing effects in NASTRAN is complicated by the fact that the element force calculation algorithm splits the problem into real and imaginary parts. The element stiffness matrices are multiplied by the real parts of the displacement vectors to calculate real force components, and the process is repeated for the imaginary components. Adding an imaginary term to the stiffness matrices causes new terms to be generated in the multiplication (imaginary stiffness x imaginary displacement and imaginary stiffness x real displacement). There is also no frequency dependence in the current algorithm, since stiffness are frequency independent. Mass matrices, however, must be multiplied by the  $-\omega^2$  term mentioned above, so they must be recalculated for every frequency.

To avoid these complications, the element force calculations were temporarily moved to McPOW. The element mass and complex stiffness matrices are recalculated on a local element level, and combined with local element displacements to solve for element forces. A force vector with 12 entries is the result; shears in the local y and z directions, moments about the local y and z directions, axial forces, and torques are solved for at each grid point. In NASTRAN only eight forces are calculated, because only moments are calculated at both ends of a beam element. Beam power flows are therefore calculated at each end of the element using only the forces at that end and the corresponding grid velocities. The average of the powers at the ends is taken to find an element power flow.

## TEST PROBLEM

### Problem Statement

The beam model that was analyzed is shown in Fig. 3. All three sections have the same cross section and material properties. Dashpots (DAMP2 elements) of value  $10^6$  were applied at the model's end in all six degrees of freedom. A unit load was applied at the top end of the model in the longitudinal direction (along the - z axis) over a frequency range of 1 to 250 Hz swept in 1 Hz increments. The finite element model consists of 152 elements and 153 grid points. Grid and element numbering starts at the left end of Link 1 and proceeds up to the end of Link 3.

Using the local beam element coordinate systems shown in Fig. 3, the following table of force balances at the corners (Link 3 to Link 2, Link 2 to Link 1) was generated.

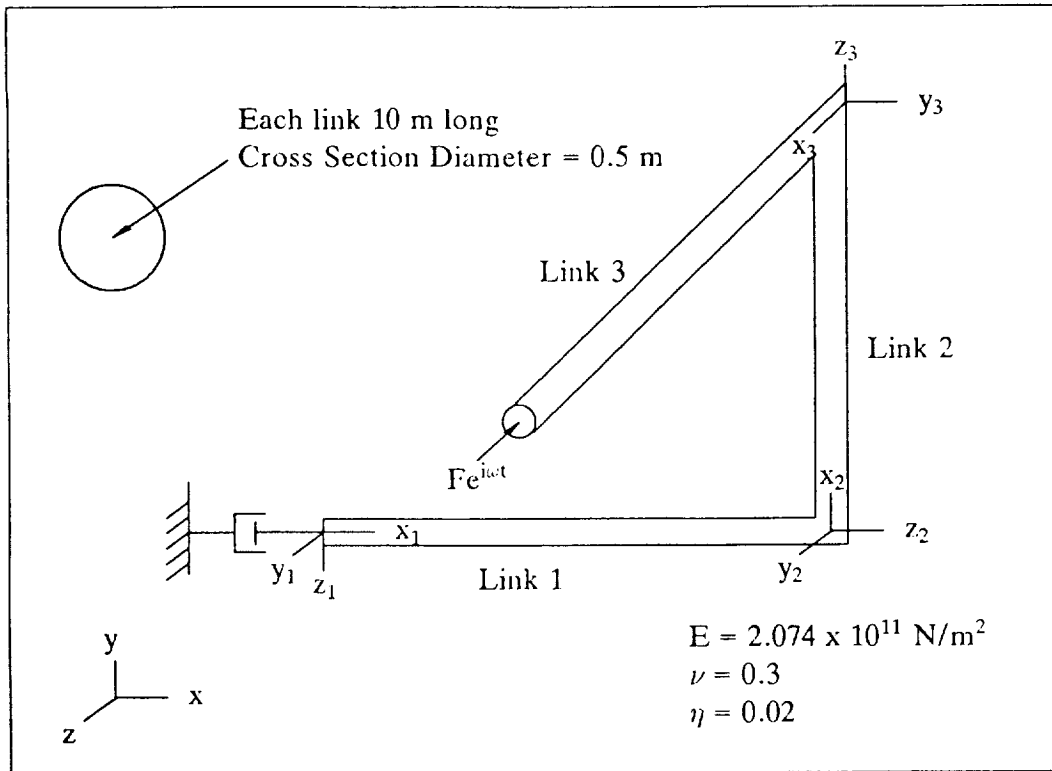


Fig. 3. Test Problem Geometry

Link 3	Link 2	Link 1
$F_x$	$V_1$	$V_1$
$T$	$M_2$	$M_2$
$V_1$	$V_2$	$F_x$
$V_2$	$F_x$	$V_2$
$M_1$	$T$	$M_1$
$M_2$	$M_1$	$T$

The subscripts on the shears and moments refer to the plane in which the forces occur (see Fig. 2). This table can be used to track the propagation of power flow through the structure. For example, the longitudinal power input to Link 3 will travel down the beam in axial waves to the first bend and become shear power flow in the  $z$  direction in Link 2. This shear power will interchange with moment power along the beam (the sum of the shear and moment components is the total flexural power flow in the beam). Any shear power that exists at the lower end of Link 2 will transition to more shear power in Link 1.

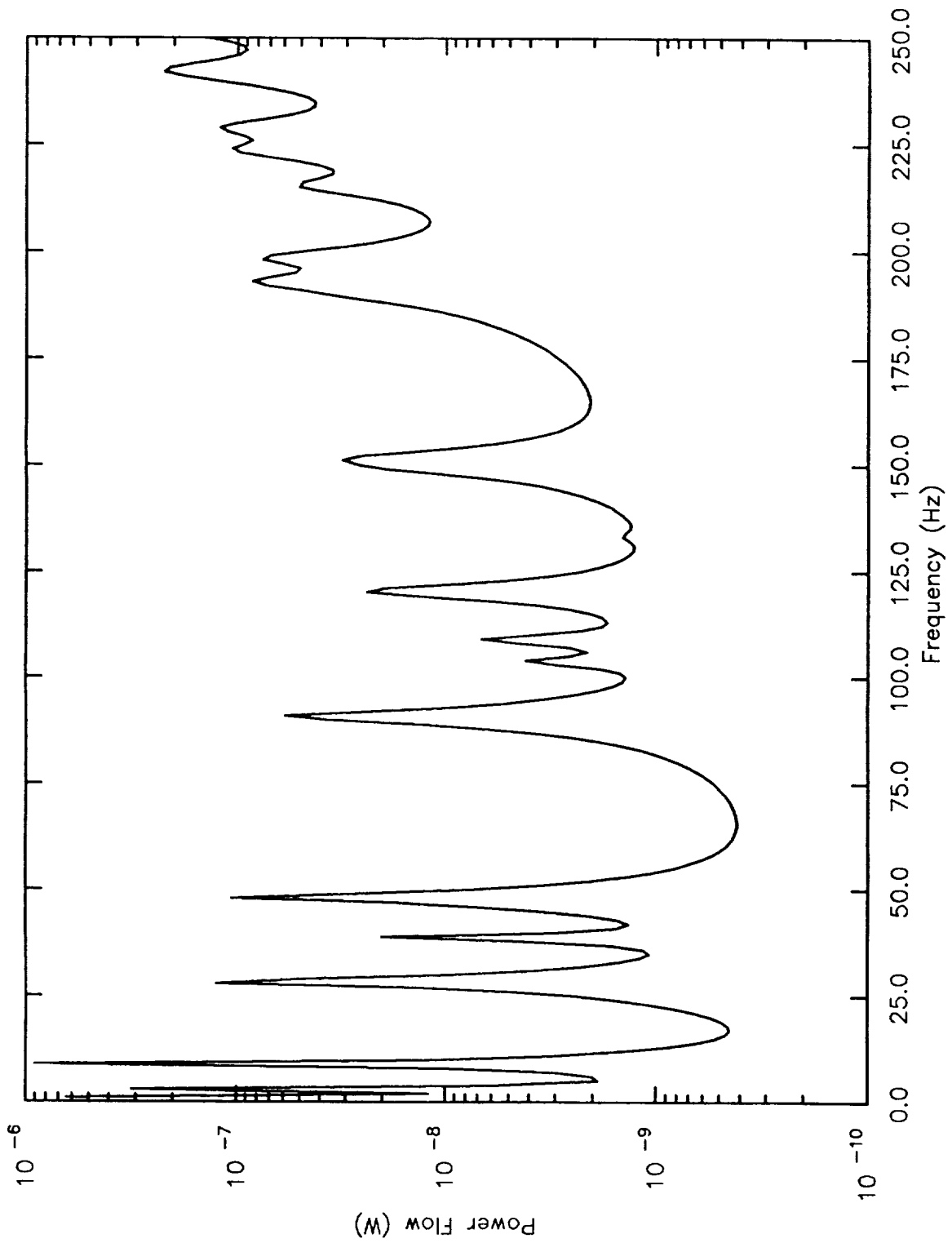


Fig. 4. Power inputs for test problem.

## Results and Discussion

The computed power input curve over the excitation frequency range is shown in Fig. 4. The power input peaks correspond to various resonances in the structure. Most are flexural, but some axial and torsional modes influence the power input curve. The longitudinal modes of Link 3 cause power input peaks (at 190 Hz and above), as well as the torsional modes of Link 1 (at 151 Hz and above).

In this model, the power flow path is independent of frequency. The total power must always flow from the input point at the end of Link 3 to the dampers at the beginning of Link 1. This simplifies the interpretation of the results, since the directions of total power flow are established.

The types of power flow in a given link are not so well-defined. Whether the dominant path in a link is flexural, axial, or torsional, depends on the motion of the structure. Fig. 5 shows the two most common types of motion paths for this problem. The displacement field of Diagram 1 occurs most often. The axial load applied to Link 3 drives the entire structure forward and backward over a frequency cycle. The dominant power flow in Link 3 is axial; the dominant power flow in Link 2 is flexural; and torsional and flexural power flows are dominant in Link 1, since the input load applies both a torque and bending moment to the link.

In Diagram 2 of Fig. 5 a different type of motion is shown. The axial load still drives the upper half of the structure in the same direction, but the lower half moves in the opposite direction. This type of motion is not what one would expect in a static problem, but the dynamic characteristics of the structure produce this type of motion in various frequency ranges.

Due to this motion path, the axial power flow travelling down Link 3 becomes flexural, torsional, and axial in Link 2. The torsional and axial components appear because the link is twisted and stretched by the opposite directions of motion of the two ends. The torsional power in Link 2 becomes flexural power in Plane 1 in Link 1, and the axial power in Link 2 turns into flexural power in Plane 2 in Link 1. The flexural power in Link 2 becomes torsional and flexural power in Link 1 as before (Diagram 1).

Considering these modes of power transitioning, the power flow plots in Figs. 6-8 may be interpreted. Each plot shows the contributions of flexural, torsional, and axial power flow as a percentage of the total power flow in the center of each link.

Fig. 8 shows the power components in Link 3. Since the input power is in the longitudinal direction, the majority of the power in this link is axial. At certain frequencies, the percentage of axial power is greater than 100 percent. The large axial percentage arises because at certain frequencies, reflected waves carry power in the opposite direction (toward the load). Three flexural resonances in the structure cause reflected power just before 50 Hz, along with

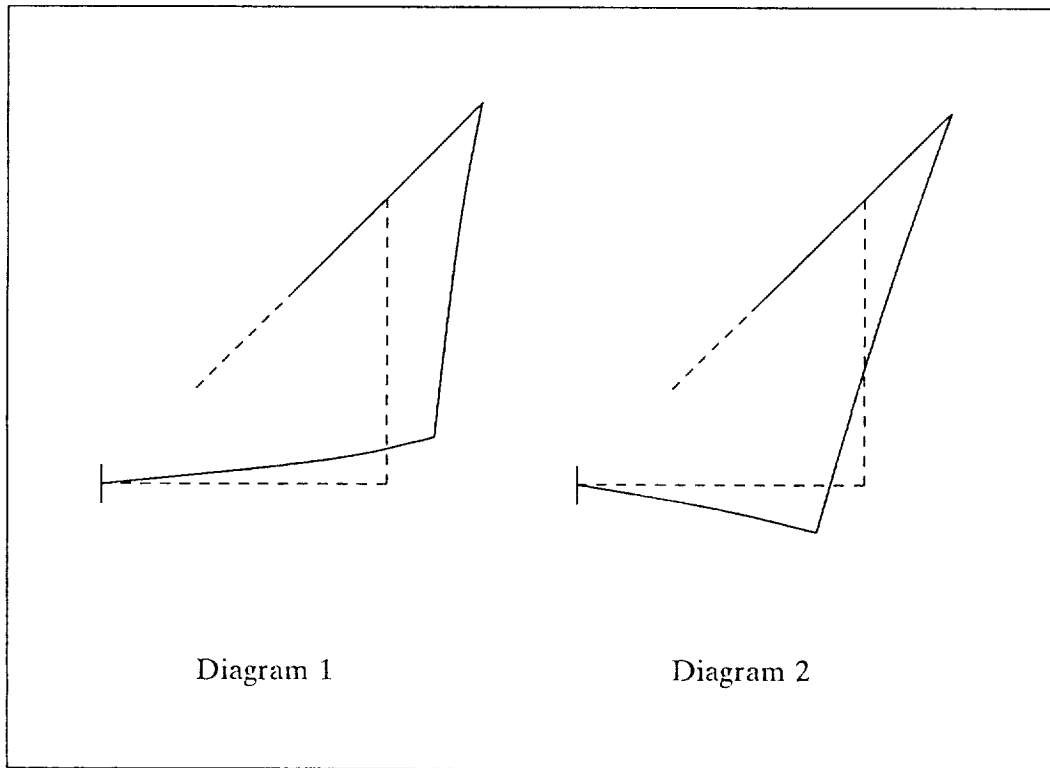


**Fig. 5.** Dominant motion paths for test problem

five others right after 100 Hz. Between 200 and 250 Hz, some flexural and torsional resonances cause more reflected powers.

Fig. 7 shows the power components in Link 2. The dominant type of power is the flexural component in Plane 1, and is denoted by the solid curve. This type of power field corresponds to the motion type shown in Diagram 1 in Fig. 5. However at certain frequencies, the power flow pattern of Diagram 2 becomes dominant, and axial and torsional power become important. In most cases, the axial power flows forward (away from the load point), and the torsional power is backward (reflected toward the load point). These tendencies occur at the same frequencies as the reflected power waves do in Link 3 (shown in Fig. 8). This behavior indicates that the flexural power in Plane 1 and the torsional power cause reflected flexural powers in Planes 2 and 1 respectively in Link 3.

Fig. 6 shows the power distribution in Link 1. In this case, all power components are positive, implying that the reflected power waves in Links 2 and 3 originate from the joint connecting Links 1 and 2. In Link 1, flexure in Plane 1 and torsion are the dominant components of power flow. Flexural

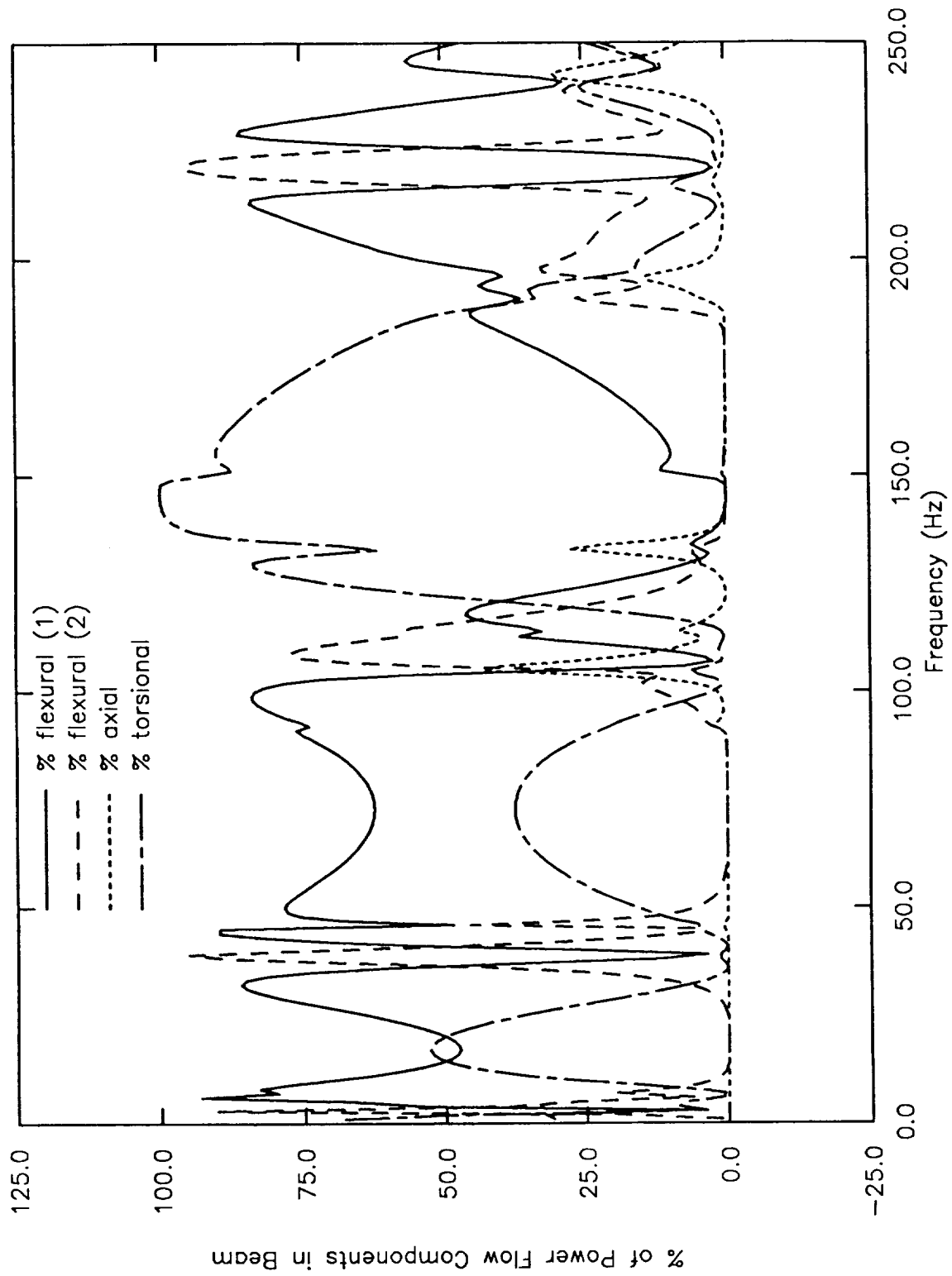


Fig. 6. Power flow types in Link 1.

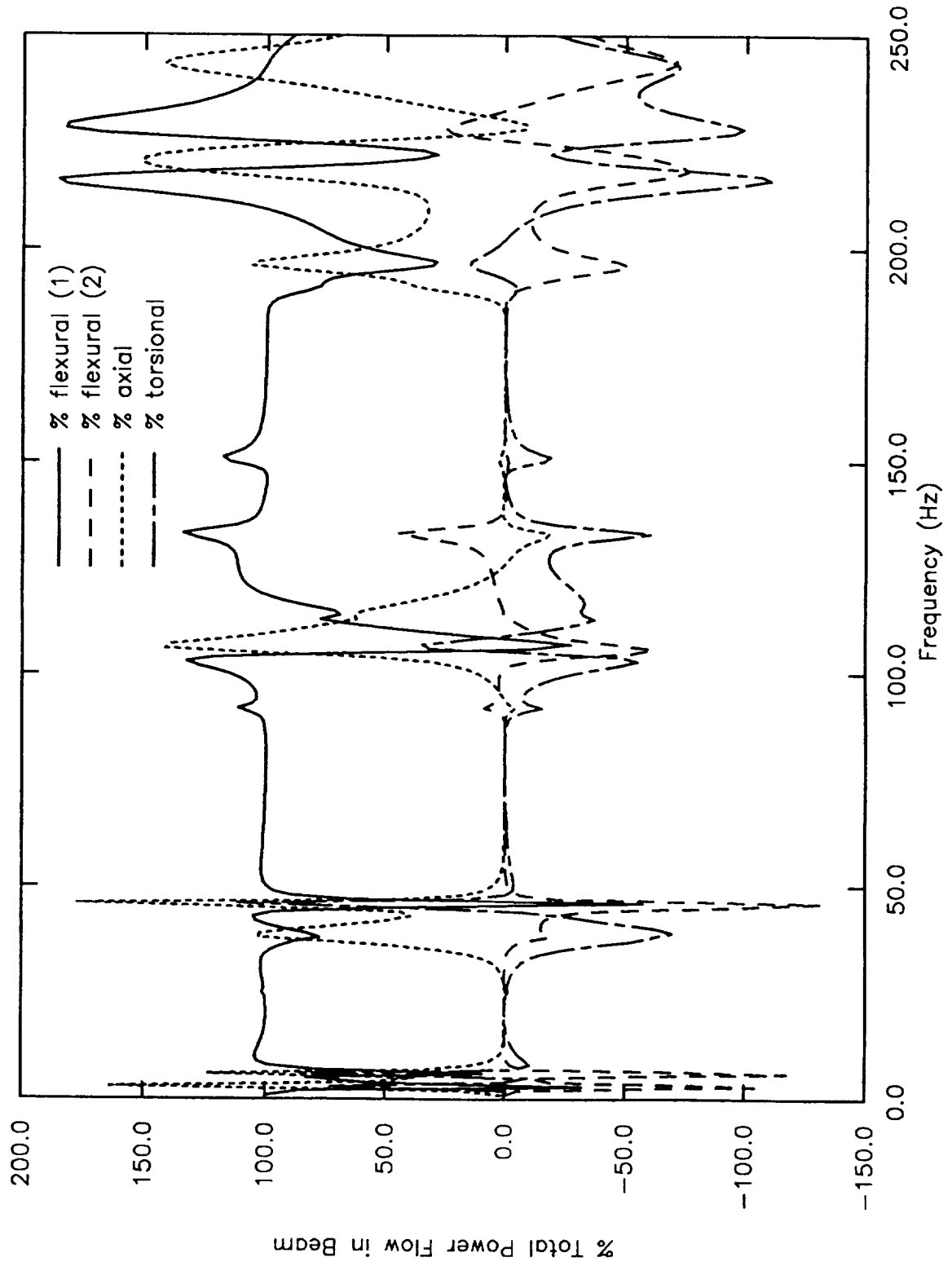


Fig. 7. Power flow types in Link 2.

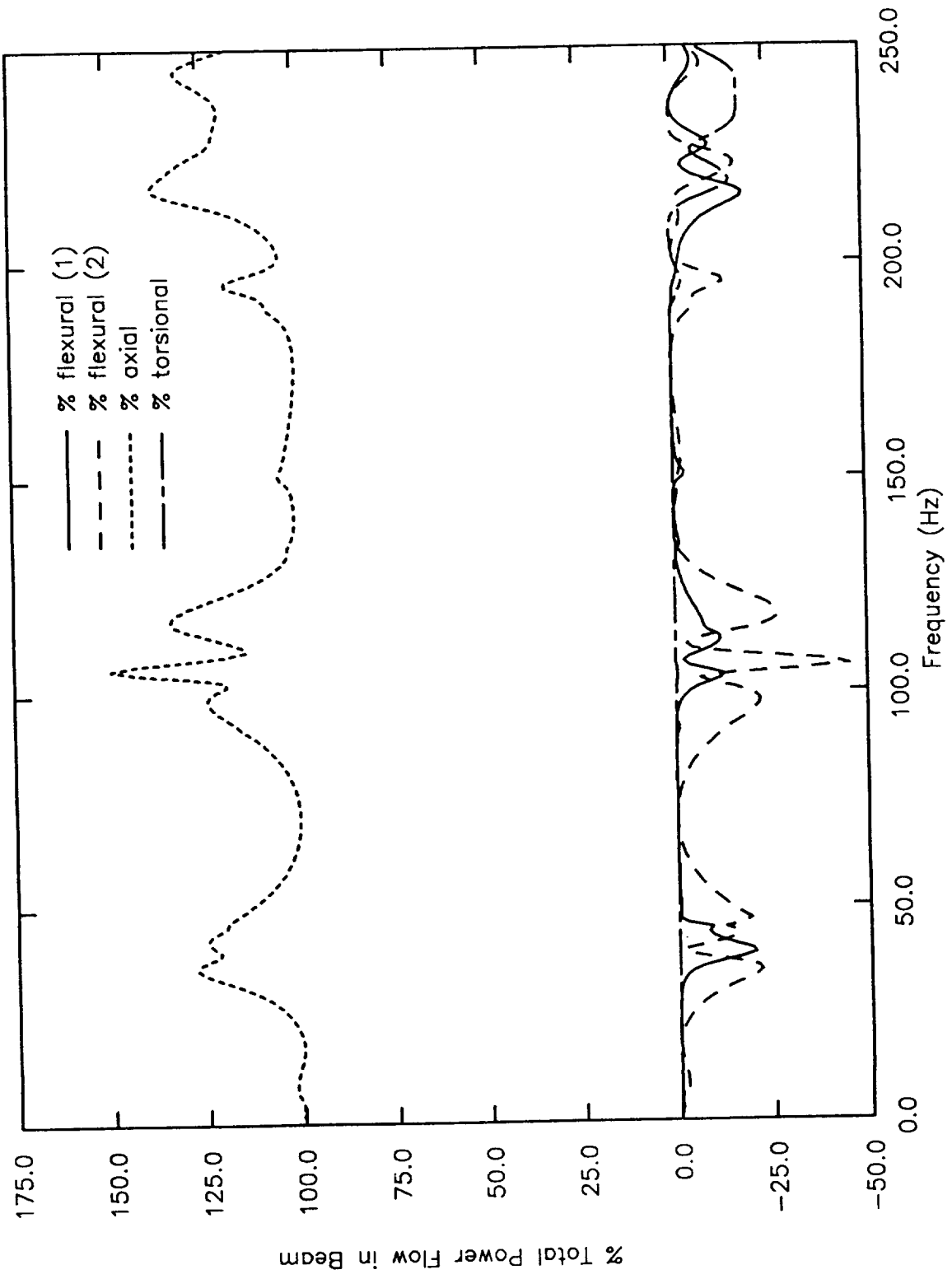


Fig. 8. Power flow types in Link 3.

motion in Plane 2 and axial motion cause power peaks at the same frequencies observed in Figs. 7 and 8, indicating the type of motion shown in Diagram 2 in Fig. 5. A torsional mode in Link 1 accounts for the peak in the torsion curve at 150 Hz, along with an input power peak at the same frequency (see Fig. 4).

In spite of the large variation in percentages of power types in the plots, all the power curves add up to 100 percent, as expected. In addition, the total power flow in the structure at all frequencies is at a maximum at the load point, and smoothly decreases to a minimum at the connection point to the dampers. The steady decrease in power is due to structural damping. The remaining power is all dissipated by the connected dampers.

This example illustrates the importance of all types of power components in a power flow analysis. Imagine trying to discern a meaningful power flow field from only flexural powers in this example. The detected powers in Link 3, which is adjacent to the input load, are all in the opposite direction, or toward the load. In Link 2, the analyst would see a sudden jump in power to values that are higher than that of the input power. Finally, in Link 1, sporadic power curves with values near the input power at frequencies below 100 Hz and values near zero after 100 Hz would be found. Confusion would surely result, with erroneous conclusions soon following. Difficulties like these would be compounded in a real application with some degree of complexity.

### CONCLUSIONS

The modifications made to NASTRAN and McPOW are critical to the power flow method. Without torsional inertias applied to the beam element mass matrices, any torsional effects in a dynamic problem are static. None of the torsional power flows present in the example problem would exist, causing incorrect total power flow fields. Adding mass and damping effects to the element force calculation algorithm is also important. In a reverberant structure where forces and velocities are nearly 90 degrees out of phase with each other, accurate calculations are necessary to guarantee good power flow results. A small change in the phase of an element force, caused by neglecting the material loss factor, could cause large errors in element power flows. Also, at higher frequencies, element mass terms can become significant and affect the element force magnitudes, and hence the element power magnitudes.

The addition of torsional inertia to the beam element mass matrix formulation was straight-forward. The addition of damping and mass effects to the element force calculation routines, however, was almost impossible. In fact, the changes had to be made to McPOW instead of NASTRAN. The implementation difficulties were due to the way NASTRAN handles complex analysis: the solutions are broken into real and imaginary parts. When the program was in its formative stages, UNIVAC computers were supported.

The UNIVAC, unfortunately, had no way of handling double precision complex arithmetic. Therefore, no complex numbers or FORTRAN complex functions are used in the element force calculation sections of the program. With this approach, a simple complex calculation like  $[-\omega^2 [M]_e + (1 + i\eta)[K]_e] \{d\}_e$  must be split up into four calculations. Also, since the calculation is frequency-dependent, the NASTRAN element force subroutines are not currently able to handle it. Since the UNIVAC has all but disappeared from the COSMIC NASTRAN computing arena and most modern computers support double precision complex arithmetic, perhaps the way NASTRAN handles complex problems should be modified.

The importance of including longitudinal and torsional components with flexural ones in a power flow analysis was shown in the example problem. Measuring flexural power alone will not give an accurate indication of the total power flow field in even a marginally complex problem. In the case of the example problem, reflected flexural waves actually indicated a reversal of power flow in the model, where the direction of flexural power was in the opposite direction of the input power. Trying to interpret power flow results that only consider flexural components will result in incorrect conclusions concerning the total power flow field.

#### REFERENCES

1. Hambric, S.A., 1988, "Power Flows and Mechanical Intensities using NASTRAN," Proceedings of the Seventeenth NASTRAN Users' Colloquium, pp. 262-289 (1989).
2. Cremer, L., Heckl, M., and Ungar, E.E., 1973, *Structure-Borne Sound*, Springer-Verlag, New York.
3. Przemieniecki, J.S., 1968, *Theory of Matrix Structural Analysis*, McGraw-Hill, New York.

310-2  
198

## COUPLED BE/FE/BE APPROACH FOR SCATTERING FROM FLUID-FILLED STRUCTURES

by

Gordon C. Everstine and Raymond S. Cheng

Applied Mathematics Division  
David Taylor Research Center  
Bethesda, Maryland 20084

### ABSTRACT

NASHUA is a coupled finite element/boundary element capability built around NASTRAN for calculating the low frequency far-field acoustic pressure field radiated or scattered by an arbitrary, submerged, three-dimensional, elastic structure subjected to either internal time-harmonic mechanical loads or external time-harmonic incident loadings. This paper describes the formulation and use of NASHUA for solving such structural acoustics problems when the structure is fluid-filled. NASTRAN is used to generate the structural finite element model and to perform most of the required matrix operations. Both fluid domains are modeled using the boundary element capability in NASHUA, whose matrix formulation (and the associated NASTRAN DMAP) for evacuated structures can be used with suitable interpretation of the matrix definitions. After computing surface pressures and normal velocities, far-field pressures are evaluated using an asymptotic form of the Helmholtz exterior integral equation. The proposed numerical approach is validated by comparing the acoustic field scattered from a submerged fluid-filled spherical thin shell to that obtained with a series solution, which is also derived in this paper.

### INTRODUCTION

Two basic problems in computational structural acoustics are (1) the calculation of the acoustic pressure field radiated by a general submerged three-dimensional elastic structure subjected to internal time-harmonic loads, and (2) the calculation of the acoustic pressure scattered by such a structure subjected to an incident time-harmonic wavetrain. The most common, as well as the most accurate, approach for solving these problems at low frequencies is to couple a finite element model of the structure with a boundary element model of the surrounding fluid. This is the approach taken by NASHUA, which is a boundary element program built around NASTRAN, a widely-used finite element computer program for structural dynamics.

Several previous papers (Ref. 1-4) described the basic formulation and development for acoustic radiation and scattering from evacuated structures. Here we describe the formulation and use of NASHUA for modeling submerged structures which are fluid-filled. Internal fluid can occur because the structure is free-flooded or contains fluid-filled tanks. It is possible to use existing NASTRAN capability to model the interior fluid with finite elements (Ref. 5-7), but three-dimensional models with large numbers of fluid degrees of freedom might result. An attractive alternative to the fluid finite element model is to represent the contained fluid using a boundary element approach. In principle, any computer

program capable of generating the appropriate boundary element matrices for an exterior fluid is also capable of generating such matrices for the complementary region (the interior region). NASTRAN's versatility in user-controlled matrix operations (DMAP) makes the implementation of such an approach straightforward.

## THEORETICAL APPROACH

The basic theoretical development for NASHUA's radiation and scattering approach for evacuated structures has been presented in detail previously (Ref. 1-4). For completeness, this paper summarizes that approach and describes the changes necessary to model the interior fluid with boundary elements in the same procedure. There is no requirement that the interior and exterior fluids be the same.

### The Surface Solution for Evacuated Structures

Consider any submerged three-dimensional, evacuated elastic structure subjected to either internal time-harmonic loads or an external time-harmonic incident wavetrain. If the structure is modeled with finite elements using NASTRAN, the resulting matrix equation of motion can be written as

$$Zv = F - G\Lambda p, \tag{1}$$

where matrix  $Z$  (of dimension  $s \times s$ ) is the structural impedance, vector  $v$  ( $s \times r$ ) is the complex velocity amplitude for all structural DOF (wet and dry) using the coordinate systems selected by the user, vector  $F$  ( $s \times r$ ) is the complex amplitude of the mechanical forces applied to the structure, matrix  $G$  ( $s \times f$ ) is the rectangular transformation of direction cosines to transform a vector of outward normal forces at the wet points to a vector of forces at all points in the coordinate systems selected by the user, matrix  $\Lambda$  ( $f \times f$ ) is the diagonal area matrix for the wet surface, and vector  $p$  ( $f \times r$ ) is the complex amplitude of total pressures (incident + scattered) applied at the wet grid points. In this equation, the time dependence  $\exp(i\omega t)$  has been suppressed. In the above dimensions,  $s$  denotes the total number of independent structural DOF (wet and dry),  $f$  denotes the number of fluid DOF (wet points), and  $r$  denotes the number of load cases. In general, the surface areas, the normals, and the transformation matrix  $G$  are obtained in NASHUA from the NASTRAN calculation of the load vector resulting from an outwardly directed static unit pressure load on the structure's wet surface.

In Eq. 1, the structural impedance matrix  $Z$ , which converts velocity to force, is given by

$$Z = (-\omega^2 M + i\omega B + K)/(i\omega), \tag{2}$$

where  $M$ ,  $B$ , and  $K$  are the structural mass, viscous damping, and stiffness matrices, respectively, and  $\omega$  is the circular frequency of excitation. For structures with a nonzero loss factor,  $K$  is complex. In addition,  $K$  can include the differential stiffness effects of hydrostatic pressure, if any (Ref. 3). A standard NASTRAN finite element model of the structure supplies the matrices  $K$ ,  $M$ , and  $B$ .

For the exterior fluid domain, the total fluid pressure  $p$  satisfies the Helmholtz differential equation

$$\nabla^2 p + k^2 p = 0, \quad (3)$$

where  $k = \omega/c$  is the acoustic wave number, and  $c$  is the fluid sound speed. Equivalently, for the exterior fluid,  $p$  is the solution of the Helmholtz integral equations (Ref. 8)

$$\int_S p(\mathbf{x}) \frac{\partial D(\mathbf{r})}{\partial n} dS - \int_S q(\mathbf{x}) D(\mathbf{r}) dS = \begin{cases} p(\mathbf{x}')/2 - p_I, & \mathbf{x}' \text{ on } S, \\ p(\mathbf{x}') - p_I, & \mathbf{x}' \text{ in } E, \\ -p_I, & \mathbf{x}' \text{ in } I, \end{cases} \quad (4)$$

where  $S$ ,  $E$ , and  $I$  denote the surface, exterior, and interior domains, respectively,  $p_I$  is the incident free-field pressure (if any),  $r$  is the distance from  $\mathbf{x}$  to  $\mathbf{x}'$  (Fig. 1),  $D$  is the free-space Green's function

$$D(\mathbf{r}) = \frac{e^{-ikr}}{4\pi r}, \quad (5)$$

$$q = \frac{\partial p}{\partial n} = -i\omega\rho v_n, \quad (6)$$

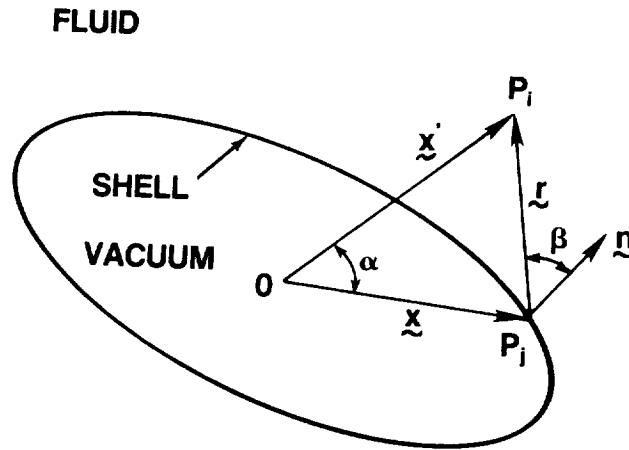


Fig. 1. Notation for Helmholtz Integral Equation

$\rho$  is the fluid mass density, and  $v_n$  is the outward normal velocity on  $S$ . As shown in Fig. 1,  $\mathbf{x}$  in Eq. 4 is the position vector for a typical point  $P_j$  on the surface  $S$ ,  $\mathbf{x}'$  is the position vector for the point  $P_i$  on the surface or in the exterior field, the vector  $\mathbf{r} = \mathbf{x}' - \mathbf{x}$ , and  $\mathbf{n}$  is the unit outward normal at  $P_j$ . We denote the lengths of the vectors  $\mathbf{x}$ ,  $\mathbf{x}'$ , and  $\mathbf{r}$  by  $x$ ,  $x'$ , and  $r$ , respectively. The normal derivative of the Green's function  $D$  is (Ref. 1)

$$\frac{\partial D(\mathbf{r})}{\partial n} = \frac{e^{-ikr}}{4\pi r} \left( ik + \frac{1}{r} \right) \cos \beta, \quad (7)$$

where  $\beta$  is the angle between the normal  $\mathbf{n}$  and the vector  $\mathbf{r}$ , as shown in Fig. 1.

All three integral equations in Eq. 4 are needed for exterior fluids. The surface equation provides the fluid impedance at the fluid-structure interface. Since the surface

equation exhibits non-uniqueness at certain discrete characteristic frequencies (Ref. 9), the interior equation is used to provide additional constraint equations which ensure the required uniqueness. The exterior equation is used to compute the exterior pressure field once the surface solution (which includes the fluid pressure and its gradient) is known.

The substitution of Eqs. 6 and 7 into the surface equation (4) yields

$$\frac{p(\mathbf{x}')}{2} - \int_S p(\mathbf{x}) \frac{e^{-ikr}}{4\pi r} (ik + \frac{1}{r}) \cos \beta dS = i\omega\rho \int_S v_n(\mathbf{x}) \frac{e^{-ikr}}{4\pi r} dS + p_I, \quad \mathbf{x}' \text{ on } S. \quad (8)$$

This integral equation relates the total pressure  $p$  and normal velocity  $v_n$  on  $S$ . If the integrals in Eq. 8 are discretized for numerical computation (Ref. 1), we obtain the matrix equation (for the exterior fluid)

$$E p = C v_n + p_I, \quad (9)$$

where vector  $p$  (of dimension  $f \times r$ ) is the vector of complex amplitudes of the total pressure on the structure's wet surface, matrices  $E$  and  $C$  (both  $f \times f$ ) are fully-populated, complex, nonsymmetric, and frequency-dependent, and vector  $p_I$  ( $f \times r$ ) is the complex amplitude of the incident pressure vector. The number of unknowns in this system is  $f$ , the number of wet points on the fluid-structure interface.

The normal velocities  $v_n$  in Eq. 9 are related to the total velocities  $v$  by the same rectangular transformation matrix  $G$ :

$$v_n = G^T v, \quad (10)$$

where  $T$  denotes the matrix transpose. If velocities  $v$  and  $v_n$  are eliminated from Eqs. 1, 9, and 10, the resulting equation for the coupled fluid-structure system is

$$(E + C G^T Z^{-1} G A) p = C G^T Z^{-1} F + p_I. \quad (11)$$

This equation is solved for the total surface pressures  $p$ , since the rest of the equation depends only on the geometry, the material properties, and the frequency. Since the two right-hand side terms in Eq. 11 correspond to mechanical and incident loadings, only one of the two terms would ordinarily be present for a given case. The details of the incident pressure vector  $p_I$  for scattering problems were presented previously (Ref. 2) and will not be repeated here.

The velocity vector  $v$  for all structural DOF is recovered by solving Eq. 1 for  $v$ :

$$v = Z^{-1} F - Z^{-1} G A p. \quad (12)$$

The surface normal velocity vector  $v_n$  is recovered by substituting this solution for  $v$  into Eq. 10.

### Modeling Interior Fluid

The theoretical development presented in the preceding section can be modified slightly to account also for an interior fluid. The wave equation, Eq. 3, applies also to interior fluids. Although all three integral equations in Eq. 4 are generally needed for exterior fluids, only the surface equation is needed to represent the surface impedance of interior fluids. Eq. 4a also applies to interior fluids if the incident pressure  $p_I$  is set to zero, and the normal vector  $\mathbf{n}$  is negated. That is, the surface integral equation applies to both exterior and interior fluids

so long as the unit normal is always directed from the structure into the fluid. One other consideration, perhaps unique to NASHUA, is that wet surface curvatures (which are needed in the calculation of the "self" terms in matrix E) are negative at some interior points (Ref. 1).

A matrix equation similar to Eq. (9) is therefore obtained for the interior fluid except that the incident pressure  $p_I$  is zero. The fluid matrices E and C are different for exterior and interior domains (even if the separating surface S has infinitesimal thickness) because the normals are of opposite sign.

### Two-Fluid Formulation

Denote the exterior fluid as Fluid 1 and the interior fluid as Fluid 2, and use the subscripts 1 and 2 to refer to these two domains. Also define new pressure and normal velocity unknowns  $p$  and  $v_n$  which include the solutions for both fluid domains:

$$p = \begin{Bmatrix} p_1 \\ p_2 \end{Bmatrix}, \quad v_n = \begin{Bmatrix} v_{n1} \\ v_{n2} \end{Bmatrix}. \quad (13)$$

Since there is no direct fluid coupling between the interior and exterior fluids, and the incident pressure vanishes in the interior domain, Eqs. 1, 9, 10, and 11 apply also to the two-fluid problem if the new definitions in Eq. 13 are used, and the matrices A, G, E, C, and  $p_I$  are re-defined as

$$A = \begin{bmatrix} A_1 & \\ & A_2 \end{bmatrix}, \quad G = \begin{bmatrix} G_1 & G_2 \end{bmatrix}, \quad E = \begin{bmatrix} E_1 & \\ & E_2 \end{bmatrix}, \quad C = \begin{bmatrix} C_1 & \\ & C_2 \end{bmatrix}, \quad p_I = \begin{Bmatrix} p_{I1} \\ 0 \end{Bmatrix}. \quad (14)$$

The principle benefit of formulating the two-fluid problem in this way is that the required modifications to extend the procedure to three or more independent fluid domains is now clear.

### The Far-Field Calculation

With the solution for the total pressures and velocities on the surface, the exterior Helmholtz integral equation, Eq. 4b, can be integrated to obtain the radiated (or scattered) pressure at any desired location  $x'$  in the exterior field. We first substitute Eqs. 5 - 7 into Eq. 4b to obtain

$$p(x') = \int_S [i\omega\rho v_n(x) + (ik + \frac{1}{r})p(x) \cos \beta] \frac{e^{-ikr}}{4\pi r} dS, \quad x' \text{ in E.} \quad (15)$$

In applications, however, the field pressures generally of interest are in the far-field, so we use instead the asymptotic form of Eq. 15 (Ref. 1):

$$p(x') = \frac{ike^{-ikx'}}{4\pi x'} \int_S [\rho c v_n(x) + p(x) \cos \beta] e^{ikx \cos \alpha} dS, \quad x' \text{ in E, } x' \gg d, \quad (16)$$

where  $d$  is a characteristic dimension of the structure, and  $\alpha$  is the angle between the vectors  $x$  and  $x'$  (Fig. 1). For far-field points,  $\cos \beta$  is computed using the asymptotic approximation

$$\cos \beta \rightarrow \mathbf{n} \cdot \frac{\mathbf{x}'}{x'}. \quad (17)$$

For both Eqs. 15 and 16, numerical quadrature is used.

### OVERVIEW OF SOLUTION PROCEDURE

The NASHUA solution procedure uses NASTRAN to generate the matrices  $K$ ,  $M$ ,  $B$ , and  $F$  and to generate sufficient geometry information so that the matrices  $E$ ,  $C$ ,  $G$ ,  $A$ , and  $p_I$  can be computed by a separate program called SURF. Then, NASTRAN DMAP is used to form the matrices appearing in Eq. 11, which is solved for the total pressures  $p$  (in both fluid domains) using the block solver OCSOLV (Ref. 10). Next, NASTRAN DMAP is used to recover the surface normal velocities  $v_n$  and the vector  $v$  of velocities at all structural DOF (NASTRAN's "g-set"). This step completes the surface solution. Then, with the total pressures and velocities on the (exterior) surface, the asymptotic (far-field) form of the Helmholtz exterior integral equation is integrated in program FAROUT to compute the far-field radiated pressures. Various tables and graphical displays are generated.

The overall setup of the solution procedure is organized into four steps. In Step 1, a separate NASTRAN structural model is prepared and run for each unique set of symmetry constraints and each fluid region. Since, for general three-dimensional analysis, up to three planes of reflective symmetry are allowed, there would be one, two, four, or eight such runs for each fluid region. Since the purpose of this step is to generate a file containing geometry information and a checkpoint file for subsequent use in the other steps, the only difference between the two runs associated with a given symmetry case is the specification of the outwardly directed unit pressure load which defines the wet surface for a given fluid region.

For each symmetry case and drive frequency, several programs are run sequentially to form Step 2. For each fluid region, the SURF program reads the geometry file generated by NASTRAN in Step 1 and, using the Helmholtz surface and interior integral equations, generates the fluid matrices  $E_1$ ,  $E_2$ ,  $C_1$ , and  $C_2$ , the area matrices  $A_1$  and  $A_2$ , the structure-fluid transformation matrices  $G_1$  and  $G_2$ , the incident pressure vector  $p_{I1}$ , and a geometry file to be used later by the far-field integration program FAROUT in Step 3. In addition, a partitioning vector is generated to facilitate the merging and partitioning of the various matrices associated with the two fluid domains.

The two SURF jobs in Step 2 are followed by a NASTRAN job which takes the structural matrices  $K$ ,  $M$ ,  $B$ , and  $F$  from Step 1 and the matrices generated by the SURF jobs and forms the matrices in Eq. 11, where the definitions in Eq. 14 apply. Eq. 11 is then solved for the total surface pressure vector  $p$  by program OCSOLV, which is a general out-of-core block solver designed specifically for large, full, complex, nonsymmetric systems of linear, algebraic equations. NASTRAN is then re-entered in Step 2 with  $p$  so that the velocities  $v$  and  $v_n$  can be recovered using DMAP operations. The surface pressures, normal velocities, and full g-set displacements are then reformatted, sorted, and merged into a single file (for each symmetry case) using program MERGE. Recall that there are one, two, four, or eight possible symmetry cases.

Steps 1 and 2 are repeated for each symmetry case. After all symmetry cases have been completed and merged, program FAROUT (Step 3) combines the symmetry cases and integrates over the surface. The far-field pressure solution is obtained by integrating the

surface pressures and velocities using the asymptotic (far-field) form of the exterior Helmholtz integral equation, Eq. 16. Output from FAROUT consists of both tables and files suitable for various types of plotting.

The remaining steps in the NASHUA procedure are for graphical display. Deformed structural plots of the frequency response are obtained by restarting NASTRAN (Step 4) with the checkpoint file from Step 1 and a results file from FAROUT. In addition, animated plots can be generated on the Evans & Sutherland PS-330 graphics terminal using the CANDI program written for the DEC/VAX computer by R.R. Lipman of DTRC (Ref. 11). X-Y plots of various quantities (both surface and far-field) versus frequency may be obtained using IPLOT or other interactive plotting programs (Ref. 12). Polar plots of the far-field sound pressure levels in each of the three principal coordinate planes can also be generated using the interactive graphics program FAFPLOT (Ref. 1).

### DMAP ALTERS

Several DMAP alters are used in the overall NASHUA procedure to implement the procedure described in preceding section. For Step 1, the following alter is used:

```

ALTER      1 $ NASHUA STEP 1, COSMIC 1988 RF8 (REVISED 12/7/89)
ALTER      2,2 $ DELETE PRECHK
ALTER      21,21 $ REPLACE GP3
GP3        GEOM3,EQEXIN,GEOM2/SLT,GPTT/S,N,NOGRAV/NEVER=1 $
ALTER      117,117 $ REPLACE FRRD
SSG1       SLT,BGPDT,CSTM,SIL,EST,MPT,GPTT,EDT,MGG,CASECC,DIT,/
           PG,,,/LUSET/NSKIP $ PG
SSG2       USET,GM,YS,KFS,GO,DM,PG/QR,PO,PS,PL $ PL
OUTPUT2    AXIC,BGPDT,EQEXIN,USET,PG $
OUTPUT2    PL,CSTM,ECT,, $
OUTPUT2    ,,,,/-9 $
PARAMR     /*EQ*/C,Y,HSP=0./0.////NOHSP $
COND       LBL4D,NOHSP $ SKIP DIFF. STIFF. IF NO HYDRO. P
PARAMR     /*COMPLEX*/C,Y,HSP=0./0./HSPC $ HSP+1*0
DIAGONAL   KAA/KDIAG/*SQUARE*/1.0 $
ADD        KAA,KDIAG/KAAD/(1.0,0.0)/(1.E-6,0.) $
RBMG2     KAAD/LLL $ FACTOR KAA
SSG3       LLL,KAAD,PL,LOO,KOO,PO/ULV,UOOV,RULV,RUOV/OMIT/
           V,Y,IRES=-1/1/S,N,EPSI $ STATIC SOLUTION
SDR1       USET,PG,ULV,UOOV,YS,GO,GM,PS,KFS,KSS,/UGV,PGG,QG/1/
           *BKI.0* $ RECOVER DEPENDENT DISPLACEMENTS
TA1        ECT,EPT,BGPDT,SIL,GPTT,CSTM/X1,X2,X3,ECPT,GPCT/LUSET/
           NOSIMP/0/NOGENL/GENEL $ TABLES FOR DIFF. STIFF.
DSMG1     CASECC,GPTT,SIL,EDT,UGV,CSTM,MPT,ECPT,GPCT,DIT/KDGG/
           S,N,DSCASET $ DIFF. STIFF. MATRIX
EQUIV     KDGG,KDNN/MPCF2 / MGG,MNN/MPCF2 $ EQUIV IF NO MPC'S
COND      LBL1D,MPCF2 $ TRANSFER IF NO MPC'S
MCE2      USET,GM,KDGG,,,/KDNN,,, $ MPC'S ON DIFF. STIFF.
LABEL     LBL1D $
EQUIV     KDNN,KDFF/SINGLE / MNN,MFF/SINGLE $ EQUIV. IF NO SPC'S
COND      LBL2D,SINGLE $ TRANSFER IF NO SPC'S

```

```

SCE1      USET,KDNN,,//KDFE,KDFS,KDSS,, $ SPC'S AND DIFF. STIFF.
LABEL     LBL2D $
EQUIV     KDFE,KDAA/OMIT / MFE,MAA/OMIT $ EQUIV. IF NO OMITs
COND      LBL3D,OMIT $ TRANSFER IF NO OMITs
SMP2      USET,GO,KDFE/KDAA $ OMITs AND DIFF. STIFF.
LABEL     LBL3D $
PARAMR    /*SUBC*///MHSPC//HSPC $ NEGATE HYDRO. P
ADD       KDD,KDAA/NEWKDD/(1.0,0.0)/MHSPC $
ADD       KFS,KDFS/NEWKFS/(1.0,0.0)/MHSPC $
EQUIV     NEWKDD,KDD//NEWKFS,KFS $
LABEL     LBL4D $ END OF DIFF. STIFF. EFFECTS (HSP)
DIAGONAL  KDD/IDENT/*SQUARE*/0. $ D-SET IDENTITY
ADD       IDENT,/IDM/(1.0,0.0) $ ANOTHER D-SET IDENTITY
ADD       IDENT,/ZERO/(0.0,0.0) $ D-SET ZERO MATRIX
FRRD      CASEXX,USETD,DLT,FRL,GMD,GOD,IDENT,ZERO,IDM,,DIT/
          UDVF,PSF,PDF,PPF/*DISP*//*DIRECT*/LUSETD/MPCF1/
          SINGLE/OMIT/NONCUP/FRQSET $ PDF, KDD=I, BDD=0, MDD=i
CHKPNT    MDD,KDD,BDD,PDF,PSF,PPF,EODYN,USETD,GOD,GMD $
CHKPNT    KFS,BGPDT,ECT,EQEXIN,GPECT,SIL $
EXIT     $
ENDALTER  $

```

The above alter does not depend on whether the fluid is interior or exterior to the structure. The Step 2 alters, however, depend on whether an interior fluid is present. For Step 2A, the following alter is used:

```

ALTER     1 $ NASHUA STEP 2A, COSMIC 1988 RF8 (REVISED 11/7/89)
ALTER     2,167 $ REPLACE ALL AFTER 'BEGIN' AND BEFORE 'END'
INPUTT2   /DAT2,,//13 $ INTERNAL FLUID
INPUTT2   /DAT,,//11 $ READ SURF MATRIX FROM UT1
MATPRN    DAT,DAT2,, $
PARAML    DAT/*DMI*/1/8/RIGD $ GET RIGID FLAG
PARAMR    /*EQ*/RIGD/0.///ELAST $ SET ELAST=-1 IF ELASTIC
COND      LBL9D,ELAST $ IF ELASTIC, JUMP OVER RIGID/SOFT
PARAMR    /*EQ*/RIGD/2.///SOFT $ SET SOFT=-1 IF SOFT BD.
COND      LBL9E,SOFT $ IF SOFT BOUNDARY, JUMP OVER RIGID
INPUTT2   /E,PI,VEKC,,//11 $ READ SURF MATRICES FROM UT1
OUTPUT2   PI,E,, //1 $ INPUTT2 FILE IS OVER-WRITTEN (UT1)
OUTPUT2   ,,, //9 $ EOF
CHKPNT    DAT,VEKC $
EXIT     $
LABEL     LBL9E $ BEGINNING OF SOFT ANALYSIS
INPUTT2   /CT,PI,VEKC,,//11 $ READ SURF MATRICES FROM UT1
TRNSP     CT/C $
ADD       PI,/MPI/(-1.0,0.0) $ NEGATE PI
OUTPUT2   MPI,C,, //1 $ INPUTT2 FILE IS OVER-WRITTEN (UT1)
OUTPUT2   ,,, //9 $ EOF
CHKPNT    DAT,VEKC $
EXIT     $
LABEL     LBL9D $ BEGINNING OF ELASTIC ANALYSIS
INPUTT5   /G2,A2,,//14 $ INTERNAL FLUID

```

```

INPUTT2      /C2T,E2,PI2,VEKC2,//13 $ INTERNAL FLUID
INPUTT5      /G1,A1,,,//12 $ READ SURF MATRICES FROM UT2
INPUTT2      /C1T,E1,PI1,VEKC,FVEC//11 $ READ SURF MATRICES
MATPRN       FVEC,,, $
MERGE        A1,,,A2,FVEC,/A/-1 $
MERGE        E1,,,E2,FVEC,/E/-1 $
MERGE        C1T,,,C2T,FVEC,/CT/-1 $
MERGE        G1,,G2,,FVEC,/G/0 $
MERGE        PI1,,,,,FVEC/PI/0 $
MATPRN       VECM,VECS,,, $
PARAML       DAT/**DMI*/1/2/FREQ $ GET FREQ FROM DAT
PARAMR       /**COMPLEX*/FREQ/0./FREQC $ FREQ+I*0
PARAMR       /**MPYC*////W/FREQC/(6.283185,0.) $ OMEGA
PARAMR       /**MPYC*////IW/W/(0.,1.) $ I*OMEGA
PARAMR       /**MPYC*////WW/W/W $ OMEGA**2
PARAMR       /**SUBC*////MWW//WW $ -OMEGA**2
ADD5         MDD,KDD,BDD,,/Y/MWW/(1.0,0.0)/IW $
MPYAD        G,A,/GA/0 $
DECOMP       Y/L,U/1//S,N,MINDIAG///S,N,SING $
FBS          L,U,GA/YIGA/1 $
FBS          L,U,PDF/YIF/1 $
ADD          YIGA,/ZIGA/IW $
ADD          YIF,/ZIF/IW $
MPYAD        G,ZIGA,/GTZIGA/1 $
MPYAD        CT,GTZIGA,E/H/1 $ LHS
MPYAD        G,ZIF,/GTZIF/1 $
MPYAD        CT,GTZIF,/Q/1 $ MECHANICAL RHS
MERGE        DUM,,PDF,,VECM,/PDF1/1 $ MERGE IN 0 COLUMNS
MERGE        DUM,,PSF,,VECM,/PSF1/1 $ MERGE IN 0 COLUMNS
MERGE        DUM,,PPF,,VECM,/PPF1/1 $ MERGE IN 0 COLUMNS
EQUIV        PDF1,PDF//PSF1,PSF//PPF1,PPF $
MERGE        DUM,,Q,,VECM,/RHS1/1 $ MERGE IN ZERO COLUMNS
MERGE        DUM,,GTZIF,,VECM,/GTZIFE/1 $ MERGE IN 0 COLUMNS
MERGE        DUM,,PI,,VECS,/RHS2/1 $ MERGE IN ZERO COLUMNS
ADD          RHS1,RHS2/RHS $ ADD MECH. AND INC. RHS
EQUIV        USETD,DUM1//GOD,DUM2//GMD,DUM3//KFS,DUM4 $
OUTPUT2      RHS,H,,, //-1 $ INPUTT2 FILE IS OVER-WRITTEN (UT1)
OUTPUT2      ,,,, //-9 $ EOF
CHKPNT       GTZIGA,GTZIFE,GA,PDF,L,U,PSF,DAT,VEKC,FVEC $
CHKPNT       USETD,GOD,GMD,KFS $
ENDALTER     $

```

The differences between this alter and one used for submerged evacuated structures are due to the need to read and combine two sets of SURF matrices, one for each fluid domain. For Step 2B, the following alter is used:

```

ALTER        1 $ NASHUA STEP 2B, COSMIC 1988 RF8 (REVISED 11/7/89)
ALTER        2,167 $ REPLACE ALL AFTER 'BEGIN' AND BEFORE 'END'
INPUTT2      /PC,,,,//11 $ READ PRESSURES FROM BLOCK SOLVER (UT1)
PARTN        PC.,FVEC/P1,,,/0 $ REMOVE INTERNAL FLUID DOF
PARTN        P1,,VEKC/P,,,/0 $ REMOVE CHIEF DOF FROM P

```

```

COND          LBL9D,ELAST $ IF ELASTIC, JUMP OVER RIGID/SOFT
OUTPUT2      DAT,P,,, //-1 $ INPUTT2 FILE IS OVER-WRITTEN (UT1)
OUTPUT2      ,,,, //-9 $ EOF
MATPRN       DAT,P,,, $ FOR SOFT BOUNDARY, P REPRESENTS VELOCITY
EXIT         $
LABEL        LBL9D $ ELASTIC ANALYSIS
MPYAD        GTZIGA,PC,GTZIFE/VNC/0/-1 $ NORMAL VELOCITIES
MPYAD        GA,PC,PDF/FA/0/-1 $ A-SET FORCES
FBS          L,U,FA/UDVF/1 $ A-SET DISPLACEMENTS
SDR1         USETD,,UDVF,,GOD,GMD,PSF,KFS,,/UPVC,,QPC/1/
              *DYNAMICS* $
PARTN        VNC,,FVEC/V1,,/0 $ REMOVE INTERNAL FLUID DOF
PARTN        V1,,VEKC/VN,,/0 $ REMOVE CHIEF DOF FROM VN
OUTPUT2      DAT,P,VN,UPVC, //-1 $ INPUTT2 FILE IS OVER-WRITTEN
OUTPUT2      ,,,, //-9 $ EOF
MATPRN       DAT,P,VN,, $
ENDALTER     $

```

This alter differs from one for evacuated structures because of the presence of several matrix partitionings to remove the internal fluid DOF from the solution vectors before the solutions are merged with the results for other frequencies.

### NUMERICAL EXAMPLE

Here we illustrate and validate the two-fluid boundary element formulation developed above by solving the problem of acoustic scattering from a submerged fluid-filled spherical thin shell. The incident loading is a time-harmonic planar wavetrain, as shown in Fig. 2. The specific problem solved has the following characteristics:

shell mean radius (a)	5 m
shell thickness (h)	0.15 m
shell Young's modulus (E)	$2.07 \times 10^{11}$ N/m <sup>2</sup>
shell Poisson's ratio ( $\nu$ )	0.3
shell density ( $\rho_s$ )	7669 kg/m <sup>3</sup>
shell loss factor ( $\eta$ )	0.01
fluid density ( $\rho$ )	1000 kg/m <sup>3</sup>
fluid sound speed (c)	1524 m/s

The same fluid is used for both the exterior and interior fluid domains. The solution of this problem exhibits rotational symmetry about the spherical axis parallel to the direction of wave propagation. The benchmark solution to which the numerical results will be compared is a series solution, the derivation of which is summarized in the next section.

### Series Solution

The series solution for scattering from a submerged evacuated spherical thin shell was presented by Junger and Feit (Ref. 13). Here we summarize that solution and indicate the modification necessary to include the addition of an interior fluid which fills the spherical

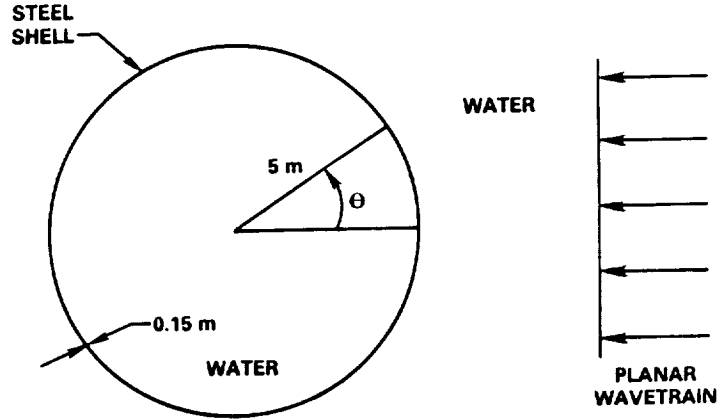


Fig. 2. Plane Wave Scattering from a Fluid-Filled Spherical Shell

volume.

In general, the series solution for plane wave scattering from a submerged, evacuated, spherical thin shell involves computing the impedances of the shell and exterior fluid, the scattered field due to rigid body effects, and the radiated field due to elastic (vibrational) effects. The shell impedance (the ratio of pressure to normal velocity) for the  $n$ th axisymmetric shell mode is

$$Z_n = -\frac{i\rho_s c_p}{\Omega} \frac{h}{a} \frac{[\Omega^2 - (\Omega_n^{(1)})^2][\Omega^2 - (\Omega_n^{(2)})^2]}{[\Omega^2 - (1 + \beta^2)(\nu + \lambda_n - 1)]}, \quad (18)$$

where  $\rho_s$  is the structural mass density,  $c_p = \sqrt{E/[\rho_s(1-\nu^2)]}$ ,  $E$  is Young's modulus,  $\nu$  is Poisson's ratio,  $\Omega = \omega a/c_p$  is the dimensionless frequency,  $h$  is the shell thickness,  $a$  is the shell mean radius,  $\beta = h/(a\sqrt{12})$ , and  $\lambda_n = n(n+1)$ . The quantities  $\Omega_n^{(1)}$  and  $\Omega_n^{(2)}$  are the upper and lower shell resonance dimensionless frequencies, respectively. They are the solutions of the characteristic equation

$$\Omega^4 - [1 + 3\nu + \lambda_n - \beta^2(1 - \nu - \lambda_n^2 - \nu\lambda_n)] \Omega^2 + (\lambda_n - 2)(1 - \nu^2) + \beta^2[\lambda_n^3 - 4\lambda_n^2 + \lambda(5 - \nu^2) - 2(1 - \nu^2)] = 0. \quad (19)$$

The impedance of the exterior fluid, found by using the Green's function and identity for the exterior fluid, is

$$z_n = i\rho c \frac{h_n(ka)}{h'_n(ka)}, \quad (20)$$

where  $h_n$  is the Bessel's function of the third kind of order  $n$ .

Thus, Junger and Feit showed that the far-field scattered pressure is

$$p(R, \theta) = -\frac{ie^{ikR} p_o}{kR} \sum_{n=0}^{\infty} \frac{(2n+1)P_n(\cos\theta)}{h'_n(ka)} \left[ j'_n(ka) - \frac{\rho c}{(Z_n + z_n)(ka)^2 h'_n(ka)} \right], \quad R \gg a, \quad (21)$$

where  $R$  is the distance to the field point,  $\theta$  is the angle from the  $z$ -axis,  $p_o$  is the incident pressure,  $P_n$  is the Legendre polynomial of order  $n$ , and  $j_n$  is the Bessel's function of the first kind of order  $n$ . The two terms in the bracketed expression correspond to rigid body and radiated effects, respectively.

The above expression for the pressure scattered from an evacuated shell can be extended to include the effects of the interior fluid merely by replacing the exterior fluid impedance  $z_n$  in Eq. 21 with the sum of the fluid impedances for the exterior and interior fluids. It can be shown, by using the Green's function and identity for the interior domain, that the interior impedance, denoted  $\zeta_n$ , is given by

$$\zeta_n = -i\rho c \frac{j_n(ka)}{j'_n(ka)}. \quad (22)$$

We note the resemblance between Eqs. 20 and 22 for the exterior and interior domains, respectively.

The computer program used to evaluate this series solution is a modification of a program called SCATSPHERE written by F.M. Henderson, a retired employee of DTRC. SCATSPHERE in turn is a variant of an earlier program called RADSPHERE (Ref. 14) for computing the radiation from an internally-driven submerged spherical shell.

### Numerical Solution

A NASTRAN finite element model of the spherical shell was prepared using 40 axisymmetric conical shell elements spanning the 180 degrees between the two poles of the sphere. Due to the axisymmetry of the incident pressure loading, only the  $N = 0$  harmonic was required. Since all structural points are in contact with both interior and exterior fluids, the resulting model therefore had 205 independent structural degrees of freedom (DOF) and 41 fluid DOF for each of the two fluid domains. System matrices for the exterior fluid were also augmented by the addition of four constraint equations associated with interior Chief points to ensure uniqueness of the integral representation at the upper frequencies. The nondimensional frequency range  $0 < ka < 5$  was swept using a frequency increment of about  $ka = 0.05$  with NASHUA and  $ka = 0.005$  with the series solution. Since the series solution is converged, we treat it as an "exact" solution for this problem.

The comparison between the computed and exact solutions is presented in Figs. 3 and 4, which plot the frequency response of the nondimensional scattered pressure  $pr/(p_o a)$ , where  $p$  is the far-field scattered pressure at distance  $r$  from the origin,  $p_o$  is the incident pressure, and  $a$  is the mean radius of the spherical shell. These two figures show very good agreement between the two scattering solutions in the backward ( $\theta = 0$ ) and forward ( $\theta = 180$  degrees) directions. In fact, the computed and series solutions are virtually indistinguishable from each other.

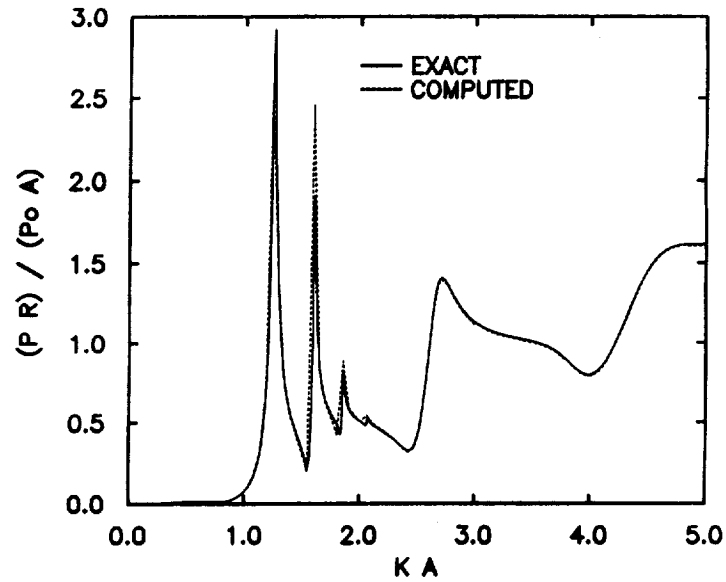


Fig. 3. Forward Scattering from a Fluid-Filled Spherical Shell

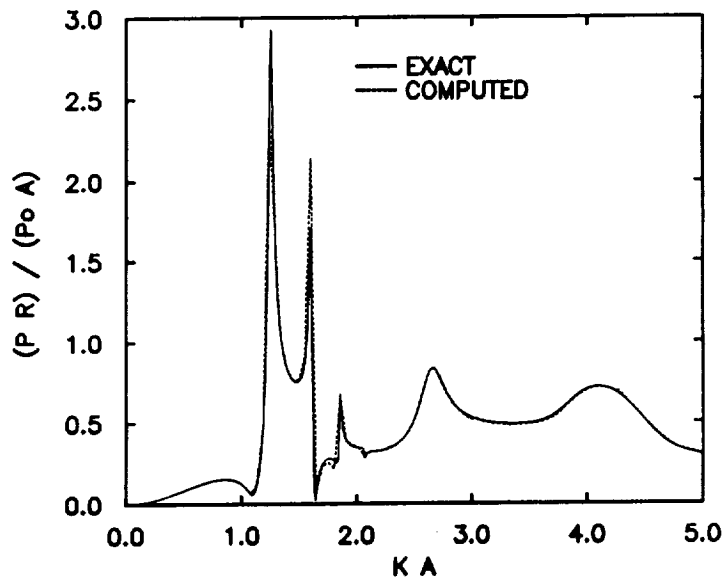


Fig. 4. Backward Scattering from a Fluid-Filled Spherical Shell

#### DISCUSSION

A very general computational capability has been described for predicting the sound pressure field radiated or scattered by arbitrary, submerged, fluid-filled, three-dimensional elastic structures subjected to time-harmonic loads. The structure is modeled with NASTRAN (in all the generality that NASTRAN allows) in combination with boundary

element models of both interior and exterior fluid domains. Sufficient automation is provided so that, for many structures of practical interest, an existing structural model can be adapted for NASHUA acoustic analysis within a few hours.

One of the many benefits of having NASHUA linked with NASTRAN is the ability to integrate the acoustic analysis of a structure with other dynamic analyses. Thus the same finite element model can be used for modal analysis, frequency response analysis, linear shock analysis, and underwater acoustic analysis. In addition, many of the pre- and postprocessors developed for use with NASTRAN become available for NASHUA as well.

#### REFERENCES

1. G.C. Everstine, F.M. Henderson, E.A. Schroeder, and R.R. Lipman, "A General Low Frequency Acoustic Radiation Capability for NASTRAN," in **Fourteenth NASTRAN Users' Colloquium**, NASA CP-2419, National Aeronautics and Space Administration, Washington, DC, pp. 293-310 (1986).
2. G.C. Everstine, F.M. Henderson, and L.S. Schuetz, "Coupled NASTRAN/Boundary Element Formulation for Acoustic Scattering," in **Fifteenth NASTRAN Users' Colloquium**, NASA CP-2481, National Aeronautics and Space Administration, Washington, DC, pp. 250-265 (1987).
3. G.C. Everstine, "Treatment of Static Preload Effects in Acoustic Radiation and Scattering," in **Sixteenth NASTRAN Users' Colloquium**, NASA CP-2505, National Aeronautics and Space Administration, Washington, DC, pp. 138-152 (1988).
4. G.C. Everstine and F.M. Henderson, "Coupled Finite Element/Boundary Element Approach for Fluid-Structure Interaction," **J. Acoust. Soc. Amer.**, to appear (1990).
5. G.C. Everstine, "Structural Analogies for Scalar Field Problems," **Int. J. Num. Meth. in Engrg.**, Vol 17, pp. 471-476 (1981).
6. G.C. Everstine, "A Symmetric Potential Formulation for Fluid-Structure Interaction," **J. Sound and Vibration**, Vol. 79, pp. 157-160 (1981).
7. G.C. Everstine, "Structural-Acoustic Finite Element Analysis, with Application to Scattering," in **Proc. 6th Invitational Symposium on the Unification of Finite Elements, Finite Differences, and Calculus of Variations**, edited by H. Kardestuncer, Univ. of Connecticut, Storrs, Connecticut, pp. 101-122 (1982).
8. D.T. Wilton, "Acoustic Radiation and Scattering from Elastic Structures," **Int. J. Num. Meth. in Engrg.**, Vol. 13, pp. 123-138 (1978).
9. H.A. Schenck, "Improved Integral Formulation for Acoustic Radiation Problems," **J. Acoust. Soc. of Amer.**, Vol. 44, pp. 41-58 (1968).
10. E.A. Schroeder, "A New Block Solver for Large, Full, Unsymmetric, Complex Systems of Linear Algebraic Equations," Report 88/003, David Taylor Research Center, Bethesda, Maryland (1988).
11. R.R. Lipman, "Computer Animation of Modal and Transient Vibrations," in **Fifteenth NASTRAN Users' Colloquium**, NASA CP-2481, National Aeronautics and Space Administration, Washington, DC, pp. 88-97 (1987).

12. G.C. Everstine, "A Portable Interactive Plotter for Digital X-Y Data," Report CMLD-86-45, David Taylor Research Center, Bethesda, Maryland (1986).
13. M.C. Junger and D. Feit, **Sound, Structures, and Their Interaction**, Second Edition, The MIT Press, Cambridge, Massachusetts (1986).
14. F.M. Henderson, "RADSPHERE – A Computer Program for Calculating the Steady-State, Axially Symmetric, Forced Response and Radiation Field of a Submerged Spherical Shell," Report 87/031, David Taylor Research Center (1987).

## MONITORING OF RITZ MODAL GENERATION

Mladen Chargin                      and  
NASA Ames Research Center

Thomas G. Butler  
Butler Analyses

In applying a Ritz modal expansion to the solution of a transient response, there is a problem as to how many modes are needed to obtain accuracy to within a specified percentage.

One of us, Chargin, has suggested a method based on the characteristics of the forcing function. The method can be incorporated into the Ritz generation algorithm such that it will automatically monitor, regulate and terminate the process according to a specified tolerance.

## FORCING FUNCTION CHARACTERISTICS

Assume that the forcing function  $F(x,t)$  can be represented as a product of a spatial function and a temporal function; i.e.

$$(1) \quad F(x,t) = F(x) \cdot f(t).$$

Develop a criterion based upon measuring the amount of power developed in the forcing function  $F(x,t)$ . The total power in  $F(x,t)$  is the product of the "power" in  $F(x)$  and  $f(t)$  owing to the assumption in equation (1). The scheme in outline is to measure the temporal power and the spatial power in  $F(x,t)$  separately then compare the corresponding power in the Ritz modes against power in each component of the forcing. Generation of

## MONITORING OF RITZ MODAL GENERATION

additional Ritz modes will continue until the power criteria are met. First a measure is taken of the total power in the temporal function.

### Temporal Power

$$(2) \quad P(\tau) = \int_0^{\tau} [f(t)]^2 dt \quad ,$$

where  $\tau$  is the interval over which the transient will act. There could very well be a separate temporal function for each spatial function. In that case of multiple loadings  $P(\tau)$  of equation (2) would be a vector "1" long.

In order to tailor this power to our use as a guide in selecting Ritz modes it will be useful to measure the amount of temporal power as a function of frequency. Expand the temporal function in a Fourier Series and sum the power versus the expansion multiple:

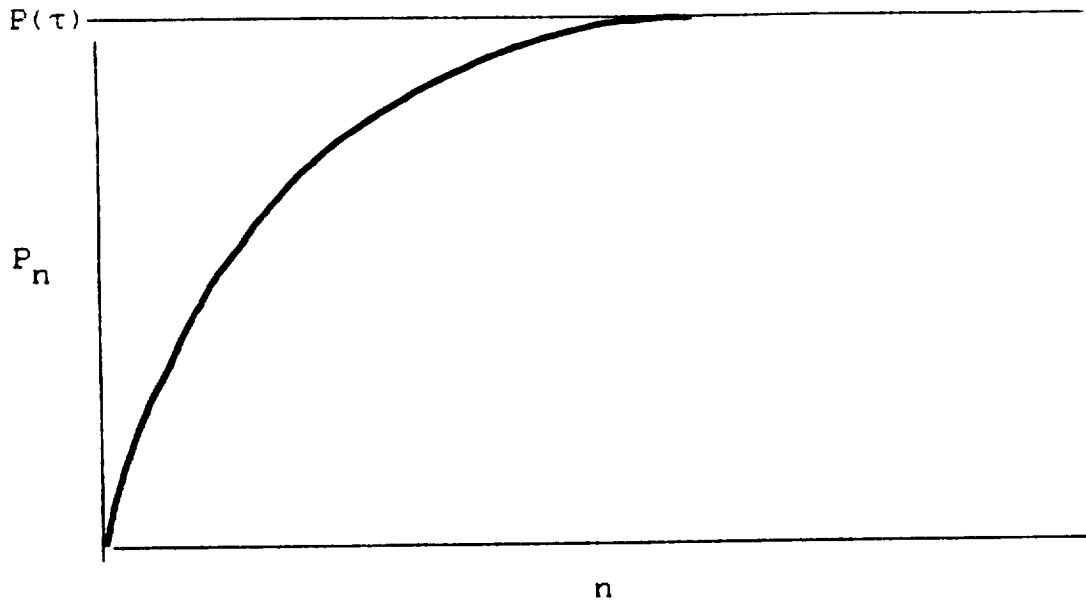
$$(3) \quad f(t) = a_0 + a_1 \cos \omega t + b_1 \sin \omega t + a_2 \cos 2\omega t + b_2 \sin 2\omega t \\ + \dots + a_n \cos n\omega t + b_n \sin n\omega t \quad .$$

The power within a band 0 to  $n\omega$  is:

$$(4) \quad P_n = \sum_{i=0}^n \left( a_i \cos i\omega t + b_i \sin i\omega t \right)^2 = \sum_{i=0}^n \left( a_i^2 + b_i^2 \right) \quad .$$

One can compare the amount of power within a given band  $P_n$  with the total power  $P(\tau)$ . When  $P_n$  is within close range of  $P(\tau)$ , say 1%, then the analyst can be satisfied that the frequency range of the truncated temporal forcing function is sufficiently broad to encompass the temporal requirements of the forcing.

## MONITORING OF RITZ MODAL GENERATION



For a certain frequency  $f_n = \frac{n\omega}{2\pi}$  ;  $\frac{P_n}{P(\tau)} = .99$ . Let this frequency be  $f_0$ .

### Spatial Power

Now turn to the spatial distribution of the forcing function  $F(x)$ , and develop a measure that is called spatial power. Make an additional assumption that all points being loaded have mass.

$$(5) \quad [\Pi(x)] = [F(x)]^T [M] [F(x)] = [C_{1a}] [F(x)] ,$$

where  $[C_{1a}] = [F(x)]^T M$  is a coefficient matrix that will be shown to be useful later.  $\Pi(x)$  is a matrix if there are a number of loading cases "l".

## MONITORING OF RITZ MODAL GENERATION

At this point we have 2 measures of the forcing function. We have  $f_0$  reflecting the desired frequency content and  $\Pi(\mathbf{x})$  reflecting the desired level of power to activate the structural mass. Now it is time to test the adequacy of the number of Ritz modes to respond to the forcing at these power levels.

First, get a spatial measure of the Ritz modes  $\theta_k$ . A simple scheme is to pattern the measure after equation (5) but substitute the matrix of  $k$  spatial Ritz functions for the post-multiply operation instead of the spatial component of loading  $F(\mathbf{x})$ .

$$(6) \quad [R_r] = \sum_{k=1}^r [F(\mathbf{x})]^T [M] [\theta_k] = \sum_{k=1}^r [C_{1a}] [\theta_k].$$

The way to use  $R_r$  is to compare each diagonal term of  $\Pi(\mathbf{x})$  with the corresponding diagonal term of  $R_r$  to see if the ratio is within a specified tolerance; i.e.

$$(7) \quad \left| \frac{\Pi_1 - R_{r1}}{\Pi_1} \right| \leq \epsilon \text{ for every } 1.$$

Keep generating additional Ritz modes  $\theta_k$   $k > r$  until an  $r$  has been reached for which every diagonal term satisfies the criterion.

### Monitoring Function

If the  $\theta_k$  satisfy the spatial power criterion of  $F(\mathbf{x},t)$  it does not necessarily hold that  $\theta_k$  will simultaneously satisfy the temporal requirements of  $F(\mathbf{x},t)$ . Therefore, use the  $\theta_k$  which have met the spatial power requirements and obtain an estimate of its frequency content by setting up the frequency equation. Use

## MONITORING OF RITZ MODAL GENERATION

an estimator that is much less demanding than solving the eigenvalue problem. Merely do the following.

Compute a  $k^{\text{th}}$  order Ritz generalized mass and stiffness; i.e.

$$(8) \quad \begin{bmatrix} v_k \end{bmatrix} = \begin{bmatrix} \theta_k^T \end{bmatrix} [M] \begin{bmatrix} \theta_k \end{bmatrix} \quad \text{and} \quad \begin{bmatrix} \kappa_k \end{bmatrix} = \begin{bmatrix} \theta_k^T \end{bmatrix} [K] \begin{bmatrix} \theta_k \end{bmatrix}$$

and construct a test matrix called  $\begin{bmatrix} S_k \end{bmatrix}$  which involves the threshold frequency,  $f_0$ , determined from the temporal power  $P_n$ .

$$(9) \quad \begin{bmatrix} \kappa_k - (2\pi f_0)^2 v_k \end{bmatrix} \equiv \begin{bmatrix} S_k \end{bmatrix}.$$

Decompose  $\begin{bmatrix} S_k \end{bmatrix}$  and extract the value of the output parameter NBRCHG issued by the DECOMP module. Param NBRCHG reports the number of negative values on the factor diagonal of  $S_k$  which is tantamount to the number of sign changes or zero crossings in the characteristic equation. If the value of NBRCHG =  $k$ , it indicates that the frequencies of all  $k$  Ritz modes are less than  $f_0$ . One would be inclined to want the frequency content of the Ritz modes to bracket  $f_0$ ; i.e. some modes with a frequency  $> f_0$ . This implies that one would seek to have the value of NBRCHG to be less than the order of matrix  $S_k$ . This idea can be built into the Ritz generation routine as a test as to whether enough modes have been generated to within a certain margin  $\alpha$  such that  $f_n > \alpha f_0$ , where the user specifies  $\alpha$ .

Obviously, one would not want to repeat the eigenvalue estimate each time a new Ritz mode is obtained, because  $\theta_k^T K \theta_k$  and  $\theta_k^T M \theta_k$  could become expensive as  $k$  becomes large. Therefore develop a scheme whereby the spatial power is reduced by some factor  $\gamma > 1$ ; i.e.  $\epsilon_{\text{new}} = \epsilon_{\text{old}} / \gamma$ . Typically, one can use a value

## MONITORING OF RITZ MODAL GENERATION

of 2 to 4 for  $\gamma$ . Once the spatial error  $\epsilon_{\text{new}}$  is satisfied, repeat the eigenvalue estimate test.

### Conclusion

A scheme has been proposed to monitor the adequacy of a set of Ritz modes to represent a solution by comparing the quantity generated with certain properties involving the forcing function. In so doing an attempt has been made to keep this algorithm lean and efficient, so that it will be economical to apply. Using this monitoring scheme during Ritz Mode generation will automatically ensure that the  $k$  Ritz modes  $\theta_k$  that are generated are adequate to represent both the spatial and temporal behavior of the structure when forced under the given transient condition defined by  $F(x,t)$ .



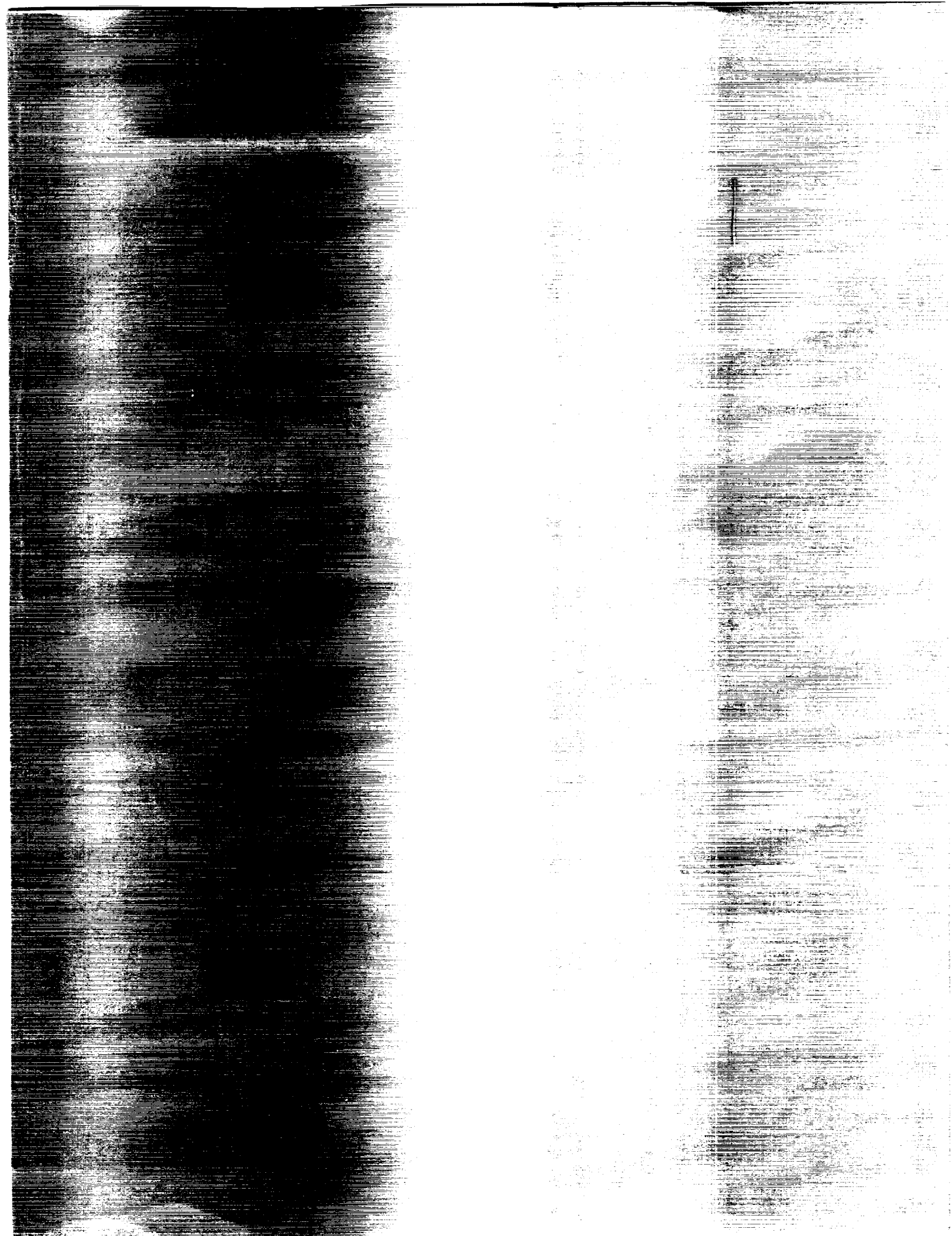




# Report Documentation Page

1. Report No. NASA CP-3069		2. Government Accession No.		3. Recipient's Catalog No.	
4. Title and Subtitle Eighteenth NASTRAN <sup>®</sup> Users' Colloquium				5. Report Date April 1990	
				6. Performing Organization Code	
7. Author(s)				8. Performing Organization Report No.	
				10. Work Unit No.	
9. Performing Organization Name and Address COSMIC, NASA's Computer software Management and Information Center The University of Georgia Athens, GA 30602				11. Contract or Grant No.	
				13. Type of Report and Period Covered Conference Publication	
12. Sponsoring Agency Name and Address National Aeronautics and Space Administration Washington, DC 20546				14. Sponsoring Agency Code	
15. Supplementary Notes Also available from COSMIC, Athens, GA 30602					
16. Abstract This publication is the proceedings of the Eighteenth NASTRAN Users' Colloquium held in Portland, Oregon, April 23-27, 1990. It provides some comprehensive general papers on the application of finite elements in engineering, comparisons with other approaches, unique applications, pre- and postprocessing or auxiliary programs, and new methods of analysis with NASTRAN.					
17. Key Words (Suggested by Author(s)) NASTRAN, Structures, Structural Analysis, Finite Element Analysis, Colloquium				18. Distribution Statement Unclassified - Unlimited  Subject Category 39	
19. Security Classif. (of this report) Unclassified		20. Security Classif. (of this page) Unclassified		21. No. of pages 170	22. Price A08





National Aeronautics and  
Space Administration  
Code NTT-4

Washington, D.C.  
20546-0001

Official Business  
Penalty for Private Use, \$300



National Aeronautics and  
Space Administration

Washington, D.C.  
20546

SPECIAL FOURTH CLASS MAIL  
BOOK

Postage and Fees Paid  
National Aeronautics and  
Space Administration  
NASA-451



Official Business  
Penalty for Private Use \$300

LI 601 OF 3049 90031380905494  
NASA  
SCIEN & TECH INFO FACILITY  
ACCESSIONS DEPT  
P O BOX 8757 BWI AIRPORT  
BALTIMORE MD 21240

